A comprehensive review on piezoelectric energy harvesting technology: Materials, mechanisms, and applications

Huicong Liu, Junwen Zhong, Chengkuo Lee, Seung-Wuk Lee, and Liwei Lin

Citation: Applied Physics Reviews **5**, 041306 (2018); doi: 10.1063/1.5074184
View online: https://doi.org/10.1063/1.5074184
View Table of Contents: http://aip.scitation.org/toc/are/5/4
Published by the American Institute of Physics

APPLIED PHYSICS REVIEWS

A comprehensive review on piezoelectric energy harvesting technology: Materials, mechanisms, and applications

Huicong Liu,[1,2,a),b)] Junwen Zhong,[3,a)] Chengkuo Lee,[2,4,5,6,7,b)] Seung-Wuk Lee,[8,b)] and Liwei Lin[3,b)]

[1]*Jiangsu Provincial Key Laboratory of Advanced Robotics, School of Mechanical and Electric Engineering, Soochow University, Suzhou 215123, China*
[2]*Department of Electrical and Computer Engineering, National University of Singapore, 4 Engineering Drive 3, Singapore 117576*
[3]*Department of Mechanical Engineering & Berkeley Sensor and Actuator Center, University of California at Berkeley, Berkeley, California 94720-1740, USA*
[4]*Hybrid-Integrated Flexible (Stretchable) Electronic Systems Program, National University of Singapore, E6 #05-4, 5 Engineering Drive 1, Singapore 117608*
[5]*NUS Suzhou Research Institute (NUSRI), Suzhou Industrial Park, Suzhou 215123, People's Republic of China*
[6]*NUS Graduate School for Integrative Science and Engineering, National University of Singapore, Singapore 117456*
[7]*Center for Intelligent Sensors and MEMS, National University of Singapore, E6 #05-11F, 5 Engineering Drive 1, Singapore 117608*
[8]*Department of Bioengineering, University of California at Berkeley, Berkeley, California 94720-1740, USA*

(Received 22 October 2018; accepted 1 November 2018; published online 27 December 2018)

The last decade has witnessed significant advances in energy harvesting technologies as a possible alternative to provide a continuous power supply for small, low-power devices in applications, such as wireless sensing, data transmission, actuation, and medical implants. Piezoelectric energy harvesting (PEH) has been a salient topic in the literature and has attracted widespread attention from researchers due to its advantages of simple architecture, high power density, and good scalability. This paper presents a comprehensive review on the state-of-the-art of piezoelectric energy harvesting. Various key aspects to improve the overall performance of a PEH device are discussed, including basic fundamentals and configurations, materials and fabrication, performance enhancement mechanisms, applications, and future outlooks. *Published by AIP Publishing.*
https://doi.org/10.1063/1.5074184

TABLE OF CONTENTS

I. INTRODUCTION OF ENERGY HARVESTING . 2
II. FUNDAMENTALS AND CONFIGURATIONS. . 3
A. Piezoelectric effect 3
B. Device configuration. 3
1. Bimorph or unimorph cantilever 3
2. Piezoelectric film configuration 4
3. Piezoelectric stack configuration. 5
III. MATERIALS AND FABRICATION TECHNOLOGIES. 5
A. Piezoelectric materials in energy harvesting. 5
1. Inorganic piezoelectric materials. 5
2. Piezoelectric polymers 7
3. Bio-piezoelectric materials. 10
B. Fabrication techniques 10
1. Micro-fabrication process. 11
2. Grow-pattern-transfer process 13
3. Nano-fabrication process 14
IV. PERFORMANCE ENHANCEMENT TECHNOLOGIES. 15
A. Multi-DOF harvesting mechanism 15
1. Multi-frequency harvesting mechanism . . 16
2. Multi-directional harvesting mechanism . 17
B. Mono-stable nonlinear PEH mechanism 17
1. Mechanical stress or stretching induced nonlinearity. 18
2. Mechanical preload induced nonlinearity 19
3. Magnetic stopper induced nonlinearity . . 19
4. Magnetic force induced nonlinearity 19
C. Bi-stable nonlinear PEH mechanism 19
1. Magnetic attraction induced bi-stability. . 21
2. Magnetic repulsion induced bi-stability. . 21
3. Mechanical load induced bi-stability 21
D. Frequency up-conversion (FUC) mechanism 22
1. Mechanical impact approach 22
2. Mechanical plucking approach 22
3. Snap-through buckling approach. 22
4. Magnetic plucking approach 23

[a)]H. Liu and J. Zhong contributed equally to this work.
[b)]Authors to whom correspondence should be addressed: hcliu078@suda.edu.cn; elelc@nus.edu.sg; leesw@berkeley.edu; and lwlin@berkeley.edu

E. Hybrid energy harvesting mechanism 24
1. Piezoelectric and electromagnetic hybrid mechanism 24
2. Piezoelectric and triboelectric hybrid mechanism 24
V. APPLICATIONS AND OUTLOOKS 25
A. Wearable and implantable energy harvesting 25
B. Self-powered wireless sensors and systems . 27
C. Future application outlooks 28
VI. SUMMARY AND CONCLUDING REMARKS. 29

I. INTRODUCTION OF ENERGY HARVESTING

Energy crisis, global warming, and environmental pollution have been increasingly discussed worldwide. Various clean and renewable energy types, such as solar energy, kinetic energy, and bio-energy as alternative energy sources to replace the traditional fossil fuel, have been widely exploited owing to their sustainability and environmental friendliness.[1,2] In the last few decades, explosive research and development efforts have been devoted to energy harvesting technologies, which scavenge the wasted energy available in the ambient environment, such as vibrations, heat, light, radiation, wind, and water, into electrical energy for low-power devices.[3–7] In general, these energy harvesting schemes could suffer from low, variable, and unpredictable ambient conditions, while the great advancements in low-power integrated circuits (ICs), wireless communication, and mobile electronics have reduced the demands in power consumption requirements and increased the attractiveness of energy harvesting approaches. An excellent commercial example comes from the Perpetuum Ltd.,[8] whose vibration energy harvesters and wireless sensor nodes can be used to monitor a wide variety of equipment and assets such as those in the rail industry.

The ambient energy sources suitable for energy harvesting applications have received varying degrees of attention such as solar, radio frequency (RF), acoustic waves, temperature gradients, and kinetic energy. Among these, kinetic energy in the form of vibrations, random displacements, or forces is ubiquitous and versatile in our ambient environment, including direct human activities from walking, running, finger tapping, heartbeat, to respiration; structural vibrations from industrial machinery, buildings, and transport vehicles; fluid flows from wind, water, ocean, etc. Some of the recent research works have focused on the design of kinetic energy harvesters based on three major transduction mechanisms,[9–15] i.e., piezoelectric, electromagnetic, and electrostatic. On the other hand, triboelectric has been known as a very competitive energy harvesting approach as well in the past few years.[16–18] There have been a number of excellent reviews in the area of energy harvesting from different aspects.[19–26] The relative advantages and disadvantages of different transduction mechanisms have been discussed thoroughly by various authors.[27–29] While each of the aforementioned techniques can provide a useful amount of energy, piezoelectric energy harvesters have received the most attention due to their higher energy density, inherent reciprocal conversion capability, and simpler architectures as compared to their counterparts.[30–33] In addition, piezoelectric material is ease of scaling in micro- and nanoscale devices,[34–36] and preferable in flexible and stretchable devices.[37,38]

The aim of this review is to provide an comprehensive overview of piezoelectric energy harvesting (PEH) technologies, including the basic configurations, materials and fabrication, performance enhancement mechanisms, applications, and future outlooks as illustrated in Fig. 1. Section II starts with the fundamentals and configurations of PEH. The performance and merits of a PEH device are strongly dependent on the operation modes and device configurations. To fully exploit the benefit of the piezoelectric effect, various piezoelectric films and stack configurations working in the 31-mode or the 33-mode with straight, tapered, or compliant cantilever shapes have been presented. The electromechanical coupling efficiency of a piezoelectric energy harvester is essentially limited by the piezoelectric properties of the material. Therefore, Sec. III gives a brief overview of recent advancements of flexible piezoelectric materials in energy harvesting, which can be classified into inorganic piezoelectric materials, piezoelectric polymers, and bio-piezoelectric materials. Furthermore, various fabrication techniques including micro-fabrication, pattern-transfer, and nano-fabrication processes have been reviewed for the integration of advanced piezoelectric materials in energy harvesters with competitive performances.

There are three main methodologies of extracting kinetic energy based on piezoelectric materials, "stain," "vibration," and "fluid." Strain energy harvesting devices directly couple the piezoelectric energy harvester to the relative deformation and movement of the mechanical sources, for example, harvesting energy from the compression of roadway vehicle, extension of muscle, pressure of pulse and heartbeat, and so on. Strain energy harvesting mechanisms do not rely on inertial force or resonance vibration. The output performance of these harvesters to a large extent is dependent on not only the electromechanical conversion efficiency of the materials

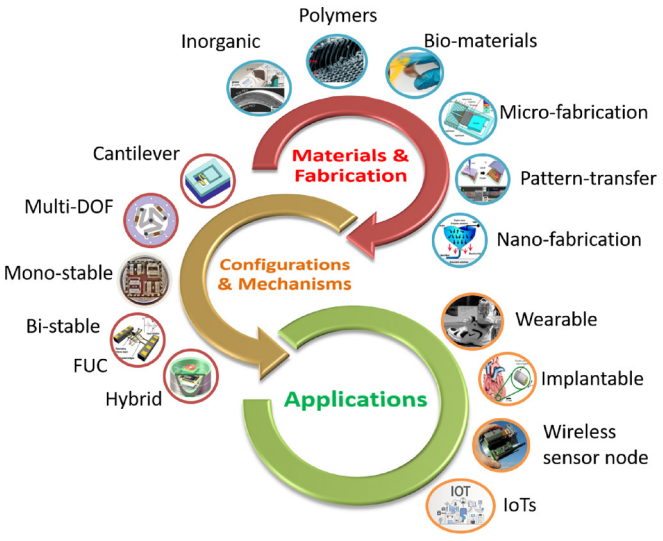

FIG. 1. A comprehensive overview of PEH including the basic configurations, materials and fabrication, performance enhancement mechanisms, and applications.

but also the extension and compression force of the mechanical stimuli. Vibration energy harvesting (VEH) is widely investigated in the literature by incorporating a basic configuration of spring-mass-damping system. The vibration amplitude of the energy harvesting device is not simply related to the base amplitude but also affected by the excitation frequency. For instance, the vibration amplitude of a device at resonance can be significantly larger than that of the base movement. In the previous studies, the majority of works focused on the development of resonant-based energy harvesting devices so as to improve the output performance at resonance, and the best performance of the device is limited to a very narrow bandwidth around the fundamental resonance frequency. Any deviation of the excitation frequency away from the resonance can result in a drastic reduction in power generation. In order to overcome this issue of the conventional linear configuration, broadening the bandwidth of the VEH device becomes one of the most challenging issues before their practical deployment. Section IV summarizes the performance enhancement techniques for vibration PEH, especially for frequency broadening approaches, such as multi-modal, mono-stable, bi-stable, frequency-up-conversion (FUC), and hybrid mechanisms.

Section V demonstrates some experiments and application examples of PEH for powering the implantable medical or wearable devices, and self-powered wireless sensors and health monitoring systems from automobile and structure vibrations. Meanwhile, some potential applications and future outlooks including wind flow, rainfall, ocean wave, roadway, and Internet of Things (IoTs) will be discussed in this section.

II. FUNDAMENTALS AND CONFIGURATIONS

A. Piezoelectric effect

The piezoelectric effect was first discovered in 1880 by the brothers Pierre Curie and Jacques Curie. Piezoelectric materials possess the unique properties of electromechanical coupling either with the generation of electric charge under an applied mechanical stress, labeled as the direct piezoelectric effect, or the induction of mechanical strain due to an applied electric field, labeled as the converse piezoelectric effect. The direct piezoelectric effect is essential for sensing and energy harvesting where the applied stresses are used to generate surface charges on the piezoelectric materials. The direct and converse piezoelectric effects are governed by the piezoelectric constitutive equations as[39] follows:

$$\begin{bmatrix} \delta \\ D \end{bmatrix} = \begin{bmatrix} s^E & d^t \\ d & \varepsilon^T \end{bmatrix} \begin{bmatrix} \sigma \\ E \end{bmatrix}, \tag{1}$$

where δ and σ represent the strain and stress components; D and E refer to the electric displacement and electric field components; s, ε, and d are the elastic compliance, the dielectric constant, and the piezoelectric coefficient, respectively; the superscripts E and T denote that the respective constants are evaluated at the constant electric field and constant stress, respectively; and the superscript t stands for the transpose.

Most piezoelectric materials for energy harvesting exhibit a well-defined polar axis, and the direction of the applied stress relative to the polar axis would affect the energy harvesting performance. For a ferroelectric ceramic or polymer,[40–43] e.g., lead zirconate titanate (PZT), $Pb(Mg_{1/3}Nb_{2/3})O_3$-$PbTiO_3$ (PMN-PT), or polyvinylidene fluoride (PVDF), the polar axis is dependent on the poling direction. However, for the non-ferroelectric crystalline materials, e.g., aluminium nitride (AlN) or zinc oxide (ZnO), the polar axis is defined by the crystal orientation (along the c-axis of the Wurtzite crystal structure). The polar axis is referred to the "3" direction. Due to the symmetry, other directions at right angles to the polar axis are equivalent and can be referred to the "1" directions. The direction of the applied stress can be either along the polar axis (3-direction) or at right angles to it (1-direction), resulting in two common PEH configurations, 33-mode and 31-mode, as illustrated in Fig. 2(a). The piezoelectric material used in the 33-mode means that the compressive stress/strain is applied in parallel to the 3-direction, while the voltage generated along the same axis. In the 31-mode, the stress/strain is applied perpendicular to the polar axis and the direction of the generated voltage is at the right angle of the applied force. The piezoelectric coefficient (d_{3i}) is used to quantify the piezoelectric material performance, which is the ratio of the open circuit charge density to the applied stress (in unit of C/N). Typically, the d_{33} coefficient is higher than the d_{31} coefficient. However, the operation in the 31-mode leads to the use of large strain in the 1-direction and thus is commonly implemented in VEH.

B. Device configuration

1. Bimorph or unimorph cantilever

Cantilever is one of the most used structures in PEH, especially for mechanical energy harvesting from vibrations, as large mechanical strain can be produced within the piezoelectric material during vibration. More importantly, the resonance frequency of the fundamental flexural modes of a cantilever is much lower than those of the other configurations. PEH usually takes the forms of bimorph or unimorph straight cantilevers.[20,21] In Fig. 2(b), the most common 31-mode bimorph cantilever contains two separate piezoelectric sheet bonded together, with a center shim in between. The structure is designed to operate in the bending mode to have the top layer of the elements in tension and the bottom layer in compression or vice versa and generates electric charge based on the piezoelectric effect. The top and bottom layers are poled either in the same direction or in the opposite direction, which are termed as parallel or series poling, to induce accumulated current or voltage by each layer, respectively.[44] The piezoelectric elements on a bending cantilever can be made of multiple layers with proper electrodes and wiring in-between each layer. In all cases, the power conversion potential is the same and theoretically the poling direction and the number of layers only affects the voltage to current ratio.

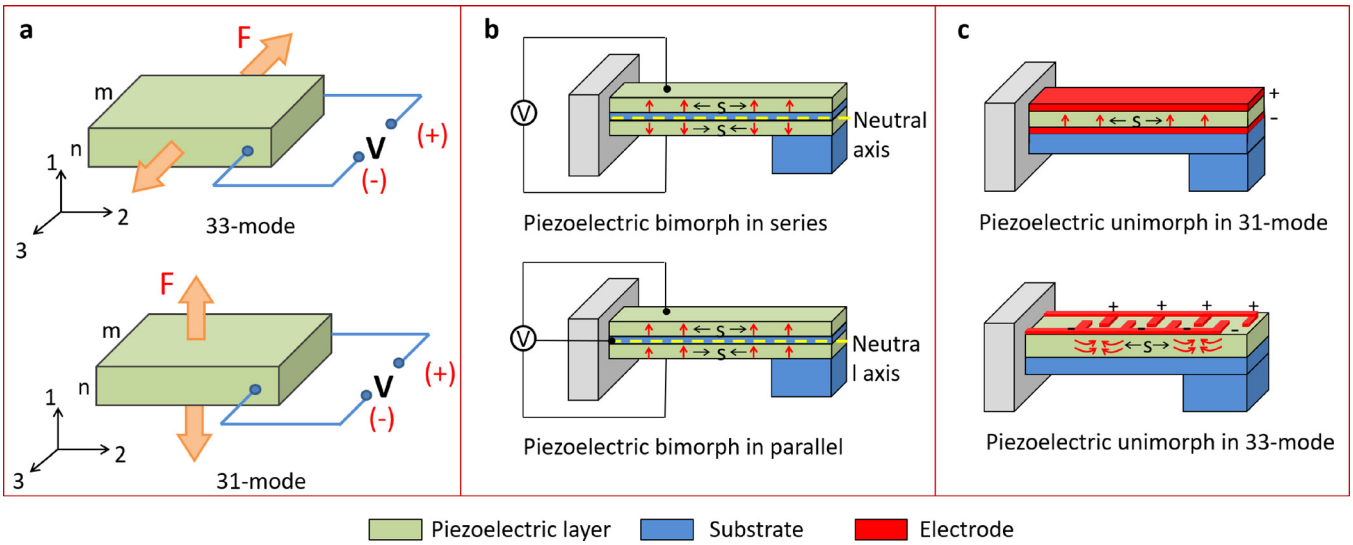

FIG. 2. (a) Piezoelectric material used in the 33-mode and the 31-mode; (b) 31-mode bimorph cantilever in series and parallel connections; and (c) 31-mode and 33-mode unimorph cantilever configuration.

Another basic configuration for vibration-based PEH is the unimorph cantilever, especially preferable for the micro-electromechanical systems (MEMS) implementation. As demonstrated in Fig. 2(c), in the 31-mode, the piezoelectric layer is sandwiched by top and bottom electrodes, while in the 33-mode, the electrode is on top of the piezoelectric layer with interdigital electrodes (IDEs) pattern. In both modes, the piezoelectric thin film layer is coated on an elastic substrate. The electric charge of the piezoelectric layer can be induced perpendicular or parallel to the direction of the applied strain in either the 31-mode or the 33-mode. The open circuit voltage of the piezoelectric layer V_{oc} is given as

$$V_{oc} = \frac{d_{ij}}{\varepsilon_r \varepsilon_0} \sigma_{ij} g_e. \tag{2}$$

From Eq. (2), it is found that the open circuit voltage V_{oc} is proportional to the applied stress σ_{ij}, the piezoelectric coefficient d_{ij}, and the gap distance between electrodes g_e. ε_r and ε_0 are the relative dielectric constant and the permittivity of vacuum, respectively.

Clearly, the performance and merits of a piezoelectric unimorph cantilever are strongly dependent on the type of piezoelectric mode. Take the most popular piezoelectric material, PZT, as an example, the piezoelectric coefficient d_{33} is approximately two times higher than that of d_{31}. Therefore, the generated voltage for the 33-mode energy harvester is expected to be higher than that of the 31-mode device by assuming that both modes have the same configuration parameters. In addition, the voltage generation is proportional to the distance between the top and bottom electrodes for the 31-mode device and to the distance between the electrode fingers for the 33-mode device. Since the thickness of the PZT layer is normally very thin, the electrode distance in the 31-mode is shorter than that in the 33-mode. It follows that the 33-mode energy harvester has the advantage of producing higher voltage output, while the 31-mode device can be superior in larger current output. In the case of the output power obtained by the product of voltage and current, a better performance in the 31-mode than in the 33-mode was reported by Lee *et al.*[45] Kim *et al.*[46] have done a similar comparison for MEMS PZT cantilevers based on the 31-mode and the 33-mode. They concluded that higher voltage and power can be obtained from the 33-mode device by optimizing the IDE design.

2. Piezoelectric film configuration

Most researchers have focused on traditional or slightly varied rectangular cantilever beams, because of their easy implementation, well-understood model, and relatively high stress distribution for a given force input. However, the stress induced in a cantilever during bending is concentrated near the clamped end and decreases in magnitude at locations further away from the clamp. As a result, the non-stressed portion of the piezoelectric layer does not actually contribute to power generation. Both theoretical analysis and experimental studies have shown that a "tapered" or triangular-shaped cantilever may achieve constant strain level throughout the length of the cantilever and can deliver more energy output than a rectangular shaped beam.[47–49] Therefore, piezoelectric cantilevers with a tapered shape have often been used to minimize the size and weight of the cantilever.

In addition to cantilevers with rectangular and tapered shapes, structural designs are explored to either match the relatively low frequency sources or increase output performances. Some studies focused on using compliant zigzag or meandering beam-shapes to lower the resonance frequency[50–52] by reducing the stiffness of the cantilever structure. However, lowering the beam stiffness is accomplished by distributing the stress throughout the structure, which reduces the generated electrical power. Sharpes *et al.*[53] have demonstrated a strategy of using the two-dimensional complaint beam-shapes to harvest energy from low frequency excitations. With the goal of maintaining the low-resonance frequency and realizing a concentrated stress structure where

a piezoelectric layer may be placed, rather than being distributed throughout the beam, three different beam shapes were proposed and characterized as shown in Fig. 3. It is shown analytically, numerically, and experimentally that the proposed "Elephant" harvester is able to provide significant increase in power production.

Another mechanical structure for PEH is the circular diaphragm. The deflection of a diaphragm structure in the pressure mode causes compressive or tensile stress at different locations. A variety of pressure fields such as fluctuating pressure,[54,55] acoustic waves,[56] and mechanical vibrations[57–59] can be converted to an AC electrical signal by piezoelectric diaphragm converters. The theoretical and experimental analyses of piezoelectric circular diaphragms operating under varying pressures were presented by Kim *et al.*[55] and Mo *et al.*[57] However, it should be noted that the circular diaphragm is considerably stiffer than a cantilever of same size, resulting in higher resonance frequencies in the vibration mode operation.

3. Piezoelectric stack configuration

To fully make use of the 33-mode, the PEH architecture composed of multiple piezoelectric layers stacked together has been developed, which has a higher coefficient d_{33} than that in the 31-mode. Xu *et al.*[60] have reported a piezoelectric energy harvester with 300-layer PZT stacks. The alternating poling directions of subsequent layers enable the direction of the electric field which is always towards the same electrode. The generated electrical power and power density were significantly improved than those of cantilever-type piezoelectric harvesters. However, due to the high stiffness of the piezoelectric stacks, it either required high compressive force in applications or be coupled to mechanical force amplifiers.

To fully exploit the benefit of piezoelectric stack, a cymbal-type force amplifying structure has been proposed.[61,62] It typically consists of a piezoelectric stack and a metal end cap on each side. When an axial stress is applied to the cymbal structure, the end caps amplify the axial stress to radial stress in the PZT stack, resulting in a higher equivalent piezoelectric coefficient d_{33} to contribute to the charge generation. They reported that at a frequency of 100 Hz and under 7.8 N force, 39 mW power was obtained across a 400 k Ω resistor. However, they are not suitable for energy harvesting from natural ambient vibration sources, which have a low magnitude of vibration. A PEH prototype consisting of a cantilever beam structure sandwiched by two cymbal transducers at the clamped end was proposed by Tufekcioglu and Dogan.[63] In order to magnify the force as high as possible with a limited physical size, a compound two-stage force amplification frame with a piezoelectric stack is developed.[64] It can obtain 21 times force amplification with an 18% energy transmission ratio to generate electrical energy up to 79 times more than that from one piezoelectric PZT stack.[65]

III. MATERIALS AND FABRICATION TECHNOLOGIES

A. Piezoelectric materials in energy harvesting

The first proposed piezoelectric material is naturally occurring quartz, which was discovered in 1880 by French physicists Jacques and Pierre Curie.[66] After about 140 years of development, researchers have found many natural piezoelectric materials and created many artificial piezoelectric materials with excellent properties to fit various application scenarios. In this section, we will review the recent developments in energy harvesting of inorganic piezoelectric materials, piezoelectric polymers, and bio-piezoelectric materials.

1. Inorganic piezoelectric materials

Inorganic piezoelectric materials are widely applied in mechanical energy harvesting and traditionally divided into two types: piezoelectric crystals and piezoelectric ceramics.[67–69] Piezoelectric crystals have a single crystal structure and natural piezoelectricity, such as quartz film and ZnO nanowires (NWs).[68] Piezoelectric ceramics are composed of many small crystals with random crystal orientations and will only show piezoelectricity after a polarization process, normally by applying a high electrical field to align the crystal orientations. The famous piezoelectric ceramics are $Pb[Zr_xTi_{1-x}]O_3$ with $0 \leq x \leq 1$, barium titanate ($BaTiO_3$), and AlN.[69]

The wurtzite ZnO NWs are easily fabricated using the hydrothermal method[70–72] and have been used to construct nanogenerators.[73–77] The crystal structure of wurtzite ZnO is shown in Fig. 4(a), in which tetrahedrally coordinated Zn^{2+}

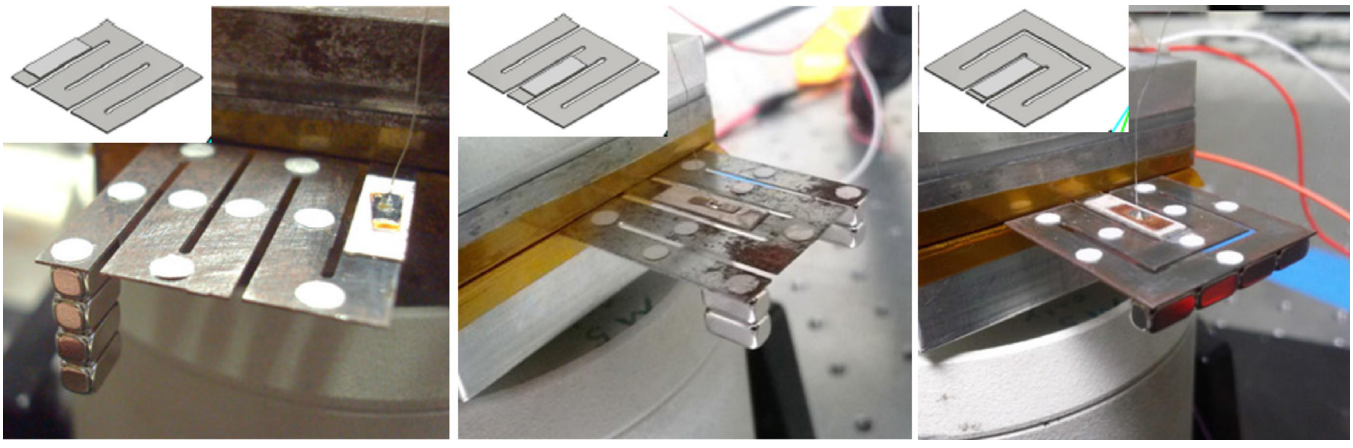

FIG. 3. Compliant zigzag or meandering beam shapes proposed by Sharpes *et al.*[53] Reprinted with permission from Appl. Phys. Lett. **107**(9), 093901 (2015). Copyright 2015 AIP Publishing LLC.

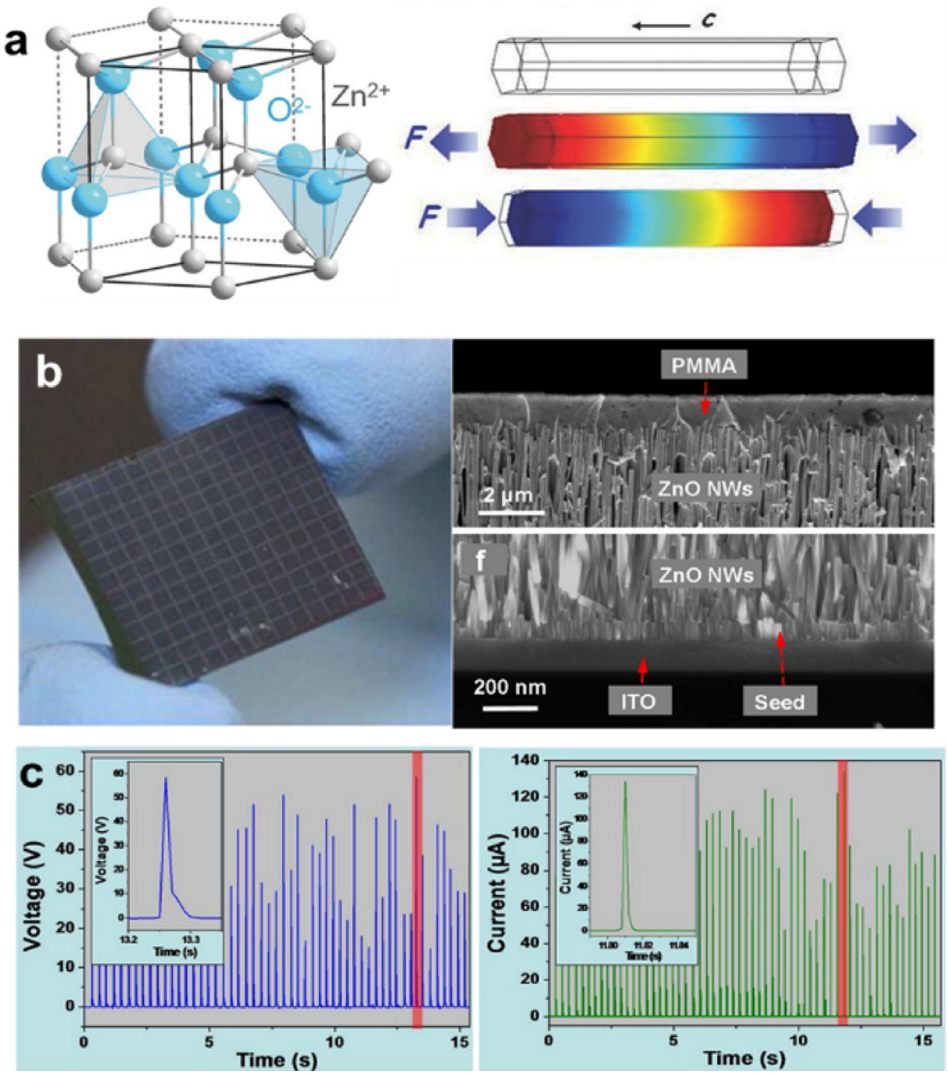

FIG. 4. (a) Atomic model of the wurtzite-structured ZnO and numerical calculation of the piezoelectric potential distribution in a ZnO NW under axial strain.[81] Reprinted with permission from J. Appl. Phys. **105**(11), 113707 (2009). Copyright 2009 AIP Publishing LLC. (b) Picture of ZnO NW-based nanogenerators array and cross-sectional view SEM image of it.[75] (c) Open-circuit voltage and short-circuit current of this nanogenerators array rectified by a bridge rectifier under impact by a human palm.[75] Reprinted with permission from Zhu *et al.*, Nano Lett. **12**(6), 3086–3090 (2012). Copyright 2012 American Chemical Society.

and O^{2-} are stacked layer-by-layer along the c-axis and the charge centers of cations and anions coincide with each other for the original state.[71] When deformation occurs, the charge centers separate to form electrical dipoles, which will generate piezo-potential between the electrodes. If the electrodes are connected with an external load, the piezo-potential will drive electrons to flow through the external load in order to partially screen the piezo-potential and achieve a new equilibrium state. As a result, mechanical energy is converted into the electrical domain. The first nanogenerator prototype was proposed by Wang and Song in 2006,[73] followed by a rapid development of the ZnO NW-based nanogenerators, with peak output voltages increasing from several milli-Volts (mV) to tens of Volts (V) and peak output currents increasing from several nano-Amperes (nA) to hundreds of micro-Amperes (μA). Since the piezoelectric effect for ZnO is not so strong (d_{33} value of about 5–10 pC/N),[78] the main way to improve the outputs is to connect many unites in parallel to improve the output current[79] and to connect many unites in series to improve the output voltage.[80]

In a typical ZnO NW-based nanogenerator with high outputs as indicated in Fig. 4(b), vertically aligned ZnO NWs grew on the patterned conductive substrate and all the units of the nanogenerator array were packaged with polymethyl methacrylate (PMMA) to enhance the mechanical strength. Such a patterned and strength-enhanced design improves not only the effectiveness of NWs for energy harvesting but also the robustness of the nanogenerator for defect toleration because each unit can work independently. The peak open-circuit voltage and short-circuit current reach a record high level of 58 V and 134 μA, respectively, as shown in Fig. 4(c). The outputs were even large enough to stimulate the neural network of a frog leg.[75]

Two-dimensional (2D) single crystal materials are also of great interest as high-performance piezoelectric materials.[82–87] Compared with one-dimensional (1D) NWs, 2D piezoelectric materials might have the morphological advantages in constructing flexible nanogenerators. The strong piezoelectricity in monolayer MoS_2 [Fig. 5(a)] is proved, with the d_{11} value of ~3 pm/V.[87] Wu *et al.*[82] assembled the mechanically exfoliated MoS_2 flakes on a flexible substrate and electrical contacts made of Cr/Pd/Au were deposited with the metal-MoS_2 interface parallel to the y axis to form a 2D nanogenerator, as indicated in Fig. 5(b). When this 2D nanogenerator is stretched, piezoelectric polarization charges of opposite polarity are induced at the zigzag edges of the MoS_2 flake. Periodic stretching and releasing of the substrate can generate piezoelectric outputs in external

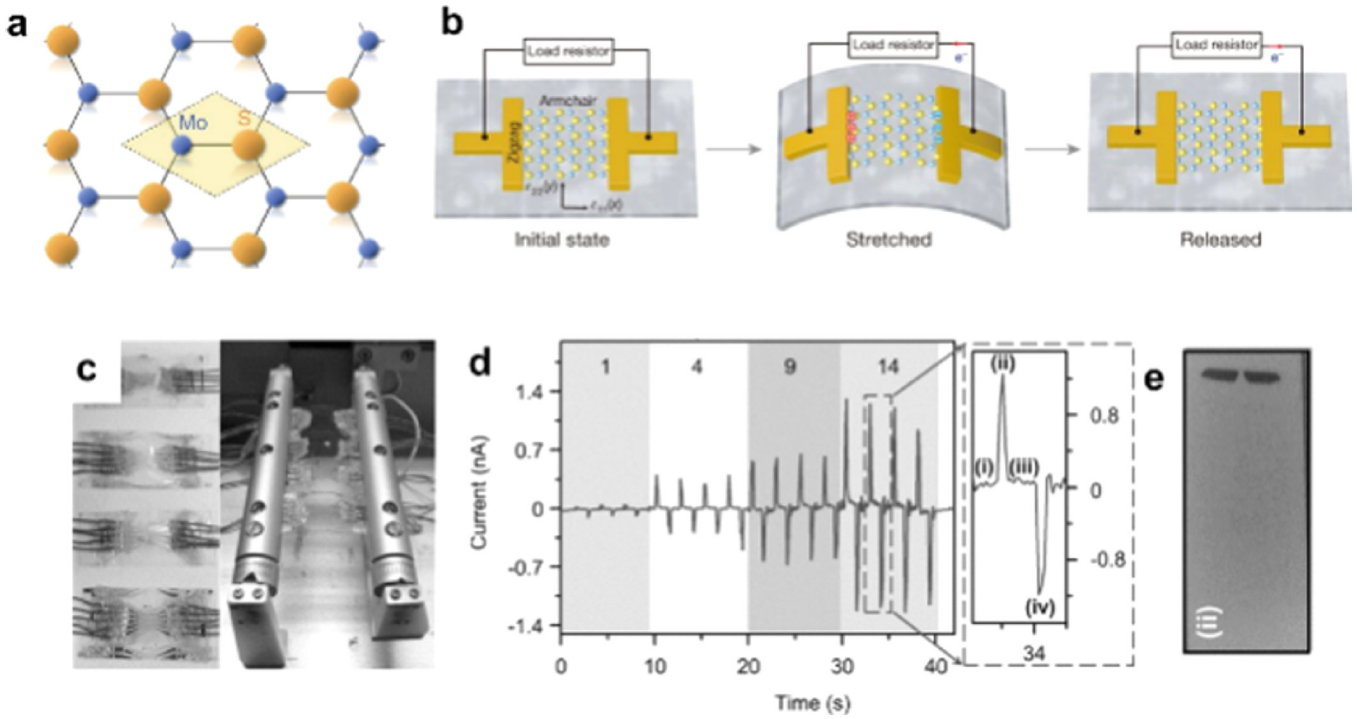

FIG. 5. (a) Atomic model of monolayer MoS_2.[83] Reprinted with permission from Cao *et al.*, Nat. Commun. **3**, 887 (2012). Copyright 2012 Springer Nature. (b) Operation scheme of the monolayer MoS_2 2D piezoelectric nanogenerator.[82] Reprinted with permission from Wu *et al.*, Nature **514**(7523), 470–474 (2014). Copyright 2014 Springer Nature. (c) Image of an array consisting of WSe_2-based 2D nanogenerators.[85] (d) Measured output currents for the integrated WSe_2-based 2D nanogenerators as a function of the number of parallel connections.[85] (e) Image of illuminating a LCD with WSe_2-based 2D nanogenerators array.[85] Reprinted with permission from Lee *et al.*, Adv. Mater. **29**, 1606667 (2017). Copyright 2017 John Wiley and Sons.

circuits with alternating polarity. A single monolayer flake strained by 0.53% generated a peak output of 15 mV and 20 pA, corresponding to a power density of 2 mW/m^2 and a 5.08% mechanical-to-electrical energy conversion efficiency. 2D-structured hexagonal boron nitride (h-BN),[84] tungsten diselenide (WSe_2),[85] and lead iodide (PbI_2)[86] were also used to build 2D nanogenerators, with device structures similar to the MoS_2 one. Currently, although the output of a single 2D nanogenerator is low, integrating many units in an efficient way will help to endow the 2D nanogenerators with really useful applications in energy harvesting. For instance, Lee *et al.*[85] integrated WSe_2-based 2D nanogenerators using a multi-electrode patterning design [Fig. 5(c)] and successfully enhanced the outputs [Fig. 5(d)] to illuminate a liquid crystal display (LCD), as shown in Fig. 5(e).

Except for aforementioned emerging nano-structured inorganic piezoelectric materials, traditional piezoelectric ceramics also possess great progress in energy harvesting, especially in the field of flexible energy harvesters, with advantages of high piezoelectric coefficients, large outputs, and good mechanical performances.[88–91] PZT [with the atomic model shown in Fig. 6(a)] and its families like PMN-PT and PMN-PZT have high d_{33} values even up to ~2000 pC/N[92,93] and are the most famous and widely used piezoelectric ceramics. Hwang *et al.*[94] deposited the PZT thin film on a flexible substrate *via* aerosol deposition (AD) and inorganic-based laser lift-off (ILLO) method, as indicated in Fig. 6(b). This flexible PZT energy harvester could generate a peak open-circuit voltage of 200 V and a peak short-circuit current of 35 μA by biomechanical bending/unbending motions and had the ability to directly light up 208 blue [Fig. 6(c)]. Furthermore, none-lead (Pb) and high-performance piezoelectric ceramics are also developed as Pb is harmful to the human body and environments. As shown in Fig. 6(d), Chang *et al.*[95] proposed a large-area flexible energy harvester based on piezoelectric alkaline niobate-based particles (KNLN), which has a d_{33} value of ~310 pC/N. This energy harvester obtained maximum output up to 140 V and 8 μA, as shown in Fig. 6(e). By virtue of the excellent energy harvesting ability of the piezoelectric ceramics-based energy harvesters, they are good for harvesting various vibration energy and have the potential to realize real self-powered systems.[96]

2. Piezoelectric polymers

Compared to inorganic piezoelectric materials, piezoelectric polymers, such as PVDF and its copolymer poly(vinylidenefluoride-co-tri-fluoroethylene) (P(VDF-TrFE)), are naturally flexile, easy for processing, and adequate mechanically strong, which are more suitable for flexible energy harvesting scenarios.[97–100] So far, there are five semi-crystalline polymorphs of PVDF, which are identified and marked as α, β, γ, δ, and ε. However, only β-phase PVDF (with the molecule model given in Fig. 7(a)] is proved to show strong piezoelectricity.[101] Thus, improving the component of β-phase PVDF is helpful for improving the abilities of PVDF-based energy harvesters.

Chang *et al.*[102] used near-field electrospinning to direct-write PVDF nanofibers with a high β-phase structure, as indicated in Fig. 7(b). This fiber-based generator could

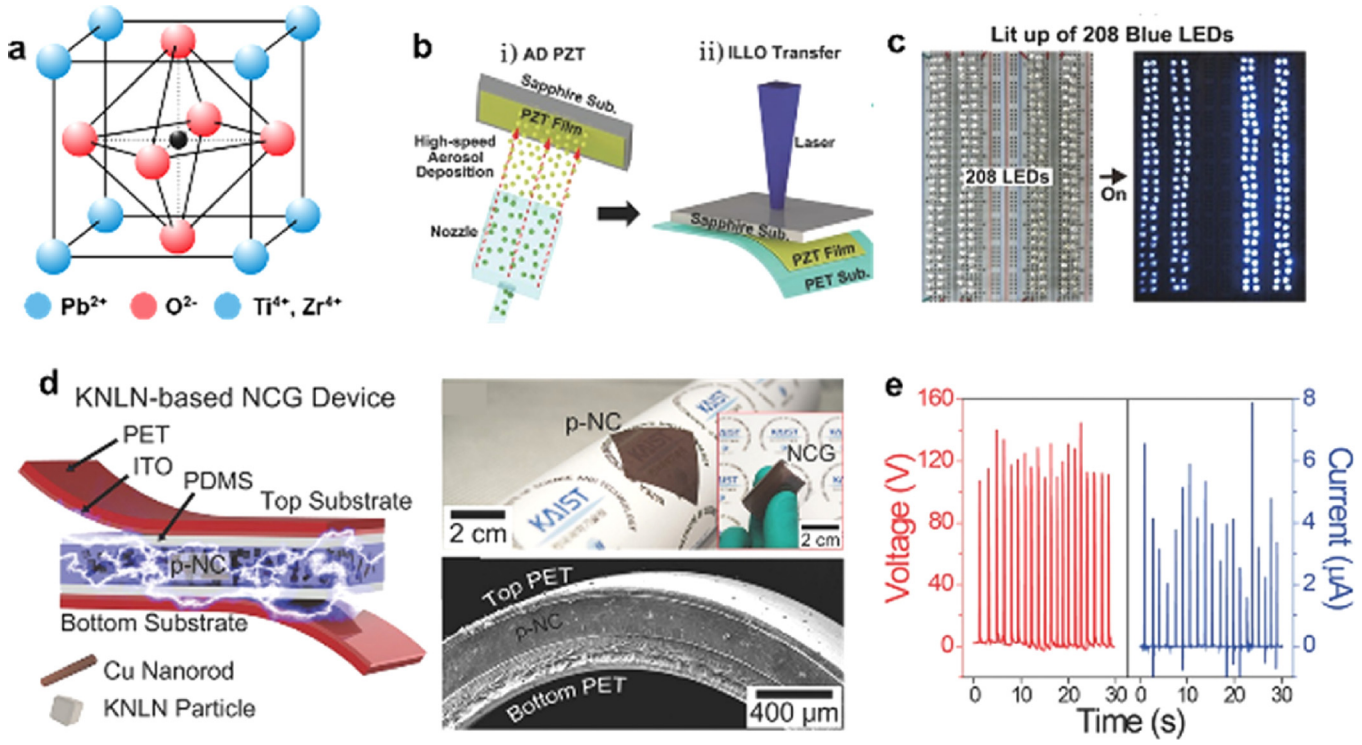

FIG. 6. (a) Atomic model of PZT.[97] (b) Schematic illustration of the device-fabrication process of a flexible AD PZT energy harvester enabled by ILLO.[94] (c) A photograph of 208 blue light emitting diode (LED)s lighting up when the flexible PZT energy-harvesting device was bent by human hand.[94] Reprinted with permission from Hwang *et al.*, Adv. Energy Mater. **6**, 1600237 (2016). Copyright 2016 John Wiley and Sons. (d) Schematic, image, and cross-sectional view SEM image of a KNLN flexible energy harvester.[95] (e) The generated output voltage and current signals from a KNLN flexible energy harvester.[95] Reprinted with permission from Chang *et al.*, Adv. Funct. Mater. **24**, 2620 (2014). Copyright 2014 John Wiley and Sons.

provide a peak short-circuit current of 0.5–3 nA and a peak open-circuit voltage of 5–30 mV, with energy conversion efficiency an order of magnitude higher than generators made of PVDF thin films [Fig. 7(c)]. To take a step further, Persano *et al.*[103] developed a large area, flexible, and free-standing piezoelectric textile that composed of highly aligned electrospun fibers of the P(VDF-TrFE), as indicated in Fig. 7(d). This textile-based generator exhibited superior flexibility and mechanical robustness, and its peak open-circuit voltage could achieve 1.5 V under bending [Fig. 7(e)]. New structural design is proposed and practiced to produce all-fiber piezoelectric textile. Soin *et al.*[104] demonstrated a "3D spacer" based all-fiber piezoelectric textile consists of high β-phase PVDF monofilaments as the spacer yarn interconnected between silver coated polyamide multifilament yarn layers acting as the top and bottom electrodes [Fig. 7(f)]. Compared to traditional 2D piezoelectric textile, this new type 3D textile-based PVDF generator provided nearly five times larger output power density, with a maximum power density of 5.07 μW/cm^2 [Fig. 7(g)].

The d_{33} value of PVDF is not high, just about 20–30 pC/N.[78] Thus, it is necessary to develop new piezoelectric polymers with high piezoelectric coefficients. Piezoelectrets are thin films of polymer foams [Fig. 8(a)], exhibiting piezoelectric-like properties after electric charging with the high voltage corona method.[105–109] Piezoelectrets usually consist of a cellular polymer structure filled with air. Polymer-air composites are elastically soft and flexible due to their high air content. The positive and negative charges inside the air bubbles compose of electrical dipoles, as indicated in Fig. 8(b). When compressed and then released, the thickness of a piezoelectret film changes, thus changing the moments of the electrical dipoles. As a result, mechanical signals are converted into electrical ones [Fig. 8(c)].[106] The traditional piezoelectret material is cellular propylene (PP), which was first proposed by Kirjavainen and co-workers in 1990.[105] The equivalent d_{33} values of cellular PP fabricated using the thermal expansion method can reach up to ~200 to 600 pC/N,[107] which is almost as high as that of commercial PZT films. Cellular polypropylene has been applied in many transducer applications, like loudspeakers and energy harvesters. For example, Wu *et al.*[106] presented a cellular PP-based flexible energy harvester with long-term stable output performance, reaching the peak power density of ~52.8 mW/m^2.

New types of piezoelectrets with higher piezoelectric coefficients are emerging. Wang *et al.*[110] proposed a porous polydimethylsiloxane (PDMS)-based piezoelectret with d_{33} values reaching ~1500 pC/N. Zhong *et al.*[111] fabricated a sandwich-structured piezoelectret with d_{33} values up to 6300 pC/N, as shown in Fig. 8(d). The flexible energy harvester based on this piezoelectret worked steadily under extreme moisture and generated peak power of ~0.44 mW and worked steadily for ~90 000 cycles, as indicated in Fig. 8(e). The aforementioned piezoelectret has very good longitudinal piezoelectric activity (high d_{33}), which is good for the conversion of vibrational energy. Specially designed piezoelectret with good transverse piezoelectricity (high d_{31}) is also developed to covert the tensile energy.[112]

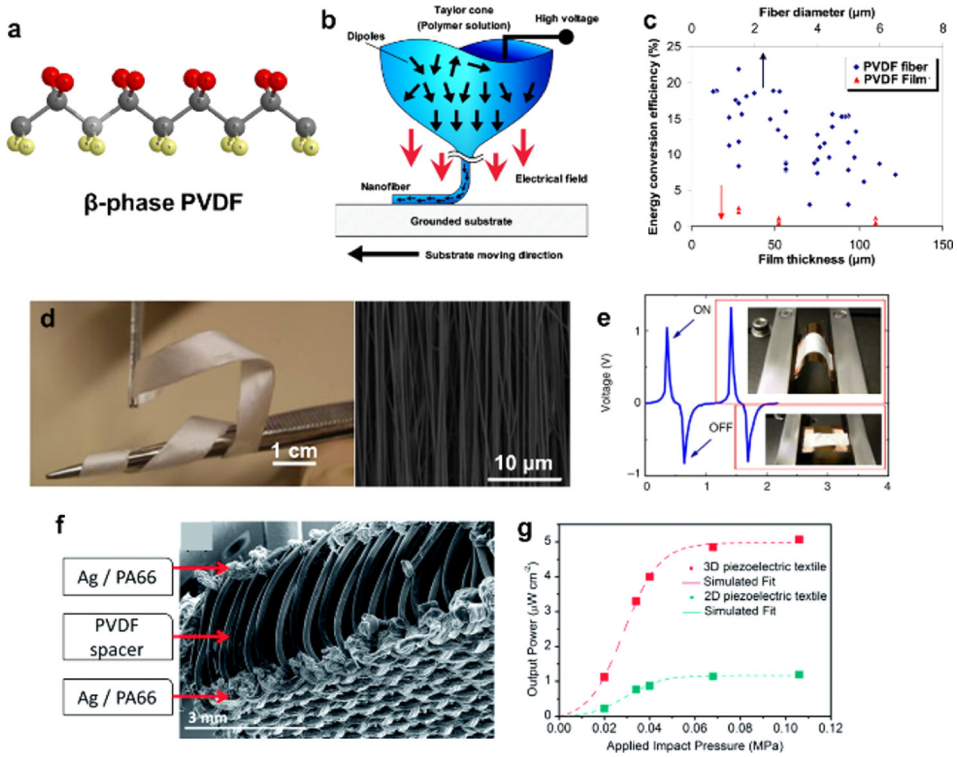

FIG. 7. (a) Molecule model of *β*-phase PVDF.[101] Reprinted with permission from Zhu *et al.*, Comput. Mater. Sci. **44**(2), 224–229 (2008). Copyright 2008 Elsevier. (b) Near-field electrospinning combining direct-write, mechanical stretching, and *in situ* electrical poling to create and place piezoelectric nanogenerators onto a substrate.[102] (c) Plots of measured energy conversion efficiency of PVDF nanogenerators and thin films with different feature sizes.[102] Reprinted with permission from Chang *et al.*, Nano Lett. **10**(2), 726 (2010). Copyright 2010 American Chemical Society. (d) Photograph and SEM image of a free-standing film of highly aligned P(VDF-TrFE) fibers.[103] (e) Open-circuit voltage for the P(VDF-TrFE)-based generator under cycling bending at 1 Hz.[103] Reprinted with permission from Persano *et al.*, Nat. Commun. **4**(3), 1633 (2013). Copyright 2013 Springer Nature. (f) Cross-sectional SEM image of the "3D spacer" all fiber piezoelectric textile.[104] (g) Variation of total output power as a function of applied impact pressure for 2D and 3D piezoelectric textile.[104] Reprinted with permission from Soin *et al.*, Energy Environ. Sci. **7**(5), 1670–1679 (2014). Copyright 2014 Royal Society of Chemistry.

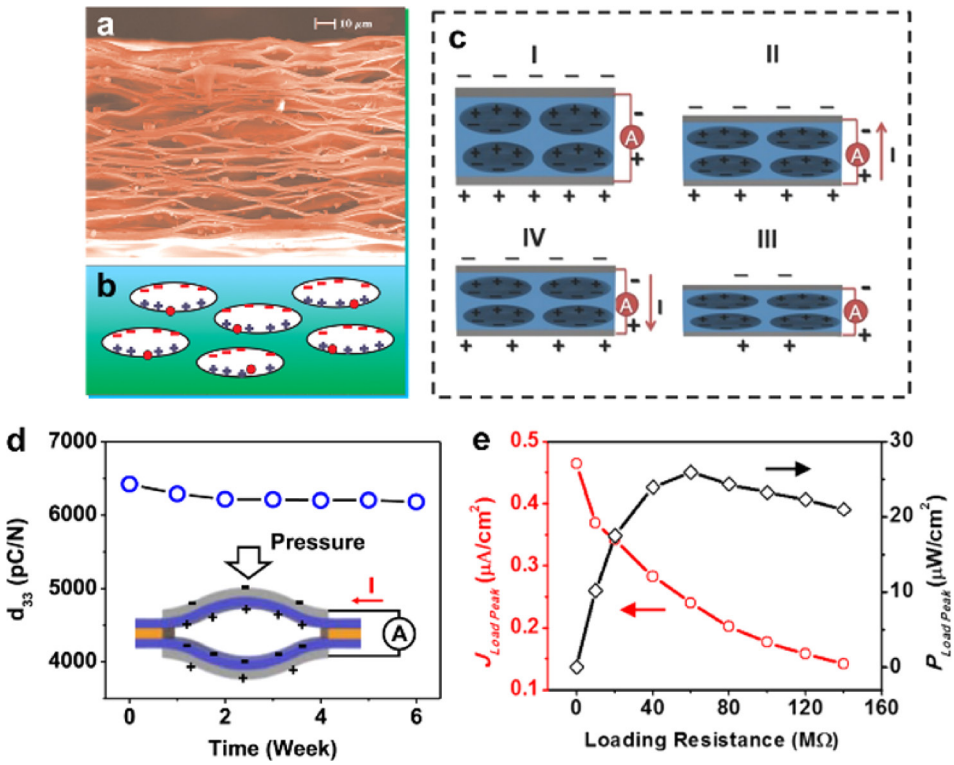

FIG. 8. (a) SEM image showing the polymer-air bubble structure of cellular PP, which is a typical piezoelectret.[105] (b) Schematic diagram showing the electrical dipoles inside the piezoelectret.[105] Reprinted with permission from Li *et al.*, Adv. Funct. Mater. **26**(12), 1964–1974 (2016). Copyright 2016 John Wiley and Sons. (c) Schematic diagram indicates the working mechanism of a cellular PP-based flexible energy harvester when it is at (I) the original, (II) the pressing, (III) the equilibrium, and (IV) the releasing states, respectively.[106] Reprinted with permission from Wu *et al.*, Adv. Funct. Mater. **25**(30), 4788–4794 (2015). Copyright 2015 John Wiley and Sons. (d) The equivalent d_{33} values of PET/ethylene vinyl acetate copolymer (EVA)/PET sandwich-structure piezoelectret.[111] (e) Load peak current and power density of a sandwich-structured piezoelectret-based energy harvester with respect to different load resistances.[111] Reprinted with permission from Zhong *et al.*, Nano Energy **37**, 268 (2017). Copyright 2017 Elsevier.

3. Bio-piezoelectric materials

It is interesting that some biological tissues and microorganisms have piezoelectricity, such as silk, bone, and specific virus.[113–115] As biotechnology techniques enable large-scale production and easy biodegradation, the bio-piezoelectric materials potentially offer a simple and environmentally friendly approach to energy generation. However, bio-piezoelectric materials are more appropriate for short-term or one-time applications due to the lifetime of the biomaterials. Lee *et al.*[116] demonstrated that M13 bacteriophage [Fig. 9(a)] could display piezoelectric property and could be used to generate electrical energy. Self-assembled thin films of M13 bacteriophage [Fig. 9(b)] could exhibit piezoelectric strengths of up to 7.8 pm/V. A piezoelectric generator based on M13 bacteriophage produced up to 6 nA of current [Fig. 9(c)] and 400 mV of potential and could operate a liquid-crystal display. Ghosh and Mandal[117] showed an efficient bio-piezoelectric nanogenerator from the swim bladder of CatlaCatla fish, as shown in Fig. 9(d). The large piezoelectric charge coefficient (d_{33} of ~22 pC/N) enabled the bio-piezoelectric generator with an open-circuit voltage of 10 V and a short-circuit current of 51 nA under a compressive normal stress (~1.4 MPa) by human finger [Fig. 9(e)]. Furthermore, the peak output power reached 4.15 μW/cm^2 with inherent piezoelectric energy conversion efficiency (~0.3%).

Various of amino acid crystals and peptide nanostructures have been studied for the piezoelectric properties. Among them, diphenylalanine (FF) has been studied intensively and fabricated for the VEH.[121–124] Lee *et al.* developed large-scale unidirectionally polarized, aligned FF nanotubes, and fabricated peptide-based piezoelectric energy harvesters.[125] They used the meniscus driven self-assembly process to fabricate horizontally aligned FF nanotubes. The FF nanotubes exhibit piezoelectric properties with unidirectional polarization. The fabricated horizontally aligned FF-peptide based piezoelectric energy harvesters could generate voltage, current, and power of up to 2.8 V, 37.4 nA, and 8.2 nW, respectively, and power multiple liquid-crystal display panels. Additionally, Nguyen *et al.* fabricated the FF-nanotube in a vertical manner by applying the high electric field.[126] The fabricated vertically aligned FF-nanotube VEH exhibited 1.4 V and a power density of 3.3 nW/cm^2.

In summary, various piezoelectric materials have been applied for mechanical strain or VEH with variable amplitude and frequency from ambient environments, such as human motions, mechanical stretching or compression, and machine vibrations. We summarize the performances of piezoelectric materials in energy harvesting as shown in Table I. These PEH devices have potential applications in distributed sensor networks and wearable electronics, aiming to establish self-powered systems.

B. Fabrication techniques

An important advantage of piezoelectric materials for energy harvesting is their scalability. Various fabrication techniques have been continuously developed to integrate advanced piezoelectric materials in energy harvesters, and hence, the output performance is improved constantly. This

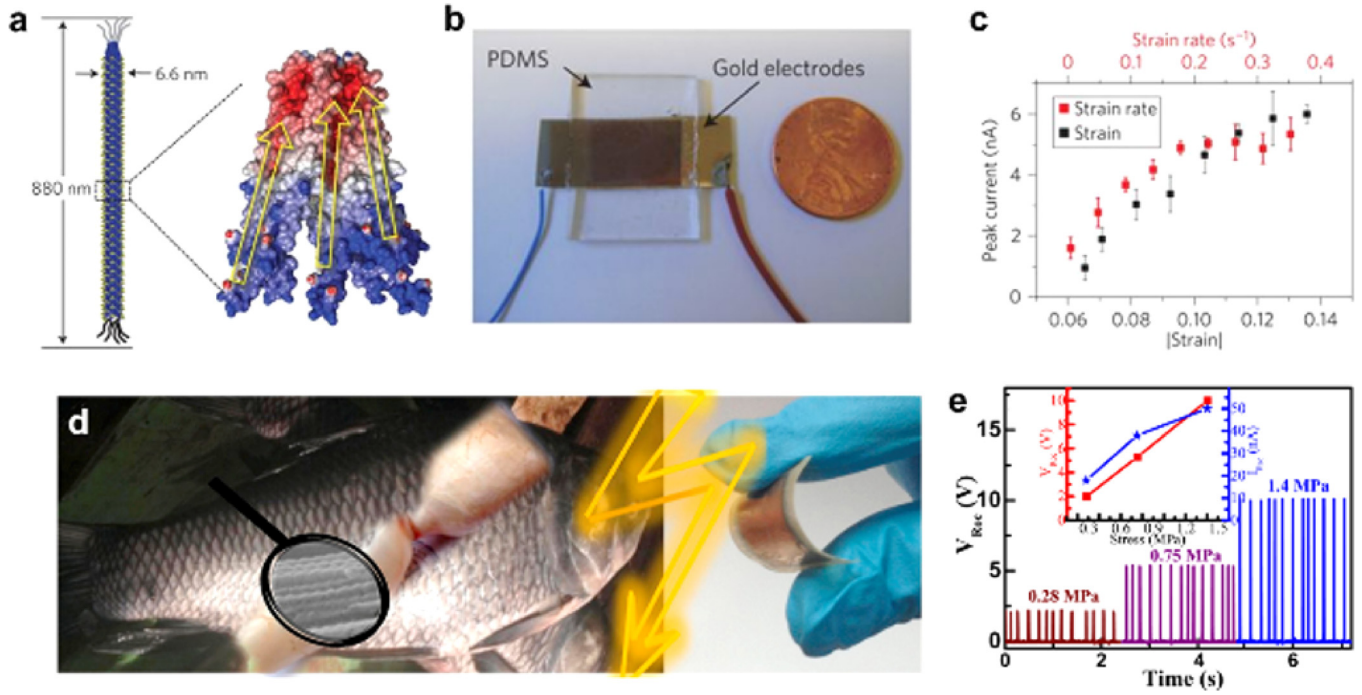

FIG. 9. (a) The M13 bacteriophage is ~880 nm in length and ~6.6 nm in diameter, is covered by ~2700 pVIII coat proteins, and has five copies each of pIII (grey lines) and pIX (black lines) proteins at either end. The dipole moments generated by ten α-helical major coat proteins are directed from the N-terminus (blue) to the C-terminus (red). Yellow arrows indicate dipole direction.[116] (b) Photograph of a M13 bacteriophage-based generator.[116] (c) Dependence of M13 bacteriophage-based generator peak current amplitude on strain and strain rate.[116] Reprinted with permission from Lee *et al.*, Nat. Nanotechnol. **7**(6), 351–356 (2012). Copyright 2012 Springer Nature. (d) Photograph of a piezoelectric generator based on swim bladder of CatlaCatla fish.[117] (e) The rectified output voltages from the swim bladder-based generator by different stresses with stress dependent output voltages and currents in inset. Reprinted with permission from S. Ghosh and D. Mandal, Nano Energy **28**(8), 356–365 (2016). Copyright 2016 Elsevier.

TABLE I. Summary for piezoelectric materials in energy harvesting.

Materials	Structure	Piezoelectric coefficient	Typical performances	Reference
ZnO	Nanowires	d_{33} of ∼5 to 10 pC/N	Peak open-circuit voltage and short-circuit current reach a record high level of 58 V and 134 μA	75,78
MoS_2	2D nanosheet	d_{11} of ∼3 pm/V	A single monolayer flake strained by 0.53% generates a peak output of 0.015 V and 2×10^{-5} μA, corresponding to a power density of 2×10^{-4} mW/cm^{-2} and an energy conversion efficiency of 5.08%	82,87
WSe_2	2D nanosheet	d_{11} of ∼3.26 pm/V	Peak current and voltage of about 0.1 V and 1.2×10^{-3} μA	85
PMN-PZT/PT	Thin film	d_{33} of ∼1500 to 2000 pC/N	Peak power of 17.18 mW/cm^3 at the resonant frequency of 406.0 Hz	92,93
PZT	Thin film	d_{33} of ∼250 to 700 pC/N	Peak voltage of 200 V and peak current of 35 μA	94
Alkaline niobate (KNLN)	Film	d_{33} of ∼310 pC/N	Peak voltage and current up to 140 V and 8 μA	95
$BaTiO_3$	Thin film	d_{33} of ∼190 pC/N	Peak voltage of up to 1 V and peak power density of ∼7 mW/cm^3	78,118
AlN	Thin film	d_{33} of ∼5 pC/N	Peak power of 1.9×10^{-3} mW at an external acceleration of 1.6 m/s^2	119,120
PVDF	Fabric	d_{33} of ∼20 to 30 pC/N	Peak currents up to 0.04 μA and peak voltage about 1.5 V	78,103
Cellular PP	Film	d_{33} of ∼200 to 600 pC/N	Maximum peak power density of 5.28×10^{-3} mW/cm^2	106,107
PDMS piezoelectret	Film	d_{33} of ∼2000 to 3000 pC/N	Peak current up to 2 V under air pressure of 12.66 kPa	110
PET/EVA/PET piezoelectret	Film	d_{33} of ∼6300 pC/N	Peak power of ∼0.444 mW and worked steadily for ∼90 000 cycles	111
fluorinated ethylene propylene (FEP) parallel-tunnel piezoelectret	Film	g_{31} of 3.0 V m/N	Peak power of 0.05 mW for an acceleration of 9.81 m/s^2 and a seismic mass of 0.09 g	112
M13 bacteriophage	Film	d_{eff} of 7.8 pm/V	Producing up to 6×10^{-3} μA of current and 0.4 V of voltage	116
Fish swim bladder	Film	d_{33} of ∼22 pC/N	Open-circuit voltage of 10 V and short-circuit current of 0.051 μA under compressive normal stress (∼1.4 MPa) by human finger	117

section is intended to give a brief overview of fabrication techniques for piezoelectric energy harvesters with competitive performance and durability.

1. Micro-fabrication process

In order to fabricate high performance PEH devices, one of the key concerns is the deposition and patterning of piezoelectric materials with high crystalline quality and controlled morphology. Standard fabrication procedures of piezoelectric film deposition include magnetron sputtering, pulsed laser deposition (PLD), chemical vapor deposition (CVD), metal organic decomposition (MOD), and chemical solution deposition (CSD) including sol-gel deposition.[127] The most popular piezoelectric materials for energy harvesting prepared by micro-fabrication process including PZT, AlN, ZnO, PMN-PT, and lead-free $K_xNa_{1-x}NbO_3$ (KNN).

a. Piezoelectric thin film deposition. Polycrystalline PZT is the most popular piezoelectric material utilized for energy harvesting applications due to its high piezoelectric coefficient. For 31-mode energy harvesting applications, the choice of the bottom electrode will influence crystalline texture, quality, and properties of the piezoelectric PZT film and thus is of primary importance. PZT/Pt/Ti/SiO_2/Si is the most widely applied deposition sequence, where a homogeneous (111) texture of the platinum (Pt) is commonly used to obtain a homogeneous nucleation of the same perovskite orientation;[128] the titanium (Ti) is not only used as an adhesion layer but also plays an important role in the diffusion phenomena.[129] In terms of topologies, the unimorph micro-cantilever design in the 31-mode with an optional proof mass is by far the most employed structure, due to their simplicity and high responsiveness. The use of silicon on insulator (SOI) wafer or bare silicon (Si)[130–132] consisting of double polished device and handle layers[133–136] to fabricate PZT micro-cantilever has been illustrated. The micro-fabrication techniques mainly involve functional film preparation and patterning, bulk Si micromachining, and structure release. Figure 10(a) shows the process flow of a PZT micro-cantilever reported by Liu *et al.*[134] The process started from the multilayer deposition of Pt/Ti/PZT/Pt/Ti/SiO_2 on an SOI wafer. The top and bottom electrodes of Pt/Ti were deposited by DC magnetron sputtering. In between, a $Pb(Zr_{0.52},Ti_{0.48})O_3$ film of 2.5–μm-thick was deposited by the sol–gel method. Step 2 shows the etch of the top and bottom electrodes by Ar ions and the etch of the PZT thin film by a mixture of HF, HNO_3, and HCl. Next, a SiO_2 thin film was deposited by RF-magnetron sputtering as an insulation layer. In step 4, the bonding pads were formed by etching and patterning of contact holes with Pt. To pattern and release the micro-cantilever structure, the SiO_2 layer and Si device layer at the frontside surface were etched by RIE using gases of CHF_3 and SF_6, respectively, while the Si handle layer and buried oxide (BOX) layer at the backside were etched using the deep reactive ion etching (DRIE) process.

The 33-mode PEH has the advantage in exhibiting approximately two times higher piezoelectric coefficient than

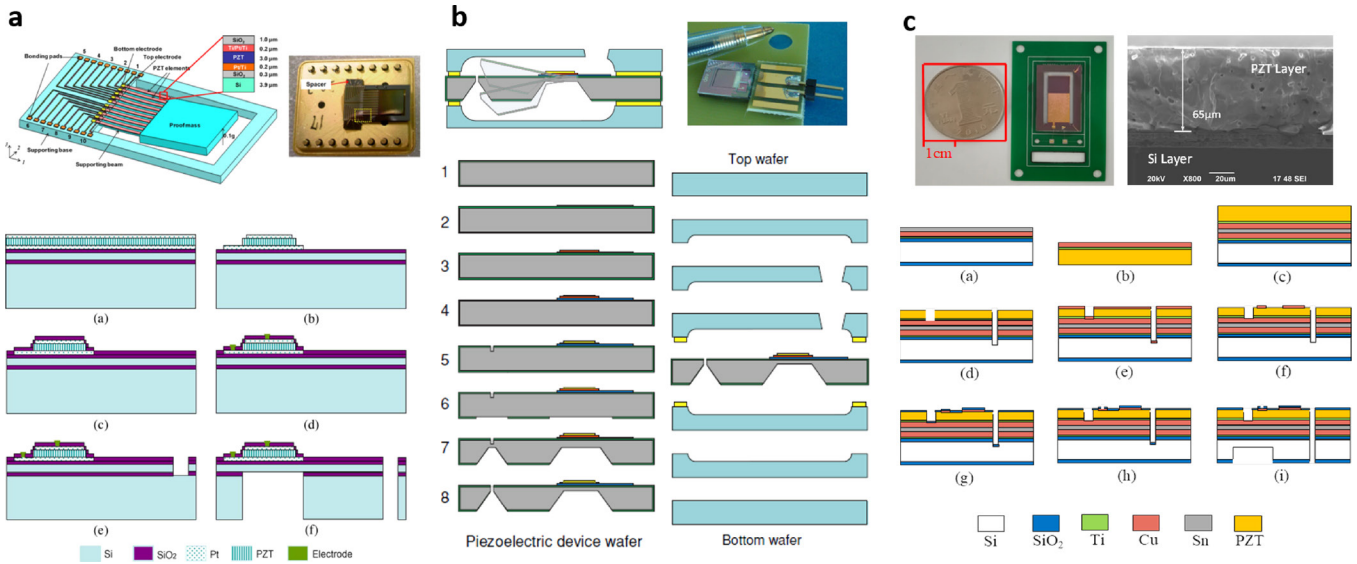

FIG. 10. The micro-fabrication process flow by using (a) piezoelectric thin film deposition of an PZT micro-cantilever reported by Liu *et al.*[134] Reprinted with permission from Liu *et al*., J. Micorelectromech. Syst. **20**(5), 1131–1142 (2011). Copyright 2011 IEEE. (b) CMOS compatible thin film deposition reported by IMEC/Holst Centre.[155] Reprinted with permission from Elfrink *et al*. J. Micromech. Microeng. **19**(9), 094005 (2009). Copyright 2009 IOP publishing. (c) Piezoelectric thick film preparation.

that in the 31-mode. Jeon *et al.*[137] have demonstrated the MEMS-based PZT energy harvesters with IDEs working in the 33-mode. The modeling, fabrication, and characterization of a similar 33-mode PZT micro-cantilever were reported by Park *et al.*[138] A $PbTiO_3$ seed layer has been applied as an interlayer between the ZrO_2 and $Pb(Zr_{0.52}Ti_{0.48})O_3$ thin film to improve the piezoelectric property. Lee *et al.*[45] have compared the output performance of the PZT micro-cantilevers in 31- and 33-modes by incorporating cantilever beam structures comprised of 5 μm aerosol deposited PZT thin films. Kim *et al.*[139] have designed a series of 33-mode PZT micro-cantilevers with the width of the IDEs ranging from 8 to 16 μm and finger spacing ranging from 4 to 16 μm. The PZT solution was synthesized and deposited by spin coating followed by a heat treatment. It is noted from the above study that a 33-mode device can be more favorable over a 31-mode device for application because higher voltage and power can be obtained with appropriate IDE designs.

The epitaxial PZT thin film grown on the Si or SOI wafer exhibits not only an excellent piezoelectric coefficient but also a low dielectric constant due to the high c-axis orientation. There have been a few reported micro-cantilever based energy harvesters based on epitaxial PZT thin films.[140–143] Reilly and Wright[140] first demonstrated the growth of the epitaxial PZT thin film with high quality by PLD for PEH. Morimoto *et al.*[141] have successfully deposited the epitaxial PZT film by RF magnetron sputtering on the substrate of (100) MgO single crystals with an epitaxial (001) Pt bottom electrode. The PZT film was later on transferred onto a stainless steel cantilever to enhance the output power efficiency and to improve the structural toughness. Isarakorn *et al.*[142] have magnetron sputtered $Pb(Zr_{0.2}Ti_{0.8})O_3$ layer on Si wafer through proper intermediate layers, including the $SrTiO_3$ (STO) buffer layer and $SrRuO_3$ (SRO) bottom electrode.

For medical implants and biomedical applications, a lead-free piezoelectric material is desirable due to the toxicity of Pb. Potassium sodium niobate ($K_xNa_{1-x}NbO_3$), or KNN, is considered to be a very promising lead-free piezoelectric material owing to its high Curie temperature and high ferroelectric orthorhombic—ferroelectric tetragonal transition temperature.[144] The lead-free KNN thin film deposition for MEMS-based PEH application was reported by RF magnetron sputtering[145] and CSD.[146]

b. CMOS compatible thin film deposition. The CMOS compatible alternatives of PZT include ZnO and AlN, which can be deposited by sputtering at relatively low temperatures.[147–149] Although both materials have similar piezoelectric coefficients, AlN has a higher resistivity and higher power generation figure of merit (FOM) due to the lower dielectric constant. A power generation FOM is defined as $d_{31}{}^2/\varepsilon_r$, where d_{31} is the piezoelectric constant and ε_r is the relative dielectric constant.[150] In addition, AlN is more compatible with Si technology and therefore is more widely used in micro-fabrication. For AlN based energy harvesting with the 31-mode configuration, the piezoelectric AlN thin film is sandwiched between two conductive metal layers with an elastic substrate layer.[151] Normally, Si is a well-known choice of elastic substrate for micro-fabrication. The choice of the electrode layer can directly influence the crystal texture of AlN, thereby affecting its piezoelectric properties. The most commonly used electrode materials are (111) textured metals having a face-centered cubic structure like Al, Pt, and Au; (110) oriented metals having a body-centered cubic structure like Mo and W; and (002) preferred oriented metals with a hexagonal structure like Ti.[152] Lee *et al.*[153] have deposited AlN films by the reactive RF sputtering method on various metal substrates including Al, Cu, Ti, and Mo, to form an Al (top)/AlN/metal (bottom)/Si configuration. It is evident that the AlN film deposited on the Mo electrode reveals a relatively dense and well-textured columnar structure with fairly uniform grains. Another potentially

CMOS compatible piezoelectric material class is the piezoelectric polymers, such as PVDF and its copolymer polyvinylidene fluoride-trifluoroethylene (PVDF-TrFE).[154]

A standard micromachining process flow for 31-mode AlN based energy harvesting cantilever demonstrated by the research group from IMEC/Holst Centre[155–157] is schematically shown in Fig. 10(b). It starts from the deposition of SiO_2 and Si_3N_4 isolation layers on a Si wafer (step 1), followed by the deposition and patterning of a Pt bottom electrode with a Ta adhesion layer (step 2). Then, an AlN film is deposited by reactive sputtering and patterning (step 3). The AlN layer typically contains a thin amorphous layer at the AlN-Pt interface and a columnar structure on top. Step 4 is the deposition and patterning of an Al top electrode to form the AlN capacitor stack. On the frontside of the wafer, a deep trench is etched to pattern the microcantilever in step 5. Then, the SiO_2/Si_3N_4 is patterned as hardmask for KOH etching on the backside of the wafer (step 6). A KOH etching is conducted to shape the proof mass of the microcantilever and is stopped before the complete release process (step 7). The complete release is done either with dry etching or wet etching with a tetramethylammonium hydroxide (TMAH) solution due to the bad etch selectivity of KOH toward Al and AlN (step 8). The harvester is finally packaged in-between two glass substrates with 400 μm deep cavities to allow enough space for the mass displacement. Besides the use of bare Si wafer, SOI wafers are also good choice for AlN based micro-fabrication.[158]

c. Piezoelectric thick film preparation. Generally, piezoelectric thick films with high piezoelectric coefficients are beneficial to improve the performance output. However, it is difficult to obtain high quality thick films on Si using conventional deposition methods, such as sputtering, CVD, PLD, or CSD. PZT thick films of more than 10 μm can be prepared using screen-printing methods.[159–162] Unfortunately, the formed thick films are not well crystallized because of the low sintering temperature. The piezoelectricity and dielectric constant are poor compared with that of bulk ceramics. For example, bulk PZT ceramics sintered at higher than 1200 °C will result in excellent piezoelectricity. Most energy harvesters with bulk PZT have relatively high power generation capabilities but at the cost of large dimensions.[163,164] Recently, useful techniques for preparing bulk PZT thick films are investigated,[165–172] based on the low temperature wafer bonding or chip bonding processes of bulk PZT and Si using an intermediate layer and then the thinning of PZT. As a result, the voltage and power output can be impressively improved. The power density of the harvester under 1 g can be as high as 70.6 mW/cm^3, at a resonant frequency of 523 Hz.[173] The basic fabrication processes for a cantilever beam structure with thinned PZT films are outlined in Fig. 10(c). First, the surfaces of bulk PZT and Si wafers are polished and bonded together at low temperature by an intermediate layer, such as epoxy resin, AuIn transient liquid phase, and polymeric adhesive WaferBOND CR-200. Following that, the bulk PZT wafer is thinned to a suitable thickness by wet-chemical etching, abrasive lapping or chemical mechanical polishing (CMP), and mechanical grinding. The thinned PZT wafer is micromachined into the desired pattern by the wet etching[174] or laser dicing[175] methods. Finally, the backside surface of the Si wafer is structured by wet or dry etching. It is well-known that oriented ferroelectric single crystals, such as PMN-PT and PZN-PT, show about 10 times larger piezoelectric coefficient than conventional PZT ceramics. It is quite promising to employ the bulk PMN-PT single crystal thick film process for improving the performance of current MEMS energy harvesters.[92]

Most of the above reported piezoelectric energy harvesters with thick films are based on the Si substrate, which can be easily broken and is limited with small vibration amplitudes. Lin *et al.*[176] successfully deposited a 15 μm high-quality PZT layer onto a stainless-steel substrate by using a modified aerosol deposition method. Later on, they developed a bimorph beam consisting of a stainless-steel substrate and double-side PZT layers, so as to improve the energy scavenging efficiency.[177] Tang *et al.*[178] have substituted the Si substrate of bulk PZT ceramics with phosphor bronze in the micro-fabrication process. On the basis, Yang's group reported a high performance bimorph piezoelectric MEMS harvester with the bulk PZT thick films on both sides of a flexible thin beryllium-bronze substrate via the bulk PZT bonding and thinning technologies.[179,180] The whole structure includes beryllium bronze as a supporting layer, upper and lower bulk PZT thick films as functional piezoelectric layers, and conductive epoxy as a low temperature bonding layer and a proof mass. The maximum effective power density reached 31.99 mW/cm^3 at 3.5 g and a resonant frequency of 77.2 Hz.

2. Grow-pattern-transfer process

To overcome the nature of brittleness and rigidity of bulk inorganic piezoelectric materials, flexible and conformal piezoelectric energy harvesters with preferable performance and durability are in demand. There are several feasible approaches to address this requirement, including the use of organic piezoelectric materials[181] as illustrated in Sec. III A, thin films growth on flexible substrates,[182,183] nanowires growth on flexible substrates[184] and "pattern-transfer" methods (i.e., first growing and/or patterning films on rigid substrates, and then transferring the patterns to plastic substrates).[185–188] The grow-transfer process is considered to be one of the most popular approach for the flexible piezoelectric energy harvesters. They can be achieved by transferring inherently high piezoelectric perovskite thin films from rigid substrates to flexible organic ones using the soft-lithographic technique, laser lift-off process, or solution-based sacrificial layer methods.

In Fig. 11(a), Lee's group[185,186] have presented the concept of the laser lift-off based grow-pattern-transfer process for the piezoelectric thin-film energy harvester. The PZT thin film was first deposited on a sapphire substrate by spin-casting a conventional sol-gel solution. After subsequent pyrolysis and calcination, the crystallised PZT thin film on the sapphire wafer was fixed to a flexible polyethylene terephthalate (PET) substrate by an ultraviolet (UV) light-enabled curing of polyurethane (PU) adhesive. Then, the PZT thin film was transferred from a sapphire wafer to a plastic substrate using an XeCl-pulsed excimer laser, which does not cause the degradation of piezoelectric properties.

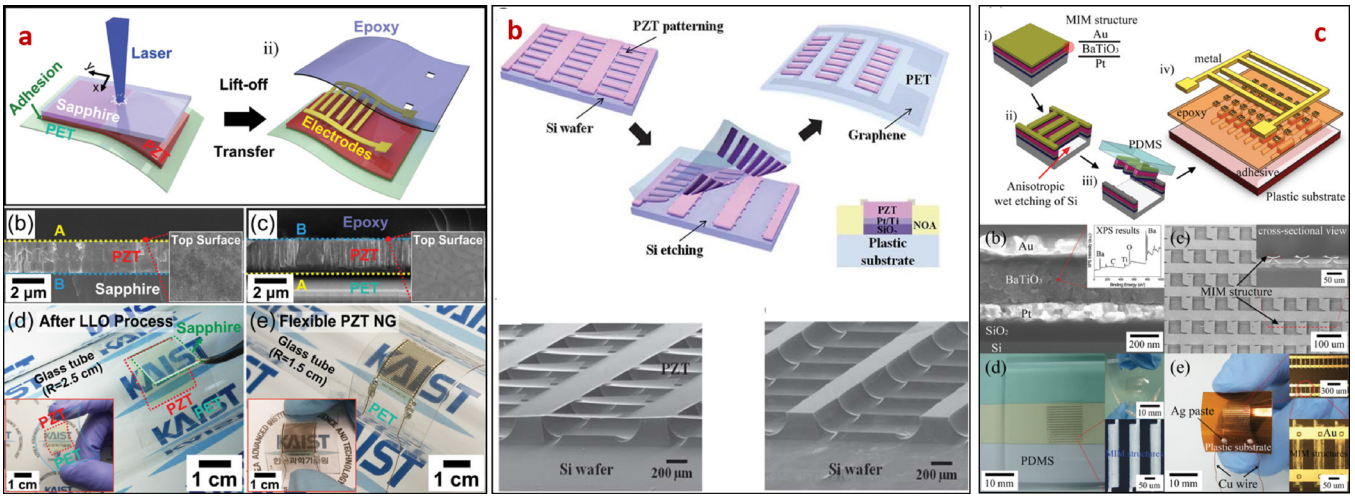

FIG. 11. Grow-pattern-transfer process: (a) Laser lift-off based grow-pattern-transfer process for the piezoelectric thin-film energy harvester.[186] Reprinted with permission from Park *et al.*, Adv. Mater. **26**(16), 2514–2520 (2014). Copyright 2014 John Wiley and Sons. (b) PZT ribbon-based nanogenerator by transfer process using solution-based sacrificial layer.[187] Reprinted with permission from Kwon *et al.*, Energy Environ. Sci. **5**(10), 8970–8975 (2012). Copyright 2012 Royal Society of Chemistry. (c) Piezoelectric $BaTiO_3$ thin film nanogenerator on plastic substrates by transfer process.[188] Reprinted with permission from Park *et al.*, Nano Lett. **10**(12), 4939–4943 (2010). Copyright 2010 American Chemical Society.

Kwon *et al.*[187] fabricated a high performance PZT ribbon-based nanogenerator with transparent graphene electrodes by a transfer process as shown in Fig. 11(b). A good quality PZT film was deposited on $Pt/Ti/SiO_2/Si$ wafer by the sol–gel method. After patterning the PZT ribbon structures, lateral etching of Si was carried out by a XeF_4 dry method. Then, the $PZT/Pt/Ti/SiO_2$ ribbons on the Si substrate were laminated by a PDMS stamp and detached on a graphene coated PET substrate by the Norland optical adhesive. Using a similar sacrificial layer method, the piezoelectric generation of perovskite $BaTiO_3$ thin films on a flexible substrate was fabricated by Park *et al.*[188] The ferroelectric $BaTiO_3$ thin films were deposited by radio frequency magnetron sputtering on a $Pt/Ti/SiO_2/(100)$ Si substrate and poled. The underneath Si layer of $BaTiO_3$ thin film ribbons were anisotropically wet-etched and successfully transferred onto a flexible substrate by PDMS stamp and then connected by IDEs [Fig. 11(c)].

3. Nano-fabrication process

The noticeable piezoelectric nanostructures, such as NWs, nanofibers, and nanobelts, by utilizing inorganic materials of PZT, PMN-PT, ZnO, $BaTiO_3$, and ferroelectric polymer of PVDF and its copolymer P(VDF-TrFE), have shown remarkable ability to harvest energy from small mechanical movements and gain higher energy conversion efficiency as compared to their micro- and macro-sized counterparts, which was attributed to size-effects, enhanced properties, and improved mechanical flexibility.[103,104,189–199] Various methods are used for the synthesis of nanostructures, such as CVD, physical vapor deposition (PVD), molecular beam epitaxy (MBE), PLD, hydrothermal and chemical synthesis, and electrospinning.

Among these, solution-based chemical synthesis methods are simple, low cost, compatible for flexible substrates, capable of large scaling up, and growth at relatively low temperatures and hence have attracted tremendous research interest. For instance, ZnO NWs can be easily grown via chemical synthesis at low temperature on any shaped substrate made of any material (crystalline or amorphous, hard or soft), such as silicon or polymers, at low cost.[196] The growth of vertically aligned ZnO NWs by the hydrothermal method usually consisted of two steps such as seed layer formation and growth of NWs on the seeds.[200] Wang *et al.* reported hydrothermal based chemical approach for the density controlled growth of aligned ZnO NWs arrays without using ZnO seeds or an external electrical field.[201] By adjusting the precursor concentration, the density of ZnO NWs arrays could be controlled within one order of magnitude (number of ZnO NWs per 100 μm^2). The laterally aligned ZnO NWs were realized by using different materials to activate or inhibit the growth.[202] Two materials are used: ZnO seeds for the growth, and Cr layer for preventing the local growth.

PVDF and its copolymer P(VDF-TrFE) nanofibers were used as the core candidate materials for wearable/implantable PEH because of the unique good properties in flexibility, stretchable, lightweight, biocompatibility, and availability in ultra-long lengths, various thicknesses, and shapes. They can be fabricated by the far-field and near-field electrospinning process via *in situ* mechanical stretching and electrical poling during fiber formation, which could transform some non-polar α-phase structures to polar β-phase structures for piezoelectricity.[203,204] Electrospun PVDF and P(VDF-TrFE) nanofibers are extensively utilized in energy conversion and wearable power generation.[102,103,205–209] Electrospinning can form nanofibers from solutions or melts and the diameters of fibers vary from tens of nanometers to micrometers. The typical setup for conventional far-field electrospinning is composed of four major components:[210,211] a syringe pump to obtain a constant flow rate of the polymer solution, a dispense needle connected to a high voltage supply as a cathode, a high voltage power supply unit, and a collector electrode which collects electrospun nanofibers (Fig. 12). When a high voltage is applied, a strong electrostatic field is excited between the needle tip and the collector electrode. The electrostatic force attracts the

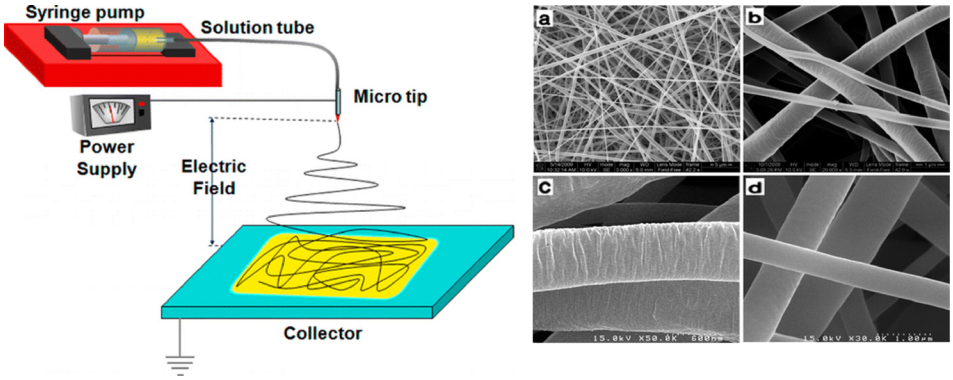

FIG. 12. Schematics of the electrospinning system and the SEM images of electrospun PVDF nanofiber morphology.[216] Reprinted with permission from Ahn *et al.*, J. Phys. Chem. C **117**(22), 11791–11799 (2013). Copyright 2013 American Chemical Society.

polymer melt out of the needle and is balanced by the surface tension force of the fluid. Figure 12 shows the scanning electron microscope (SEM) image of PVDF nanofiber fabricated using a far-field electrospinning process.

In order to improve the piezoelectric properties of PVDF fibers, a near-field (direct-writing) electrospinning technique[212,213] was developed to produce orientation controllable depositions of fibers of various materials. The same group has reported nanogenerators based on electrospun PVDF nanofibers with high energy conversion efficiency for potential wearable "smart clothes" to power hand-held electronics through body movements.[102] Some of the modified electrospinning techniques focus on the doping of different types of inorganic nanofillers [i.e., multi-walled carbon nanotubes (MWCNTs), ZnO, MoS_2, $BaTiO_3$, and $(Na,K)NbO_3$] to improve the β-phase content of PVDF fiber.[214–217]

IV. PERFORMANCE ENHANCEMENT TECHNOLOGIES

VEH devices exploit the ability of piezoelectric materials to generate an electric potential in response to mechanical stimuli and external vibrations.[218,219] However, the frequency range and the acceleration magnitudes of environmental vibration sources are normally below the operational mode of a PEH system. Furthermore, most reported vibration-based PEH devices exhibit low power generation as restricted by the input energy sources, their output performance, and operating bandwidth. Therefore, improving the performance and increasing the operating bandwidth become two significant and urgent research focuses in past years.[220–222] It is required advanced methodologies to maximize their performance and broaden the effective operating frequency region. The performance enhancement mechanisms especially for frequency bandwidth broadening and power amplification technologies can be classified into five mainstream: (1) multi-degree-of-freedom (multi-DOF) harvesting mechanism, (2) mono-stable, (3) bi-stable nonlinear mechanism, (4) frequency-up-conversion mechanism, and (5) hybrid harvesting mechanism. A summary and evaluation of the most significant approaches, exploited in the literature, based on the advantages and disadvantages are discussed below.

A. Multi-DOF harvesting mechanism

In order to address the aforementioned operation bandwidth limitation, a number of resonance adjustment methods have been investigated. For a simply supported cantilever beam configuration, the resonant frequency can be calculated by using the following equation:[223]

$$f_r = \frac{\upsilon_n^2}{2\pi}\frac{1}{L^2}\sqrt{\frac{EI}{mw}}, \tag{3}$$

where E is the Young's modulus; I is the moment of inertia; m is the mass per unit length of the cantilever beam; L *and* w are the length and width of the cantilever beam, respectively; and $\upsilon_n = 1.875$ is the eigenvalue for the fundamental vibration mode. For a cantilever with proof mass attached to the free end, Eq. (3) can be approximated into Eq. (4) as

$$f_r = \frac{\upsilon_n'^2}{2\pi}\frac{1}{L^2}\sqrt{\frac{K}{m_e + \Delta m}}, \tag{4}$$

where $\upsilon_n'^2 = \upsilon_n^2\sqrt{0.236/3}$; $m_e = 0.236mwL$ is the effective mass; Δm is the proof mass of the cantilever; and K is the effective spring constant of the cantilever. Based on the above equation, resonance adjustment can be considered to either effectively change the spring stiffness or the inertial mass of the system such that the resonant frequency can be tuned to match the frequency of ambient vibration. Zhu *et al.*[224] have presented a comprehensive review of the principles and operating strategies for frequency tuning approaches. However, most of these methods require extra system and energy for frequency tuning and respond to only one frequency at a time, which is inconvenient for practical applications. Alternatively, resonance adjustment can be realized by utilizing multiple vibration modes of a multi-DOF system in a single or multiple directions working together to broaden the effective operating range. Although ambient vibrations are ubiquitous, different vibration sources produce vibrations of different frequencies and amplitudes with various cyclic movements in different directions. A multi-DOF harvester is designed to scavenge energy from vibration sources with multiple frequency peaks along the same or different directions. A straightforward concept is to integrate an array of single-DOF oscillators with distinct resonant frequencies.[225–227] The power spectrum of the harvester array is a combination of each single harvester. Thus, the effective operating bandwidth can be thus essentially increased. The drawback of this approach is the inefficiency of device volume since at a particular vibration frequency, only a single or a few individual harvesters contribute to the power output. On the other hand, it is a good idea to use

multiple spring-mass elements in one structure for multi-DOF harvesters. In general, it can be classified into two main categories, i.e., multi-frequency and multi-directional harvesters.

1. Multi-frequency harvesting mechanism

Unlike a non-linear wideband energy harvester that broadens the operating range of the first resonant mode in a continuous range, a multi-frequency energy harvester utilizes a specific spring-mass structure to achieve multiple resonant modes at discrete frequencies. Each vibration mode of the device matches with a particular frequency peak of ambient vibration source so as to achieve more efficient VEH overall. In practice, most of the reported multi-DOF PEH systems can be classified into two main configurations as shown in Fig. 13. In configuration I, the cascaded PEH contains multiple springs (k_1, k_2, … k_i) and proof masses (m_1, m_2, … m_i) connected in series with a free end or fixed-fixed end. The PEH transducers (f_1, f_2, … f_i) can be implemented at any of the spring-mass hierarchy. In configuration II, it contains multiple spring structures connected with a larger inertial mass m in parallel. To achieve various resonant modes, their variable parameters are constructions, geometries, and number of the spring-mass hierarchies. We will give some examples for each configuration in the following.

The cascaded PEH configuration I as shown in Fig. 13(a) normally consists of several spring-mass hierarchies connected in series. In the spring-mass hierarchy, each spring-mass element of a child stage is used as the adjustable mass of the previous parent stage, and multiple resonant modes can be formed by pure bending of every stage. The vibration amplitude can be significantly enlarged by series connected spring-mass hierarchy. Theoretical investigations of cascaded harvesters have proved that they are able to provide multiple close and effective peaks in output response and significantly enhanced the magnitude of power than a single-spring-mass configuration.[228–232] Experimental implementation of spring-mass elements connected in series has been realized by a number of groups[233–241] for wideband PEH performance. Vullers *et al.*[234] utilized a packaged MEMS piezoelectric cantilever attached at the tip of a metal beam to form a dual-spring-mass system. The generated power is significantly boosted of more than 51 times due to the large packaged mass and the secondary beam oscillator. Meanwhile, the bandwidth of the harvester is increased by the dual resonant peaks. Kim *et al.*[235] and Hu *et al.*[236] have proposed wideband and high-efficiency PEH prototypes based on a two-stage folded and three-stage folded cantilever, respectively. El-Hebeary *et al.*[237] have investigated multi-frequency VEH ranging from 8 to 19 Hz by employing a three-stage open delta-shaped plate as shown in Fig. 13(b). The plate structure with multiple magnets attached on it can be modeled as a three-stage spring-mass hierarchies.

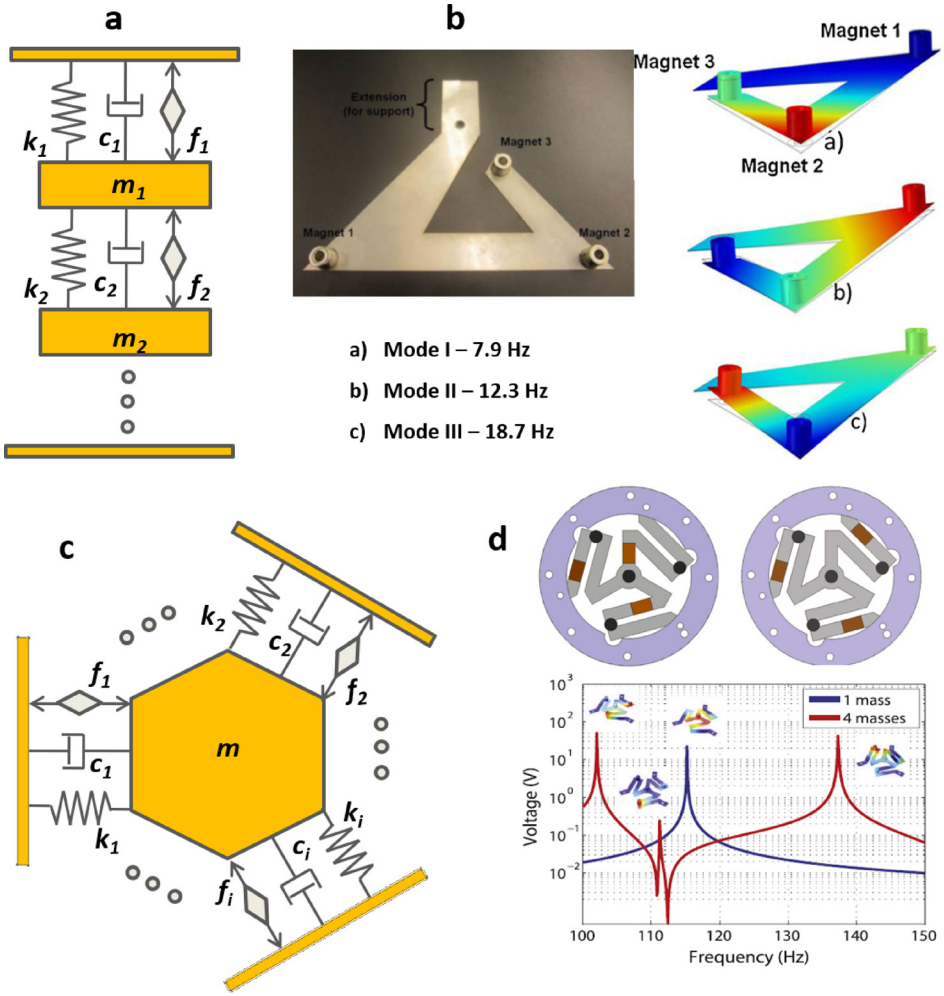

FIG. 13. Configurations of the multi-DOF spring-mass structures: (a) configuration I; (b) a three-stage open delta-shaped piezoelectric plate.[237] Reprinted with permission from El-Hebeary *et al.*, Sens. Actuators, A **193**, 35–47 (2013). Copyright 2013 Elsevier. (c) Configuration II; (d) wideband multi-mode PEH based on the compliant tri-spring structure.[244] Reprinted with permission from Appl. Phys. Lett. **106**(16), 163903 (2015). Copyright 2015 AIP Publishing LLC.

Toyabur *et al.*[238] proposed a primary spring bridge connected with four piezoelectric element in parallel, which can obtain four peak values in the range of 10–20 Hz. It is also an effective approach to use several piezoelectric beams series stacked to form a folded or L-shaped structure in 3D space.[239–241]

In PEH configuration II [Fig. 13(c)], the multiple springs are connected with a center or distributed inertial mass in parallel. The spring structures are normally designed in zigzag/meandering, spiral, and circular arc shape, so as to achieve compliant stiffness and multiple resonance modes. A significant performance improvement or bandwidth broadening with multiple resonant peaks can be observed. Berdy *et al.*[242] exploited a distributed mass in combination with two meandering piezoelectric bimorph structures to increase the fractional bandwidth to 19.9%, which is a 4 times increase compared with that of typical single mode devices. Rezaeisaray *et al.*[243] presented a multi-frequency AlN based MEMS PEH device by using two L-shape folded beams. The beam length is as long as the length of the proof mass, providing larger deflection in response to a given excitation. In Fig. 13(d), a wideband multi-mode PEH based on the compliant tri-spring structure and multiple masses with piezoelectric plates attached at three different locations is proposed by Dhote *et al.*[244,245] He and Jiang[246] proposed a complementary multiple low-frequency piezoelectric energy harvester which is mainly composed of three chiral folded beams in a light hexagonal matrix. A multi-modal four-leaf clover structure proposed by Iannacci *et al.*[247,248] is based on four petal-like double mass-spring systems through four straight beams anchored to the surrounding Si frame.

2. Multi-directional harvesting mechanism

Most of the above reported multi-frequency devices are focused on the energy harvesting from uni-directional vibration. This is a strong limitation because the vibration may come from various directions in practical applications. The two- and three-directional magnetically coupled PEH systems have been proposed[249–251] that enables scavenging energy from vibrations in orthogonal directions. In the system, each primary and auxiliary beam is designed to be sensitive to an orthogonal vibration direction. Chen *et al.*[252] proposed a dandelion-like multi-directional PEH structure, consisting of a number of piezoelectric cantilevers. Each cantilever is fixed on the multi-faceted support body in different directions, so that they were sensitive to vibration in different directions, respectively.

Besides the use of multiple cantilevers in different directions, multi-directional PEH systems can also be realized by specially designed spring-mass structures. Hung *et al.*[253] demonstrated a single-proof-mass at the center of a cross beam to convert either the x-axis or y-axis in-plane and z-axis out-of-plane ambient vibrations into piezoelectric voltage responses. There is an interesting cantilever-pendulum design for multi-directional PEH proposed by Xu and Tang.[254] The structure only consisted of a pendulum attached to the tip of a piezoelectric cantilever. This design took advantage of the nonlinear coupling between the pendulum motion in three dimensional space and the beam bending vibration at resonances. Both Yu *et al.*[255] and Zhang *et al.*[256] exploited the spiral cylindrical spring to extract the external vibration with arbitrary directions resulting in not only a three-dimensional response to external vibration but also a bandwidth broadening behavior. Then, they developed the impacting mass and rolling bead, respectively, to collide with the surrounding piezoelectric cantilevers so as to produce electrical outputs.

B. Mono-stable nonlinear PEH mechanism

In order to enhance the coupling between the excitation and harmonic oscillation to a wider range of frequencies, considerable research has been focused on exploiting the nonlinearity of the PEH system. Usually, the nonlinearity can be introduced from the large strain deflection of an oscillation system[257] or can be resulted from a nonlinear constitutive relationships of piezoelectricity.[258] However, these inherent nonlinearities have limited effects and cannot be easily controlled. The intentional introduction of nonlinearity in the design of PEH has received widespread attention.[222] The most common approach is to introduce nonlinear restoring force for the oscillation system using magnetic or mechanical forces.[259–262] The results have indicated that, by carefully introducing nonlinearity in the system, the operation bandwidth can be broadened and, hence, allow for more efficient energy transduction under the ambient random and non-stationary sources.

The governing equation of the relative displacement X(t) of an inertial mass m for an underdamped, single-DOF oscillator excited by base acceleration $\ddot{Z}(t)$ can be formulated by

$$m\ddot{X}(t) + c\dot{X}(t) + \frac{dU(\dot{X})}{dX} = -m\ddot{Z}(t), \tag{5}$$

where c is the viscous damping constant and the overdot denotes the differentiation with time. The potential energy function of the oscillator U(X), which is also known as the Duffing potential, may be expressed as

$$U(x) = \frac{1}{2}k_1(1-\gamma)X^2 + \frac{1}{4}k_3X^4, \tag{6}$$

where k_1 and k_3 are linear and nonlinear stiffness coefficients, respectively, while γ is introduced to permit variations in the linear stiffness around its nominal value. From Eq. (6), the restoring force-displacement relationship of a Duffing-type nonlinear spring is given by

$$F(x) = \frac{dU(X)}{dX} = k_1(1-\gamma)X + k_3X^3. \tag{7}$$

According to the tuning parameter γ and nonlinearity strength $\delta = k_1/k_3$ of the potential energy function, the energy harvesting system can be classified into three major categories as shown in Figs. 14(a) and 14(b). Case I ($\gamma < 1$, $\delta = 0$) represents a linear VEH system, where the restoring force is a linear function of the displacement. Case II ($\gamma < 1$, $\delta \neq 0$) represents the nonlinear mono-stable VEH

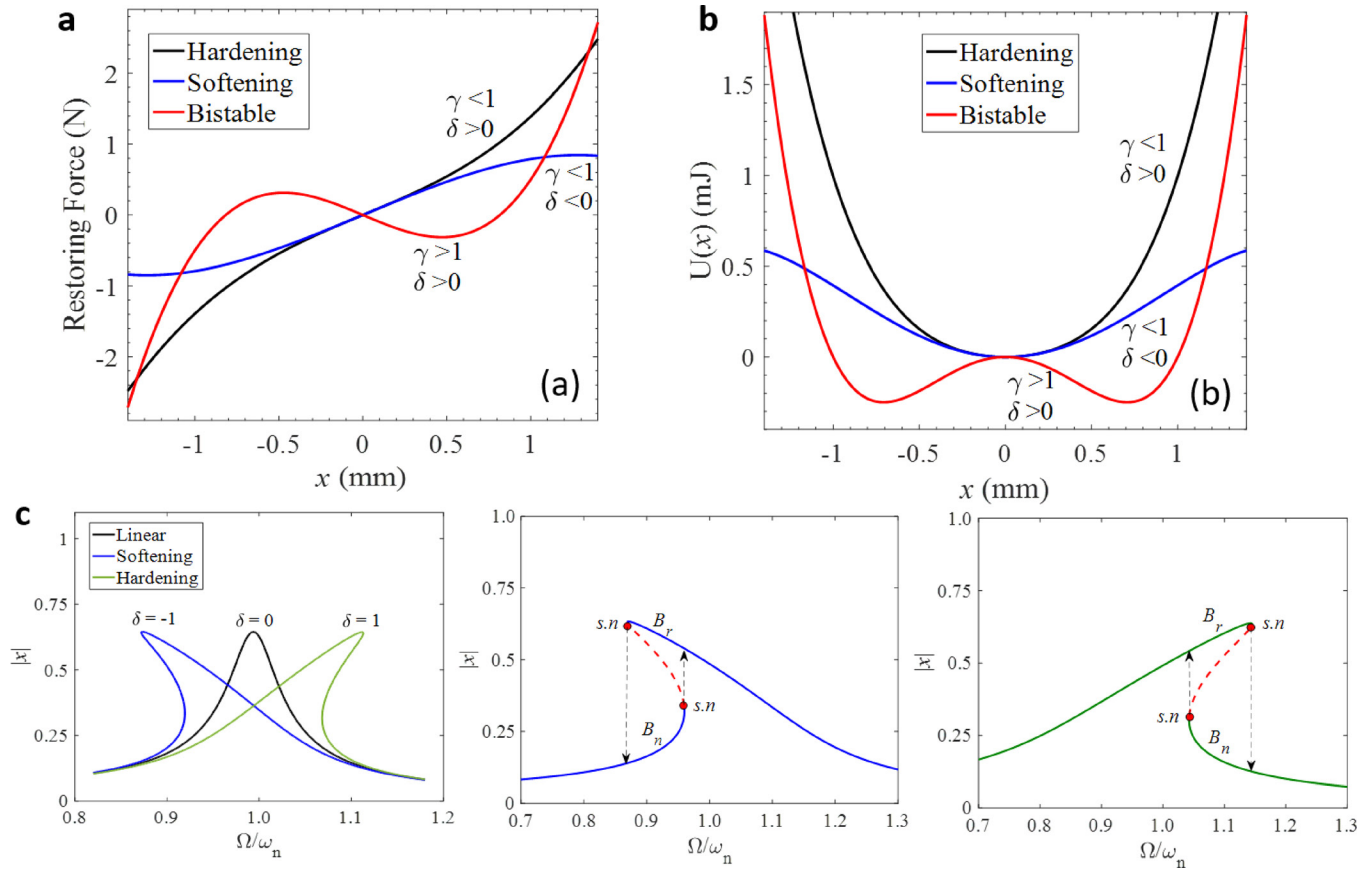

FIG. 14. (a) Restoring force and (b) energy potentials of different nonlinear vibratory energy harvesters; (c) frequency response of the particle in the mono-stable potential.

system. When $\delta > 0$, the restoring force increases with the displacement, which indicates a spring stiffness hardening condition. On the other hand, when $\delta < 0$, the restoring force decreases with the displacement and it indicates a spring stiffness softening condition. Case III ($\gamma > 1$, $\delta > 0$) represents the nonlinear bi-stable VEH system, where the potential energy function has two potential wells separated by a potential barrier.

In a mono-stable VEH system, the frequency response curves will bend to the right or to the left in the absence of the external excitation, indicating either a hardening nonlinearity ($\delta > 0$) or a softening nonlinearity ($\delta < 0$), as shown in Fig. 14(c). The nonlinear curve can be divided into three branches, namely, the upper resonant branch (B_r), the non-resonant branch (B_n), and the unstable branch (in dashed line). The stable branches collide with the unstable branch at two saddle nodes. It should be noted that the frequency response of the mono-stable PEH system depends on the direction of frequency sweep. For a hardening nonlinearity, as the excitation frequency sweeps up to the resonant frequency, the mass motion follows the upper resonant branch (B_r) up to the higher saddle-node bifurcation, where it drops to the nonresonant branch (B_n) and continues on the branch as the frequency increases further. When the process is reverse, the mass motion follows the nonresonant branch until the lower saddle-node bifurcation, where it jumps to the upper resonant branch. The mass motion will remain on the upper orbit branch as the frequency sweeps downward. For a softening nonlinearity, the response curve follows just the opposite trace. It is found that as long as the mass motion follows the upper orbit branch until the higher saddle-node bifurcation, the operation bandwidth can be increased greatly. The hardening and softening nonlinearity phenomena encourage researchers to exploit various mono-stable mechanisms for the bandwidth broadening of the PEH system. We reviewed recent advances in mono-stable PEH systems by introducing mechanical stress, stretching, preload, stopper and magnetic force, as illustrated in Fig. 15.

1. Mechanical stress or stretching induced nonlinearity

Usually, a hardening Duffing of the spring structure can be induced by a clamped-clamped beam or membrane that experiences mechanical stress or stretching at large deflections or displacements. This approach is very simple to be implemented within MEMS devices and requires no additional power source. Marzencki *et al.*[263] reported a MEMS PEH device by using a clamped–clamped beam with centrally located big seismic mass. The nonlinearity can be introduced by designing interlayer stresses in the clamped-clamped beam, where the high p+ doping of the top silicon layer introduces a tensile shear stress on the interface with the AlN piezoelectric thin film layer. Thus, the fabricated MEMS structure is highly prestressed and the frequency adaptability of over 36% is achieved at an input acceleration

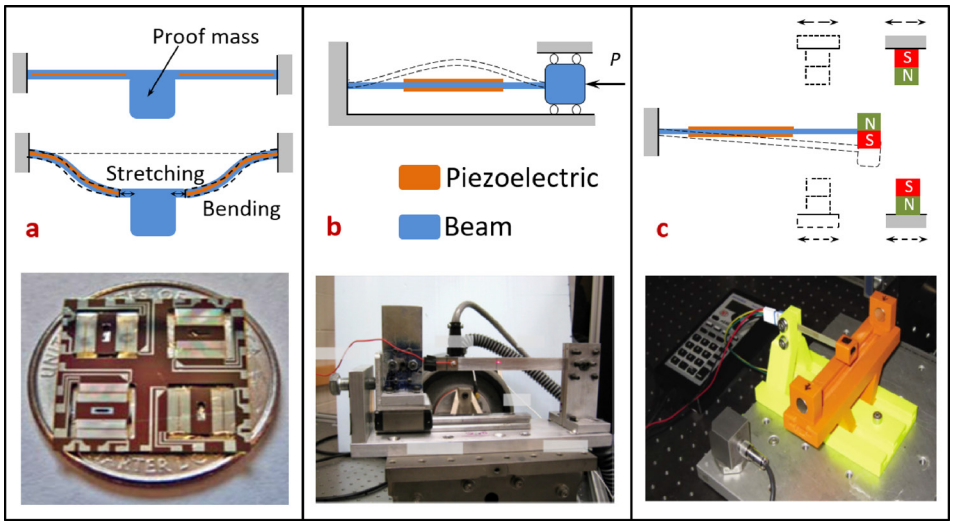

FIG. 15. Three common mono-stable PEH configuration by introducing (a) mechanical stretching.[264] Reprinted with permission from Appl. Phys. Lett. **99**(8), 083105 (2011). Copyright 2011 AIP Publishing LLC. (b) Mechanical preload.[268] Reprinted with permission from R. Masana and M. F. Daqaq, J. Sound Vib. **330**(24), 6036–6052 (2011). Copyright 2011 Elsevier. (c) Magnetic force.[275] Reprinted with permission from Appl. Phys. Lett. **95**(17), 174103 (2009). Copyright 2009 AIP Publishing LLC.

of 2 g. Hajati and Kim[264] have exploited an ultra-wide bandwidth MEMS PEH device by using a similar doubly clamped PZT beam with a center proof mass, as shown in Fig. 15(a). The nonlinear PEH device provided a power bandwidth exceeding 50% of the center frequency and 2 orders of power magnitude improvement. The hardening nonlinearity induced by large deflections of four fixed-fixed piezoelectric beams with inertial proof mass has also been demonstrated by Huang *et al.*[265] and Marinkovic and Koser,[266,267] which were shown to have a wide steady state response bandwidth.

2. Mechanical preload induced nonlinearity

The hardening Duffing of the PEH device can also be produced by a clamped-clamped beam axially loaded at one end. It is demonstrated that the axial load enhances the energy transfer efficiency, amplifies the effect of the external excitation on the structure, and enhances the effective nonlinearity of the device. These factors combined can increase the steady-state response amplitude, output power, and bandwidth of the harvester. In Fig. 15(b), Masana and Daqaq[268,269] have investigated the nonlinear behavior of the axially loaded piezoelectric beam subjected to harmonic base excitations. The harvester operated in the mono-stable (pre-buckling) and bi-stable (post-bucking) configurations, respectively, as the axial load is below and above the critical bucking force.

3. Magnetic stopper induced nonlinearity

In addition to the mono-stable piezoelectric energy harvesters with continuous nonlinear restoring forces, researchers also investigated another type of piecewise-linear hardening restoring effect, which can be physically realized by means of adding mechanical stoppers to conventional linear energy harvesters. Such nonlinear mechanism is most adequate for meso-scale and micro-scale PEH due to the simple configuration. A piecewise-linear model with two-sided mechanical stoppers contains a primary linear suspension system and two secondary suspension systems, where the spring stiffness jumps as the contact between the cantilever and stopper takes place. Some researchers[270–273] have investigated a one-side stopper arrangement for bandwidth enhancement in meso-scale PEH and Liu *et al.*[134,135] successfully realized the wideband response of PEH in micro-scale by using the one-sided packing stopper. Liu *et al.* also employed the MEMS devices and investigated the restoring effect of the one-sided and two-sided models.[274] The operation bandwidth of such piecewise-linear model depends on the inherent stiffness characteristics of the harvester, the level of excitation, and/or the presence of nonlinear restoring force components.

4. Magnetic force induced nonlinearity

By carefully incorporating with nonlinear magnetic restoring force, both the hardening and softening Duffing behavior can be invoked in a PEH system. Figure 15(c) shows the typically configuration which contains a PEH cantilever and a tip oscillating magnet interacting with the two oppositely poled stationary magnets. Stanton *et al.*[275] and Sebald *et al.*[276] showed that the effective nonlinearity of the system can be changed by altering the distance between the stationary magnets and the oscillating magnet. In particular, a hardening hysteresis response occurs when the stationary magnets are set behind the tip magnet, while the softening response results otherwise. Tang and Yang[277] established lumped parameter models for the conventional linear PEH, the nonlinear PEH with a fixed magnet, and the nonlinear PEH with a magnetic oscillator. In the experiment, nearly 100% increase in the operating bandwidth and 41% increase in the magnitude of the power output are achieved at an excitation level of 2 m/s^2 for the nonlinear PEH interacted with an oscillating magnet. Fan *et al.*[278] proposed a mono-stale PEH device by introducing symmetric magnetic attraction to a piezoelectric cantilever and a pair of stoppers to confine the maximum deflection of the beam. Experimentally, a 54% increase in the operating bandwidth and a 253% increase in the magnitude of output power were achieved as compared to those of its linear counterpart.

C. Bi-stable nonlinear PEH mechanism

For a nonlinear bi-stable PEH system, the potential energy function has two potential wells separated by a

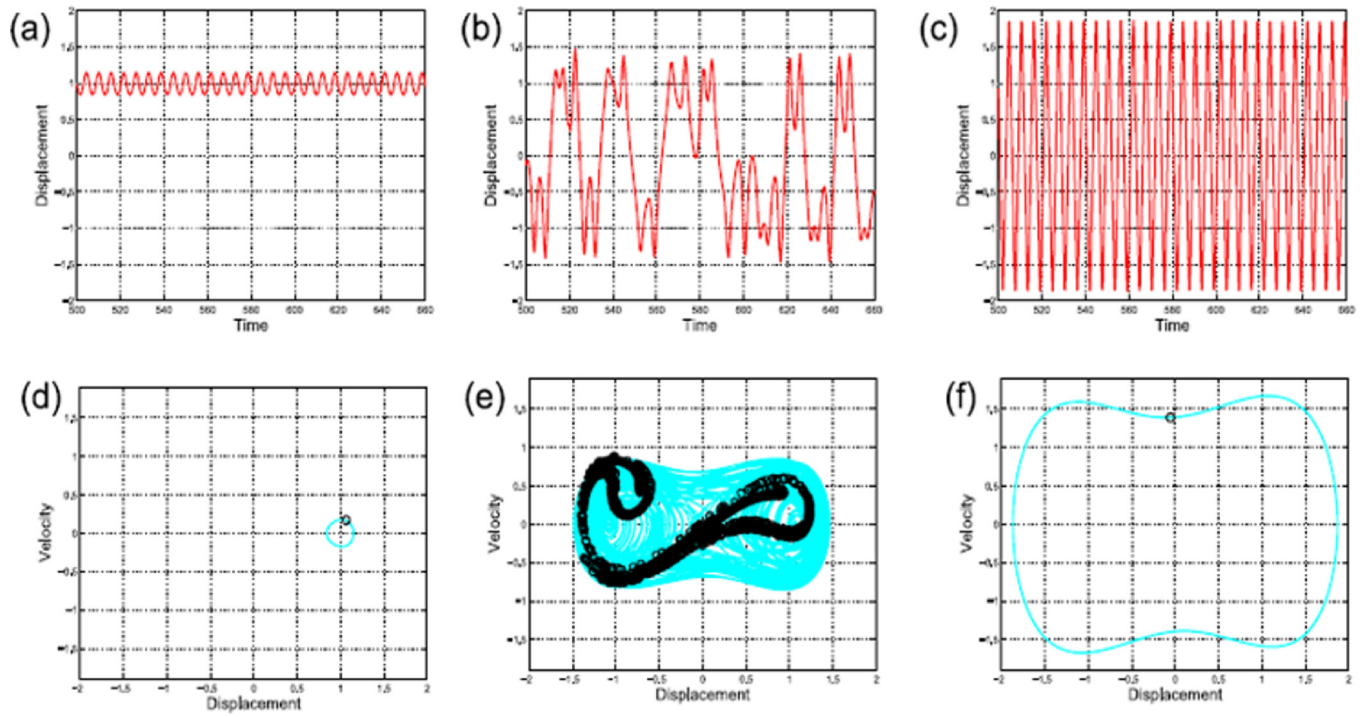

FIG. 16. Example displacement–time responses (top row) and phase plots with an overlap Poincare map as black circles (bottom row) for three dynamic regimes of bi-stable oscillators: (a) and (d) intrawell oscillations, (b) and (e) chaotic vibrations, and (c) and (f) interwell oscillations.[280] Reprinted with permission from Harne *et al*., Smart Mater. Struct. **22**(2), 023001 (2013). Copyright 2013 IOP publishing.

potential barrier, as depicted in Fig. 14(b). Depending on the input amplitude, the bi-stable system may exhibit three distinct trajectories, which are intrawell oscillation, chaotic interwell vibration, and interwell oscillation.[279,280] For a low input amplitude, the inertial mass of the bi-stable system experiences low-energy intrawell oscillation around one of the potential well. Figures 16(a) and 16(b) show the example displacement–time response trajectory and phase portrait with an overlay Poincare map. As the excitation amplitude grows to a critical value, the bi-stable oscillator exhibits aperiodic or chaotic vibrations between potential wells, as seen in Figs. 16(c) and 16(d). As the excitation amplitude is increased still further, the oscillator may experience a periodic interwell oscillation, as depicted in Figs. 16(e) and 16(f). The snap-through characteristics of the bi-stable system is considered as an effective means to dramatically improve the energy harvesting performance. Compared with the intrawell and chaotic vibration, snap-through oscillation displaces a much greater displacement and velocity of the inertial mass and high energy orbits, which is preferable for energy harvesting. In addition, the snap-through oscillation may be triggered regardless of the excitation frequency, and large operation bandwidth can be achieved in the system.

These benefits have attracted a rapidly growing research of literature on bi-stable energy harvesting, among which three common bi-stable PEH configurations are depicted in Fig. 17. In 2008, McInnes *et al.*[281] used the concept of stochastic resonance phenomenon[282] to enhance the harvested power by adding periodic forcing to a VEH mechanism. Thereafter, Cottone *et al.*[283] and Erturk *et al.*[284] proposed the first two bi-stable PEH configurations, both of which induced magnetoelastic buckling in a piezoelectrically laminated

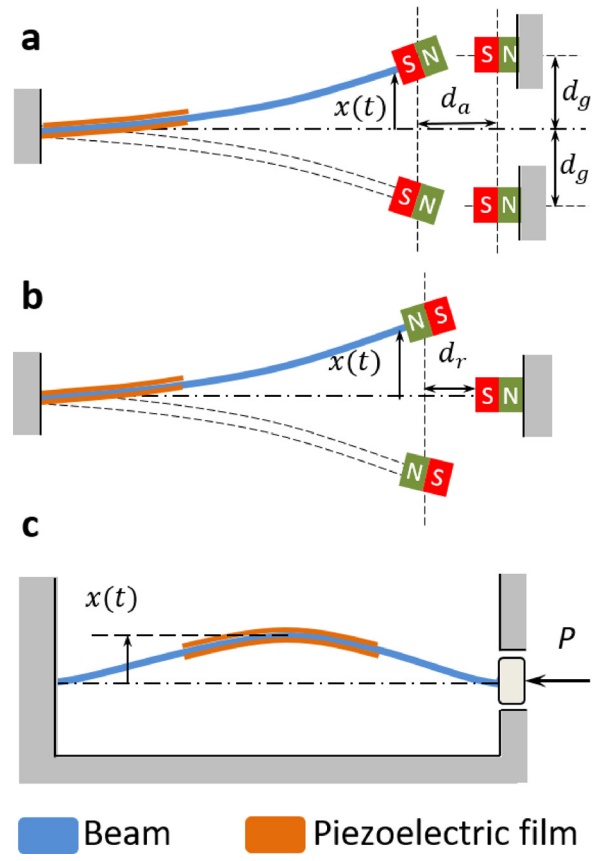

FIG. 17. Three common bi-stable PEH configurations by (a) magnetic attraction induced bi-stability; (b) magnetic repulsion induced bi-stability; and (c) mechanical load induced bi-stability.

beam by using different magnetic attraction and repulsion arrangements. Researchers have proposed other mechanical methods, including purely elastic buckling due to axial load,[268] pre-compressed spring,[285] and so on. The detailed analysis of the bi-stable VEH systems has been reviewed by Pellegrini *et al.*[286] and Harne and Wang.[280]

1. Magnetic attraction induced bi-stability

As shown in Fig. 17(a), the use of magnetic attraction to induce the bistability of a piezomagnetoelastic energy harvester was investigated by Erturk *et al.*[284,286] over a range of excitation frequencies. Zhao and Erturk[287] from the same group have numerically and experimentally studied the mono-stable and bi-stable configurations under the stochastic excitation. It reveals that a bi-stable PEH device can potentially be preferred only if it is carefully designed to operate in the neighborhood of a specific random excitation intensity. It is crucial to check the available noise intensity to justify the advantage of using a bi-stable configuration in harvesting random vibration energy, since there is a strong possibility of drastically reducing the power output due to bi-stability even with shallow potential wells.

The bi-stable PEH is preferable to high-energy interwell oscillations under the appropriate excitations. However, when the excitation level is low, the PEH cannot break through the constraint of potential wells resulting in low-energy intrawell oscillations. This fact provides motivation to study the magnetic coupled PEH with shallower potential wells, so as to accomplish the large amplitude motion and higher energy output for lower level excitations. Lan *et al.*[288] developed an improved bi-stable PEH mechanism by adding a small magnet at the middle of two fixed magnets. It is proved that the attractive force originated from the additional magnet can minimize the potential well and enable the device to realize snap-through easily even at fairly weak excitation. Cao *et al.*[289,290] have investigated a nonlinear PEH mechanism based on rotatable external magnets. The magnet inclination angle plays an important role in broadening the operating bandwidth and changing the dynamic characteristics from bi-stable to mono-stable Duffing oscillation. Based on a similar configuration with the magnet at a particular inclination angle, a tri-stable PEH system was theoretically and experimentally investigated by the same group.[291,292] In comparison to the bi-stable nonlinear PEH with a deeper potential well, the tri-stable one with three shallower potential wells can be easily excited to pass the potential well for generating high energy outputs over a wider range of frequencies. Wang *et al.*[293] have conducted the experiments and resistance optimization of a tri-stable PEH device from human motions excitation.

2. Magnetic repulsion induced bi-stability

There are numerous studies on bi-stable PEH using magnetic repulsion in the literature. Figure 17(b) shows a typical bi-stable configuration with two potential wells induced by repelling magnetic dipoles. Cottone *et al.*[283] and Gammaitoni *et al.*[294] provided experimentally validated models with electromechanical coupling considerations in the presence of exponentially correlated noise. While a detailed mathematical model was derived from energy principles in various studies.[295,296] Ferrari *et al.*[297,298] and Vocca *et al.*[299] used the bi-stable PEH design to white noise stochastic excitation and real measured environmental vibrations, respectively, both numerically and experimentally and found significant improvement in the voltage response. Tang *et al.*[300] also studied the bi-stable piezoelectric beam with magnetic repulsion. A considerable increase in broadband power could be harvested for an optimum magnetic repulsion gap. The voltage was approximately 50% greater than that of the linear harvester when the system was excited by low-pass filtered stochastic vibration. Ando *et al.*[301] have successfully fabricated and validated a true micro-scale bi-stable PEH device, which composed of a MEMS cantilever with a couple of permanent magnets, thus extending the advantages of bi-stable mechanism at the macroscopic scale towards the microscale regime.

In order to broaden the bandwidth of a bi-stable system further, Yang and Towfighian[302] presented an improved model that consists of a piezoelectric cantilever beam carrying a movable magnet facing an externally fixed magnet. Bi-stability is introduced by the magnetic repulsive interaction, while the movable magnet generates internal resonance. The combination of bi-stability and internal resonance effects could theoretically induce two times larger in the frequency bandwidth compared to that of a bi-stable model with fixed magnets. Recently, Zhou *et al.*[303,304] have developed a novel quad-stable PEH to overcome the defects of bi-stable PEH under weak stochastic excitation. The configuration is composed of a piezoelectric cantilever beam with a tip magnet and three externally fixed magnets. By adjusting the positions of the tip and fixed magnets, four stable equilibrium positions can be realized with shallower and wider potential wells, implying that it can execute jumping across the potential barrier easily. Experimental results showed that the bi-stable PEH could create larger deflection and generate higher output voltages than those of a bi-stable PEH nearly over the whole range of excitation intensity.

3. Mechanical load induced bi-stability

The bi-stability characteristic of a PEH system can be induced by mechanical design and loading, including methods inspired by biological structures.[305] As shown in Fig. 17(c), the bi-stable configuration of a clamped–clamped piezoelectric beam buckled by an adjustable axial load has been proposed and investigated thoroughly,[268,269,306–308] where the post-buckled beam snapped from one stable state to the other when excited by enough input acceleration. Results illustrated that, for a bi-stable PEH with shallow potential wells, super-harmonic resonances can activate the interwell dynamics even for a small acceleration, thereby producing large voltages. Ando *et al.*[309] described a millimeter-scale bi-stable PEH device in a snap-through-bucking configuration. Aiming to improve the functionality of a buckled beam, a midpoint proof mass and magnetic force[310] are utilized to enable snap-through motions under low-frequency and small amplitude excitations.

Alternatively, bi-stability can be induced by using an inverted clamped piezoelectric beam and a tip mass, demonstrated by Friswell *et al.*[311] The configuration has an advantage for extremely low-frequency vibration environments, while is not easily excited to interwell oscillation in experiments. The inertial tip mass was designed such that the beam was subjected to a near-critical buckling load to produce the most expected dynamics. Arrieta *et al.*[312] employed a carbon fiber epoxy bi-stable composite plate with seismic masses and piezoelectric patches attached. Unlike the bi-stable magnetoelastic cantilevers, the bi-stability of the plate does not require magnetic interaction. Large average power was achieved from limit cycle and chaotic oscillations for broadband responses with initially stable states. Betts *et al.*[313] have further investigated the dynamics of a similar bi-stable piezoelectric asymmetric composite energy harvester for broadband application. Van Blarigan *et al.*[314] reported a PEH device with two flexible ceramic piezoelectric elements arranged in a buckled configuration. Experimental results showed an enhanced harvesting of energy both for periodic and stochastic vibrations relative to a comparable cantilever design.

D. Frequency up-conversion (FUC) mechanism

It has been reported that the maximum power generation occurs at resonant frequency and power flow decreases with the decrease in resonant frequency. However, most ambient vibrations take place in low frequency range (typically 1 to 30 Hz). Harvesters with low resonant frequencies typically suffer from reduced electrical power generation.[315] In order to effectively manage the challenges of harvesting low-frequency environmental vibrations, the FUC mechanisms, up-converting low-frequency vibrations to high-frequency self-oscillations, have attracted great research interest and shown the highest efficiency to date. On the basis of the frequency broadening approaches using nonlinear mono-stable and bi-stable mechanisms, the FUC approaches produce more efficient power generation at low frequencies and simultaneously possess a wide operating bandwidth. Based on either contact or non-contact excitation strategies, the FUC mechanisms can be classified by mechanical impact, mechanical plucking, snap-through bulking, and magnetic force approaches.

1. Mechanical impact approach

The up-conversion approach for vibrational PEH was first demonstrated by Umeda *et al.*,[316,317] who investigated the power transformation by the falling impact of a steel ball on a piezoelectric membrane. Renaud *et al.*[318] and He *et al.*[319] demonstrated the up-converted piezoelectric generating beams driven by the non-resonant impact of a sliding or rolling mass in an open-ended guiding channel, which showed good performance for low-level, broadband, and low-frequency VEH. Halim and Park[320] introduced a flexible sidewall structure which response to the low-frequency consecutive impact of the rolling ball and transferred the deformation to the respective connected piezoelectric beam with high-frequency oscillation of 60 Hz.

Besides the mechanical impact by a non-resonant moving mass, researchers[321–325] have investigated various impact-driven FUC PEH configurations as shown in Fig. 18(a), which are realized by the periodic impact between the compliant driving beams and the piezoelectric beams, with improved power outputs at low frequencies and broadened operating bandwidth. Liu *et al.*[326] have successfully realized a MEMS-based FUC PEH device, by utilizing the periodic impact between an S-shaped low-frequency driving cantilever and a straight high-frequency PZT generating cantilever. The operating bandwidth is extended from 12 to 26 Hz and the power density of the device is significantly improved. Zhang *et al.*[327] reported a novel rope-driven FUC approach, in which the high-frequency generating beam is driven by an array of low-frequency driving beams using ropes. The mechanism takes the advantages of FUC and multimodal harvesting techniques, which not only produces high output power but also has the potential to achieve unlimitedly wide bandwidth with the increasing number of beams.

2. Mechanical plucking approach

Using the mechanical plucking approach, kinetic energy from the low frequency vibrations can be transferred to the high frequency piezoelectric harvesting structures. There are several plucking-based FUC designs proposed in the literature. Lee *et al.*[328] realized mechanical plucking between an atomic force microscope (AFM)-like piezoelectric harvesting beam and a set of superelastic ridges. Janphuang *et al.*[329] have used a similar up-conversion mechanism of an AFM-like MEMS piezoelectric cantilever plucked by the teeth of the rotating gear. The voltage generation of this configuration depends on the depth and spacing of a ridge or gear with the AFM-like cantilever. Pozzi *et al.*[330,331] implemented a FUC strategy to harvest energy from the rotation of a knee joint, by deflecting and releasing the piezoelectric cantilevers through a plectrum. Kuang and Zhu[332] studied similar plucking mechanism from a low-speed rotation motion. Because of the overlap between the piezoelectric bimorph and the plectrum, the bimorph was plucked consecutively, achieving FUC and high electrical energy output. Priya[333] harvested the wind energy to rotate a wheel with notches that pluck a series of piezoelectric windmill. Liu *et al.*[334] have demonstrated a MEMS-based piezoelectric energy harvester with FUC behavior, which is achieved by a scrape-though process using a low-frequency piezoelectric plucking cantilever of 36 Hz and a high-frequency PZT harvesting cantilever of 618 Hz assembled with a pre-determined gap and overlap [Fig. 18(b)]. Such approaches have the potential to offer the benefit of resonance, but with the difficulty of fine adjusting the overlapping distance. The aforementioned mechanical impact or plucking methods may cause increased risk of breakage and is harmful to long-term durability.

3. Snap-through buckling approach

When a clamped-clamped buckling beam is subjected to a low-frequency vibration above the threshold acceleration, it will snap through and activate the harvesting structure to resonate at high frequencies. The snap-through buckling phenomenon of a clamped-clamped beam is adapted to achieve

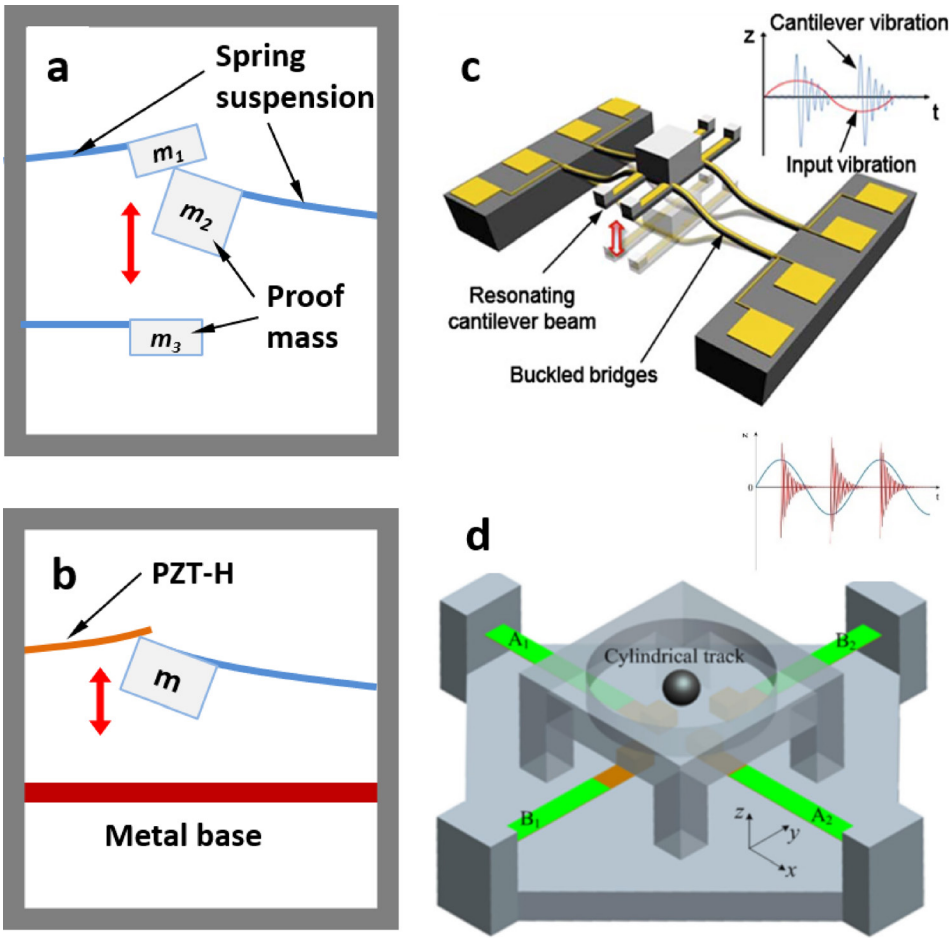

FIG. 18. Typical FUC mechanisms realized by (a) mechanical impact;[326] (b) mechanical plucking;[334] and (c) snap-through bulking.[335] Reprinted with permission from Appl. Phys. Lett. **96**(11), 111906 (2010). Copyright 2010 AIP Publishing LLC. (d) Magnetic force approaches.[343] Reprinted with permission from Fan *et al.*, Energy Convers. Manage. **96**, 430–439 (2015). Copyright 2015 Elsevier.

highly efficient energy harvesting even at ultra-low and wide off-resonance conditions.

Jung and Yun[335] have demonstrated a non-impact PEH without magnetic coupling using the snap-through action of a pre-buckled beam. The prototype illustrated in Fig. 18(c) consists of two pre-buckled slender bridges and four cantilever beams at the center of the bridges. The rapid transition between the two equilibrium states generates a highly accelerated impulse like excitation and thereby caused the attached cantilever beams to vibrate at their high resonant frequencies. In this work, the high threshold acceleration is required to induce snap-through, which restricted its application to very limited areas. Han and Yun[336] presented a modified bi-stable PEH concept with a compliant mechanism on the sidewalls. During the snap-through transition, the flexible sidewalls deflected outwards, thus lowering the threshold acceleration value for the bi-stable buckling. Ando *et al.*[337,338] have presented an impact-based PEH with the nonlinear snap-through buckling configuration. The two PEH cantilevers placed at the stable minima of the potential energy function were excited by the snap-through buckling beam.

4. Magnetic plucking approach

The mechanical impact or plucking method may cause increased risk of breakage thereby is detrimental to long-term durability. Nevertheless, the non-contact magnetic plucking has been widely utilized to overcome the aforementioned drawbacks.[339] Galchev *et al.*[340] have successfully fabricated a micro piezoelectric frequency-increased generator (FIG) system based on the magnetic attractive force. The driving FIG is comprised of a large inertial mass on a compliant suspension to couple kinetic energy from the ambient. As the inertial mass moves, it pulls and initiates high-frequency oscillation of the piezoelectric FIG spring, converting the stored mechanical energy into electrical energy. Tang and Li[341] developed a micro PEH device with a two-stage vibratory structure. The first stage picks up ambient low-frequency vibration and excites the second stage to vibrate at its resonant frequency, thereby realizing FUC by magnetic plucking force and improving power generation capability. Chung *et al.*[342] report a novel magnetic-force-configured three axial FUC piezoelectric energy harvester, so as to harness 3-D or three-axial mechanical energy by using one single mechanism.

The resonant-based driving oscillation structure of a FUC mechanism has wideband range but suffered from an uni-directional vibration sensitivity, while the naturally occurring vibration may come from various directions. Non-resonant structures have been proposed where a slower moving inertial mass magnetically plucks a piezoelectric cantilever beam which converts mechanical energy to electrical energy at a higher frequency. Fan *et al.*[343] reported a FUC beam-roller harvester to sense the low frequency sway and multi-directional vibration by a non-resonant cylindrical roller and a piezoelectric cantilever beam [Fig. 18(d)]. The

FUC is also achieved through this beam-roller configuration which converts the low-frequency sway and vibration to the higher-frequency vibration of the beam by magnetic attractive force. They also developed a nonlinear FUC PEH via introducing the magnetic plucking between a ferromagnetic ball and four piezoelectric cantilever beams. The introduction of the ferromagnetic ball enables the PEH to harvest energy from both the rotation motion and the sway motion.[344] To further harvest the rotational and sway motion, Pillatsch *et al.*[345,346] employed a non-resonant semi-circular rotor as the driving structure for irregular human motion application. The magnetic plucking induced FUC is in the form of piezoelectric beam plucking through magnetic coupling with a rotating rotor. Ramezanpour *et al.*[347] have investigated pendulum-based piezoelectric FUC energy harvester with a high number of magnets on the rotating proof mass. By applying an appropriate number of rotating magnets, the extracted power from FUC excitations can be enhanced. Fu and Yeatman[348] have analyzed the methodology for low-speed rotational energy harvesting using piezoelectric transduction and the magnetic plucking FUC approach. Xue and Roundy[349] have investigated several feasible magnet configurations to achieve a typical magnetic plucking implementation.

E. Hybrid energy harvesting mechanism

In order to develop compact and efficient PEH systems with high power density and provide enough power for real applications, the power amplification techniques have been evaluated in this section. These techniques include the above-mentioned FUC mechanism to amplify the power performance at low environmental frequencies, as well as the combination of the electromagnetic and triboelectric transduction mechanisms with PEH to improve the power density efficiently. Vibration-based energy harvesting devices employ one of the following energy transduction mechanisms: piezoelectric, electromagnetic, electrostatic, and triboelectric mechanisms. Normally, the energy exploited from the mechanical strain or relative displacement by a single transduction mechanism is not enough to meet the power requirement of the electronics. In order to overcome the drawbacks of each individual mechanism, the hybrid energy harvesting devices would be an option to deal with the low power generation issue.

1. Piezoelectric and electromagnetic hybrid mechanism

From a hybrid design perspective, the energy harvested from the electromagnetic mechanism must be greater than the decrease in the energy from the piezoelectric mechanism to result in a net increase in power output of the hybrid device. A comparative study of piezoelectric and electromagnetic energy harvesters for portable devices has been presented by Poulin *et al.*[350] As a guideline, piezoelectric energy harvesters usually produce high voltages and lower current. In contrast, electromagnetic energy harvesters tend to produce relatively low voltage but higher current because of the low internal impedance. Wacharasindhu and Kwon[351] proposed a hybrid VEH device to harness energy from typing motions on a computer keyboard by combining piezoelectric (using typing force) and electromagnetic (in terms of typing speed and frequency) mechanisms.

A typical hybrid VEH configuration integrated with piezoelectric and electromagnetic mechanisms is composed of a piezoelectric cantilever with the proof mass of a magnet on the tip and fixed coils beside [Fig. 19(a)].[352,353] Sang *et al.*[354] have studied four kinds of cantilever-based prototypes. A maximum power of 10.7 mW is generated at its resonant frequency, with an increase in 81.4% compared with 5.9 mW of single electromagnetic technique. In order to optimize the overall efficiency from the perspective of electrical damping, Wischke *et al.*[355] illustrated the design considerations and limitations that one must consider to enhance device performance through the coupling of multiple harvesting mechanisms within a single energy harvesting device. The drawback of clamped-free cantilever is the inclination between magnet and coil, which results in the partial straining of piezoelectric layer. The double-clamped suspension was proposed, in which the center displacement generates a bending stress as well as a longitudinal elongation stress. Li *et al.*[356,357] have investigated the double-clamped hybrid configuration under harmonic and random excitation theoretically and experimentally. Compared with piezoelectric-only and electromagnetic-only energy harvester, 3 dB bandwidth and output power of the hybrid device increase 67%, 25% and 38%, 118%, respectively.

To broaden the bandwidth, researchers also developed various nonlinear hybrid mechanisms with softening or stiffening Duffing behavior. For example, Li *et al.*[358,359] reported a nonlinear double-clamped hybrid configuration by incorporating two magnets inside the up and down coils. The center oscillating magnet of the piezoelectric beam will interact with the two oppositely poled stationary magnets such that the nonlinearity can be induced by the magnetic force. Lin *et al.*[360] integrated a piezoelectric cantilever with a basic nonlinear construction of suspension magnet and coil at the end tip. Fan *et al.*[361] employed two piezoelectric cantilevers at the end tube of the basic nonlinear construction. In both designs, the suspended nonlinear magnet not only induces the coil to generate electricity but also actuates the PEH to work, achieving the simultaneous energy extraction from one excitation through two conversion mechanisms.

2. Piezoelectric and triboelectric hybrid mechanism

In recent few years, triboelectric energy harvesting mechanism first proposed by Wang's group has gained signification attention for harvesting low frequency motion energy. To effectively harvest vibration energy from the environment, the hybrid energy harvesters based on piezoelectric and triboelectric mechanisms have been proposed. For example, Han *et al.*[362] employed the piezoelectric PVDF cantilever to vibrate and impact the PDMS film on the substrate, producing both piezoelectric and triboelectric output at the same time. Chen *et al.*[363] proposed a hybrid

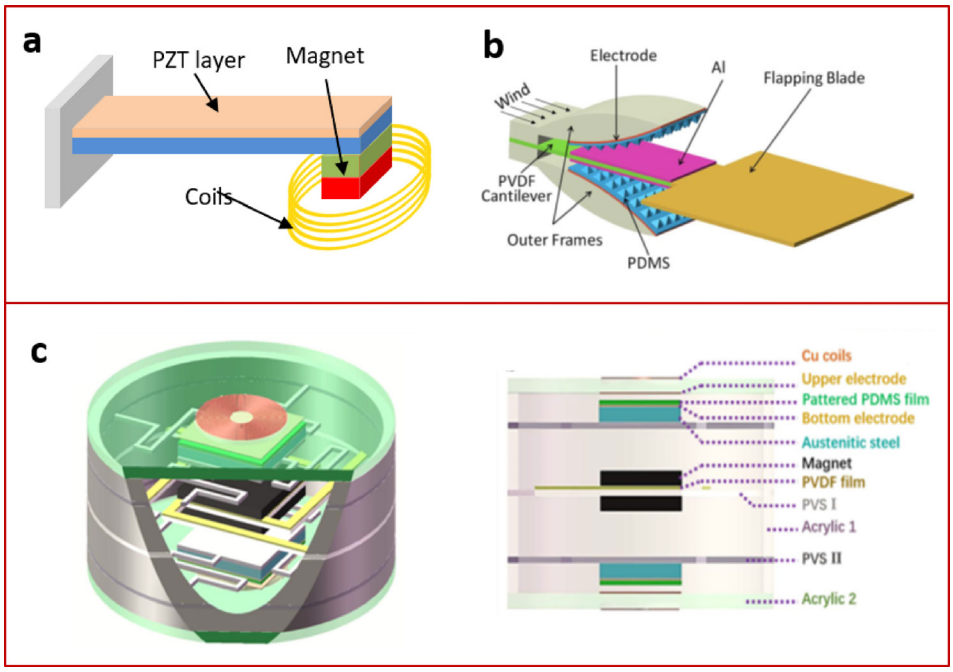

FIG. 19. (a) A typical hybrid VEH configuration integrated with piezoelectric and electromagnetic mechanisms. (b) A hybrid piezoelectric and triboelectric-based wind energy harvester.[363] Reprinted with permission from Chen *et al.*, J. Microelectromech. Syst. **25**(5), 845–847 (2016). Copyright 2016 IEEE. (c) A multilayered hybrid VEH device based on piezoelectric-electromagnetic-triboelectric mechanism.[364] Reprinted with permission from He *et al.*, Nano Energy **40**, 300–307 (2017). Copyright 2017 Elsevier.

piezoelectric and triboelectric-based wind energy harvester with high output performance based on the vortex shedding effect [Fig. 19(b)]. As wind flows through the device, the PVDF cantilever driven by the flapping blade deforms and the Al surface on the PVDF cantilever contacts with the upper and lower inner PDMS surfaces of the outer frames. Hence, piezoelectric and triboelectric-based voltage outputs can be generated simultaneously. He *et al.*[364] illustrated a multilayered hybrid VEH device based on piezoelectric-electromagnetic-triboelectric mechanism [Fig. 19(c)], which was designed to achieve broadband behavior at low acceleration and enhance the electric output. It mainly consists of three parts: the piezoelectric and electromagnetic hybrid VEH based on the four L-shaped spring-mass structure, and the upper and bottom triboelectric parts based on the four folded spring-mass vibration structure to achieve broadband behavior at low acceleration.

V. APPLICATIONS AND OUTLOOKS

Recent advances in energy harvesting have been intensified due to urgent needs of portable or wireless electronics and system with extensive life span for a wide potential applications. The PEH devices are intensively developed to capture environmental energy and support the sensor in a standalone module, or working along with the electronics to extend its lifetime. This section demonstrates some tentative experiments and applications for piezoelectric energy harvesters, which includes the energy harvesters from human activities for powering the implantable medical or wearable devices, harvesting the vibration energy from automobile and structures for self-powered wireless sensors, and health monitoring. Meanwhile, energy harvesting outlooks for other potential applications including wind flow, rainfall, ocean wave, roadway, and Internet of Things (IoTs) will be generally illustrated in this section.

A. Wearable and implantable energy harvesting

With the decrease in power consumption of both portable electronics and biomedical devices, it has become feasible by harvesting electrical energy to power these devices from the human activities, such as arm swings, walking, running, breathing, or keyboard typing as well as by extremely tiny biomechanical movements of muscles and organs inside the body (e.g., heartbeat, blood flow, eye blinking or muscle stretching, contraction/relaxation of the diaphragm and lungs, etc.).[365,366] A wearable energy harvesting system typically contains a harvester to convert human motion into electrical power, a power conditioning circuit to provide power rectification and regulation, and a storage element (e.g., a capacitor or a rechargeable battery) to store the harvested energy.[367] The harvested energy is used to extend the lifetime of batteries, thus enabling self-powered wireless sensors and systems.

González *et al.*[368] have presented an overview of various energy sources from human activities, such as continuous breathing, blood flow, and discontinuous walking and limb movement. Niu *et al.*[369] found that ankle, knee, hip, elbow, and shoulder motion can generate power up to 69.8, 49.5, 39.2, 2.1, and 2.2 W, respectively. A large amount of research in biomechanical energy harvesting of discontinuous human activities has been conducted. Shoe-inserted energy harvesters have been one of the earliest attractive research for biomechanical application because of their ability to convert everyday human activity into useful energy and their ease of implementation. Shenck and Paradiso[370] at the MIT Media Laboratory proposed a pioneer energy harvesting unit that constituted a shoe-mounted piezoelectric generator with a complete subsequent power conditioning circuit [Fig. 20(a)]. The circuit supports an active RF tag that transmits a short-range, 12-bit wireless identification (ID) code, while the wearer walks. Ishida *et al.*[371] developed a shoe insole pedometer as a first step toward the application

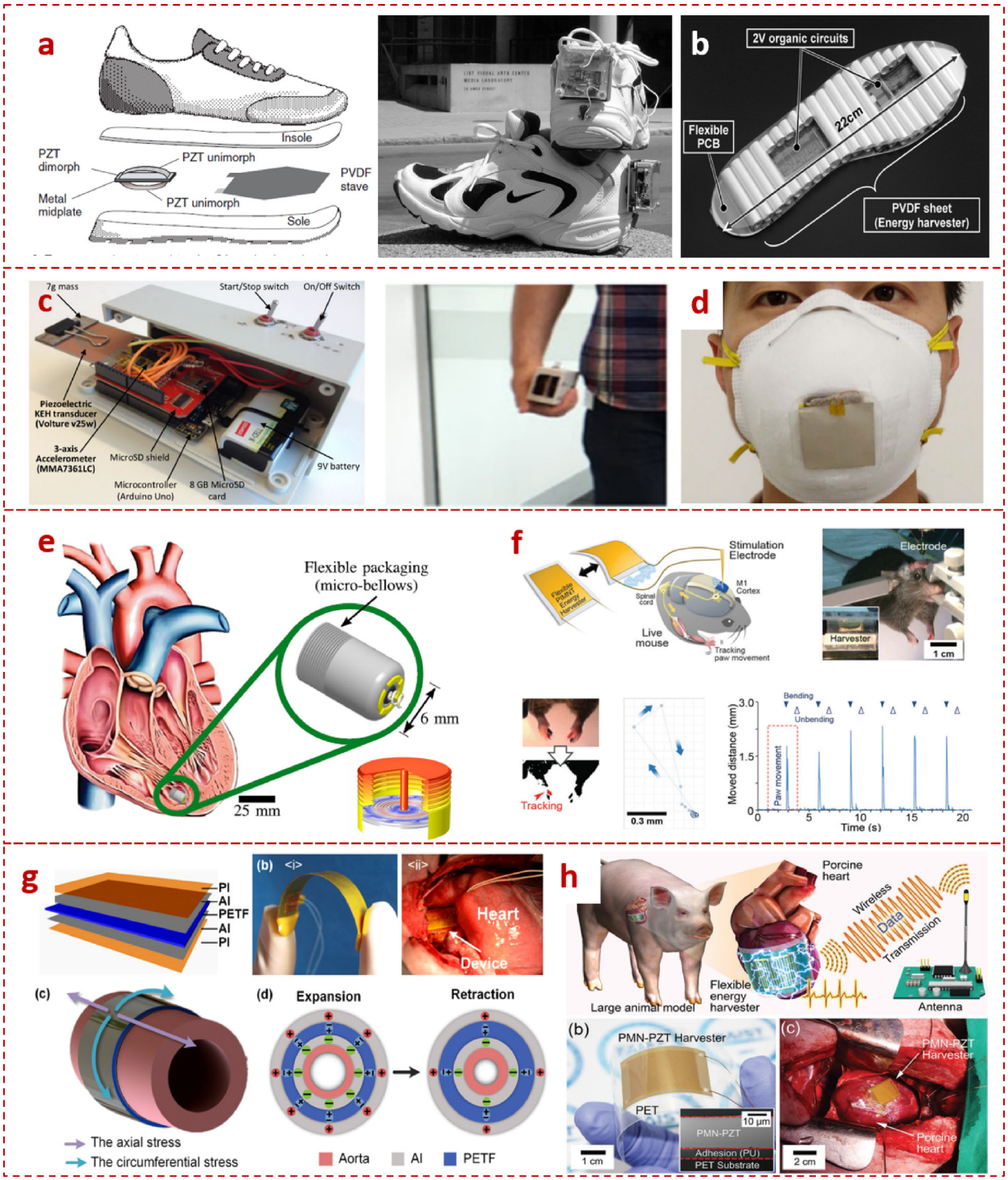

FIG. 20. (a) Piezoelectric-powered radio frequency identification (RFID) shoes with mounted electronics.[370] Figure 20(a) Reprinted with permission from Shenck and Paradiso, IEEE Micro **21**(3), 30–42 (2001). Copyright 2001 IEEE. (b) Photograph of the shoe insole pedometer using PVDF rolls.[371] Figure 20(b) Reprinted with permission from Ishida *et al.*, IEEE J. Solid-State Circuits **48**(1), 255–264 (2013). Copyright 2013 IEEE. (c) Human activity recognition from kinetic energy harvesting data logger.[367] Figure 20(c) Reprinted with permission from Khalifa *et al.*, IEEE Trans. Mobile Comput. **17**(6), 1353–1368 (2018). Copyright 2018 IEEE. (d) A wearable pyroelectric nanogenerator and self-powered breathing sensor.[380] Reprinted with permission from Xue *et al.*, Nano Energy **38**, 147–154 (2017). Copyright 2017 Elsevier. (e) Micro blood pressure energy harvester for intracardiac pacemaker.[398] Figure 20(e) Reprinted with permission from Deterre *et al.*, J. Microelectromech. Syst. **23**(3), 651–660 (2014). Copyright 2014 IEEE. (f) The real-time self-powered deep brain stimulation using the flexible PIMNT energy device.[399] Reprinted with permission from Hwang *et al.*, Energy Environ. Sci. **8**(9), 2677–2684 (2015). Copyright 2015 RSC Publishing. (g) Implantable and self-powered blood pressure monitoring based on a piezoelectric thin film.[391] Reprinted with permission from Cheng *et al.*, Nano Energy **22**, 453–460 (2016). Copyright 2016 Elsevier. (h) Self-Powered wireless transmission using biocompatible flexible energy harvesters.[401] Reprinted with permission from D. H. Kim and K. J. Lee, Adv. Funct. Mater. **27**(25), 1700341 (2017). Copyright 2017 John Wiley and Sons.

of flexible large-area energy harvesting, which consists of a 2 V organic pedometer circuit, a PVDF roll for pulse generation, and others for power generation [Fig. 20(b)]. A wearable insole made of a PVDF stave sandwiched by two wavy plates that not only can harvest energy from foot pressure during walking but also can serve as a self-powered human motion recognition sensor was reported.[372,373] A portion of these studies[345,346,374–378] focus on the development of PEH mechanisms to improve output performance from low frequency and irregular human motions. In light of this, Khalifa *et al.*[367] envision and propose a HARKE system which employs PEH both as a power generator and a sensor for human activity recognition [Fig. 20(c)]. The system infers human activity directly from the energy harvester patterns without using any accelerometer, saving 79% of the overall system power consumption. Sun *et al.*[379] demonstrated a PVDF microbelt for harvesting energy from human respiration. Xue *et al.*[380] designed and fabricated a wearable PEH by integrating the PVDF thin film in a N95 respirator for scavenging energy of human respiration as shown in Fig. 20(d).

On the other hand, recent advances focus on the self-powered flexible and stretchable energy harvesters from body movement, muscle contraction/relaxation, cardiac/lung motions, and blood circulation for biological pressure/strain sensing, or direct intervention of them for some special self-powered treatments.[381,382] These pliable energy harvesters used organic or inorganic piezoelectric materials on flexible or stretchable thin films such as polyethylene terephthalate (PET), polyimide (PI), and polydimethylsiloxane (PDMS) as illustrated in Sec. III. These functional devices can generate electric power under tiny irregular deformation and mechanical vibration revealing a tremendous potential to be applied in different medical devices. The most challenges and opportunities lie in the integration of fully bio-compatible self-powered energy harvesting systems for implantable biomedical devices *in vivo*, such as implanted pacemaker and defibrillators. Since traditional implanted batteries have limited lifetime, replacement of implanted batteries requires frequent, costly surgeries with increased risk of complications.[383–386] Considering the feasibility of bio-implantable applications, the concept of scavenging continuous organ or blood movement as self-powered implantable power supplies has the potential to reduce the patient's physical/psychological pain and financial burden. Triboelectric energy harvesters have recently been attempted to scavenging biomechanical energy,[387–390] but they have intrinsic limitations such as susceptibility to humidity, stability, and surface damage from friction. In contrast, PEH has attracted much attention as a self-powered energy source.[391–395] Platt *et al.*[396,397] have presented an implant of a self-powered knee replacement by embedding a sensor to provide *in vivo* diagnosis data via RF transmission. When subjected to 900 N standard force profile, the harvester is able to output 4.8 mW of continuous raw power, which is sufficient for providing power to a microprocessor and a sensor node. Deterre *et al.*[398] presented the design, fabrication, and tests of a micro spiral-shaped piezoelectric energy harvester and its associated microfabricated packaging that collects energy from ordinary blood pressure variations in the cardiac environment [Fig. 20(e)]. This device could become a life-lasting, miniaturized energy source for active implantable medical devices such as leadless pacemakers. Hwang *et al.*[399] demonstrated a self-powered deep brain stimulation via a flexible Pb(In1/2Nb1/2)O3–Pb(Mg1/3Nb2/3)O3–PbTiO3 (PIMNT) energy harvester for neural prosthetics and brain–computer interfacing [Fig. 20(f)]. Dagdeviren *et al.*[400] reported a conformal piezoelectric energy harvester that can yield significant electrical power from the natural contractile and relaxation motions of the heart, lung, and diaphragm, up to and exceeding levels relevant for practical use in implants. Kim and Lee[401] demonstrated the self-powered wireless data transmission enabled by harvesting *in vivo* biomechanical energy with a high-performance piezoelectric PMN-PZT energy harvester in a large animal model [Fig. 20(h)]. This successful self-powered wireless data transmission system shows the possibility of powerful application to health systems directly using biomechanical energy harvesting.

B. Self-powered wireless sensors and systems

With the relatively mature development of energy harvesting devices and power conditioning electronics, self-powered wireless sensors, and systems targeting ubiquitous, standalone and movable sensor networks have been investigated for intelligent monitoring applications. The sensor unit could contain a battery or not, as the incorporated energy harvesting module either provides continuous or intermittent electric power to prolong battery usage, or combines the function of sensing and harvesting by using a single unit. Elvin *et al.*[402] studied the possibility of combining functions of strain sensing and energy harvesting using a single piezoelectric PVDF device. The harvested energy enables the wireless transmission of the sensed data to a remote receiver. Roundy *et al.*[20] designed a small-sized piezoelectric cantilever that a total size of the bimorph and mass is approximately 1 cm^3. It is demonstrated to self-power a custom designed radio transceiver that consumes 12 mW when transmitting at a duty cycle of 1.6%. Arms *et al.*[403] presented a fully integrated wireless temperature and humidity sensor powered by a piezoelectric energy harvester unit from ambient vibrations [Fig. 21(a)]. Aktakka *et al.*[404] presented a self-powered MEMS energy harvester with its power management circuitry for autonomous charging of an energy reservoir. The proposed packaging of the harvester is of $<0.3\,cm^3$ [Fig. 21(b)]. Zhu *et al.*[405] reported a credit card sized self-powered smart sensor node consisting of a piezoelectric bimorph for energy harvesting, a power conditioning circuit, the sensors, and an RF transmitter [Fig. 21(c)]. The generated power is sufficient to enable periodic sensing and transmission. MicroGen Systems, Inc., has launched BOLT energy harvesting products[406] for industrial and building wireless sensor applications [Fig. 21(d)]. The Power Cells include piezoelectric MEMS AlN energy harvesters, electronics for rectification, impedance matching and voltage regulation, and a small capacitor for energy storage.

Self-powered energy harvesting devices have also attracted attention in automotive industry applications.

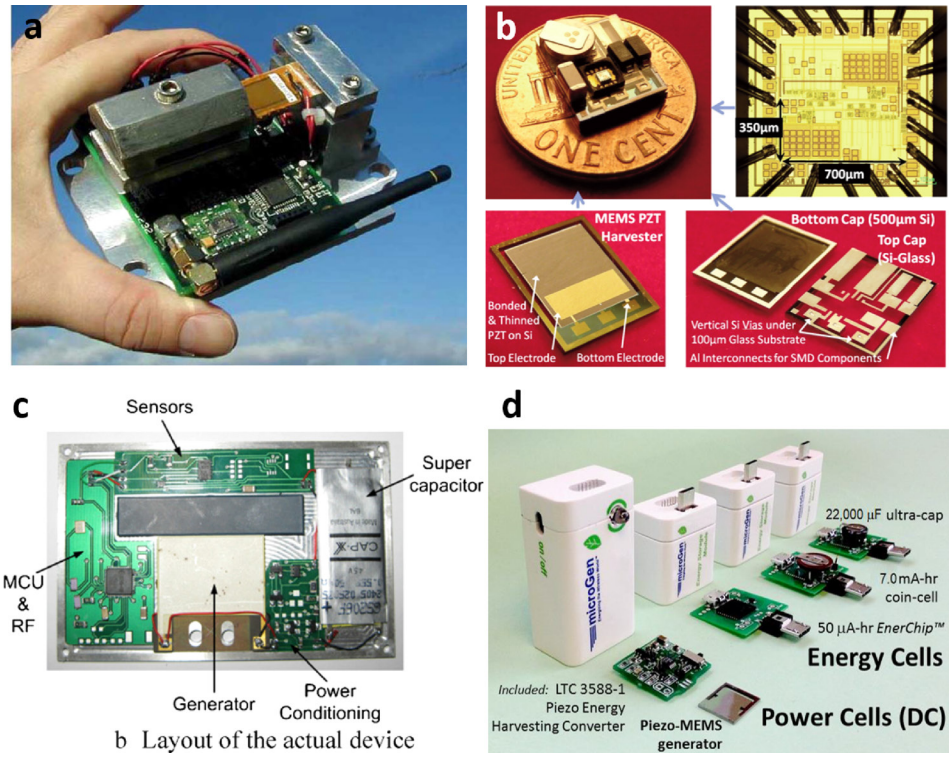

FIG. 21. (a) A wireless temperature and humidity wireless sensor by Arms *et al.*[403] Reprinted with permission from Arms *et al.*, Proc. SPIE **5763**, 267–275 (2005). Copyright 2005 SPIE. (b) The generator, with MEMS harvester, its packaging, placement of the chip and surface-mount device (SMD) components, and chip micrograph by Aktakka *et al.*[404] Figure 21(b) Reprinted with permission from Aktakka *et al.*, *Proceeding of the IEEE Conference on Industrial Automation and Control Emerging Technology Applications* (2011), Vol. 6, p. 409. Copyright 2011 IEEE. (c) A credit card sized self-powered smart tag by Zhu *et al.*[405] Reprinted with permission from Zhu *et al.*, Sens. Actuators, A **169**(2), 317–325 (2011). Copyright 2011 Elsevier. (d) Micro-power product for industrial & building wireless sensor applications by MicroGen Systems, Inc.[406] Reprinted with permission from MicroGen BOLT energy harvesting product (https://www.microgensystems.com/).

Because the rotating wheels can provide significant vibration energy, which may be a potential energy source for the intelligent tire with monitoring sensors. Due to the various road conditions and travel speed, the vibration frequency of a rotating wheel usually varies in the low frequency range (1–100 Hz).[407] The main challenges of a harvester mounted on or inside the tire are that it should accommodate broadband frequency range and high acceleration. In order to collect the vibration energy effectively at varied resonant frequencies, a wideband piezoelectric energy harvester using magnetic coupled FUC mechanism has been proposed.[408] A MEMS based piezoelectric energy harvester for Tire Pressure Monitoring System (TPMS) has been developed for noise and shock excitations.[409] The module measures accelerations up to 2000 g with a sample rate of 2 kHz. The data can be transmitted with a 2.4 GHz wireless link or stored in a 8 GB small memory card. Lee and Choi[410] presented a self-powered system for measuring the power directly from the tire, which supplies the wireless sensor system installed inside the tire. The piezoelectric composite with integrated electrodes and piezofibers has been utilized for scavenging vertical deformation from the car weight and inner liner deformation while driving. Zhang *et al.*[411,412] have utilized a piezoelectric bi-stable structure for rotational tyre-induced energy harvesting with the advantage that it can broaden the rotating frequency bandwidth and simultaneously stabilize high energy orbit oscillations. The maximum power generation can reach 0.24 mW with a mean power of 61 μW.

C. Future application outlooks

Throughout our surrounding environment, the applicable scenarios for PEH are not limited to the most reported mechanical vibrations and human motions and can be extended to wind flow, rainfall, ocean waves, roadway loading, and so on. Among the ambient available energy sources, wind energy is ubiquitous and abundant. The flowing power of wind is usually from a typical intensity of 0.1–0.3 kW/m^2 to 0.5 kW/m^2 on the earth surface along the wind direction. There are a considerable number of research studies focused on flow induced energy harvesting technology based on a piezoelectric transducer in the literature.[413–421] These harvesters can be used to power small electronic devices and deployed in many locations, such as urban areas, high wind areas, ventilation outlets, rivers and ocean, ducts of buildings, and lifting components in aircraft structures. Tropical climate countries have abundant annual rainfall. Hence, raindrop impact energy harvesting is a feasible form of alternative energy source for rainy outdoor environment.[422,423] Over recent years, there has been a handful of groups reported and studied the rainfall energy harvesters using piezoelectric materials by the impact of raindrops, but the potential has not been fully realized.[424–429]

The traffic-induced roadway loading can also be a potential clean and reliable energy source. In the United States, the total energy wasted annually by the motor vehicles on tires is estimated to be about 2.218×10^{16} kJ.[430] If 1/1000 of this energy can be captured, it will be enough to supply about 6 million houses in United States.[431] In recent years, a number of studies have begun to focus on harvesting energy from traffic-induced vibrations in transportation infrastructures. Generally, piezoelectric stacks or symbol structures are embedded into pavement to capture the deformation and vibration from the roadway loading of vehicles and convert them into electrical energy in transportation infrastructure.[432–440]

In addition, it is noted that there is a plenty of sustainable and clean ocean energy on the earth. The flowing power

of ocean waves is around 2–3 kW/m^2 under the ocean surface along the direction of the wave propagation.[68] In view of considerable large energy density from water flows and wave motions, energy harvesting has been pursued as an alternative or self-contained power source. An energy harvester using a piezoelectric polymer "eel" to convert the mechanical flow energy, available in oceans and rivers, to electric power was first presented by Taylor *et al.*[441] Later on, various types of piezoelectric energy harvesters and representative mathematical models are proposed and studied in the literatures.[442–446] However, to harness the ultra-low frequency and high amplitude ocean wave energy with high efficiency, the PEH development from ocean waves still faced with many challenges.

VI. SUMMARY AND CONCLUDING REMARKS

This paper gives an overall review of the recent research on piezoelectric energy harvesters. Various types of harvester configurations, piezoelectric materials, and fabrication techniques were discussed. Most of the PEH devices studied today have focused on scavenging vibration and strain energy from ambient sources due to their abundance in both natural and industrial environments. Aside from/In addition to the most studied cantilever beam structure, various compliant piezoelectric film structures and configurations, as well as piezoelectric stacks, are developed. The power output of a particular piezoelectric energy harvester depends upon many intrinsic and extrinsic factors, which leads to great variations in power output, ranging from nanowatts to milliwatts. The utilization of inorganic, organic, and bio piezoelectric materials has been explored by researchers using various fabrication techniques for specific requirements in a great range of harvesting applications. To date, the low output performance and narrow bandwidth are still the most challenging issues before their practical deployment. To enhance the output performance and broaden the working bandwidth, a large number of performance enhancement solutions in the field of vibration energy harvesting have been proposed by researchers. Many promising mechanisms have been proposed and some of them were verified to be quite efficient for hostile environment conditions.

On the whole, with the current rapid development of the Internet of Things (IoTs), energy harvesting offers significant advantages and opportunities to the development and application for smart cities, smart homes, smart health, smart agriculture, intelligent transportation, industry, security, marine, and so on. It is a critical and promising solution for creating an enhanced class of autonomous self-powered terminal nodes that can operate for much longer periods of time without the need of battery charges. It can also induce cost savings by significantly delaying battery replacement and the energy harvesting solutions can further increase the robustness in all IoTs applications.

ACKNOWLEDGMENTS

The authors acknowledge the financial support from the following research grants: National Natural Science Foundation of China Grant Nos. 51875377 and 41527901; Ministry of Education (MOE) Faculty Research Committee (FRC) Grant No. R-263–000-B56-112 at the National University of Singapore; NRF-CRP8-2011–01 Grant No. R-263–000-A27-281 by the National Research Foundation (NRF), Singapore; and HIFES Seed Funding-2017–01 Grant No. R-263–501-012–133.

[1]M. Z. Jacobson, M. A. Delucchi, Z. A. F. Bauer, S. C. Goodman, W. E. Chapman, and M. A. Cameron, Joule **1**(1), 108–121 (2017).
[2]T. W. Brown, T. Bischof-Niemz, K. Blok, C. Breyer, H. Lund, and B. V. Mathiesen, Renewable Sustainable Energy Rev. **92**, 834–847 (2018).
[3]J. A. Paradiso and T. Starner, IEEE Pervasive Comput. **4**(1), 18–27 (2005).
[4]P. D.Mitcheson, E. M. Yeatman, and G. K. Rao, Proc. IEEE **96**(9), 1457–1486 (2008).
[5]C. Wei and X. Jing, Renew. Sust. Energy Rev. **74**, 1–18 (2017).
[6]A. Dewan, S. U. Ay, M. N. Karim, and H. Beyenal, J. Power Sources **245**(1), 129–143 (2014).
[7]K. V. Selvan and M. S. Mohamed Ali, Renewable Sustainable Energy Rev. **54**, 1035–1047 (2016).
[8]See https://perpetuum.com/ for commercial energy harvester from Perpetuum Ltd.
[9]J. He, T. Wen, S. Qian, Z. Zhang, Z. Tian, J. Zhu, J. Mu, X. Hou, W. Geng, and J. Cho, Nano Energy **43**, 326–339 (2018).
[10]D. P. Arnold, IEEE Trans. Magn. **43**(11), 3940–3951 (2007).
[11]Y. Suzuki, IEEJ Trans. Electr. Electron. Eng. **6**(2), 101–111 (2011).
[12]H. Liu, K. H. Koh, and C. Lee, Appl. Phys. Lett. **104**(5), 053901 (2014).
[13]H. Liu, Z. Ji, T. Chen, L. Sun, S. C. Menon, and C. Lee, IEEE Sens. J. **15**(9), 4782–4790 (2015).
[14]K. Tao, L. H. Tang, J. Wu, S. W. Lye, H. L. Chang, and J. M. Miao, J. Microelectromech. Syst. **27**(2), 276–288 (2018).
[15]Y. Zhang, T. Wang, A. Luo, Y. Hu, X. Li, and F. Wang, Appl. Energy **212**, 362–371 (2018).
[16]S. H. Wang, L. Lin, and Z. L. Wang, Nano Lett. **12**(12), 6339–6346 (2012).
[17]W. Jiang, H. Li, Z. Liu, Z. Li, J. Tian, B. Shi, Y. Zou, H. Ouyang, C. Zhao, L. Zhao, R. Sun, H. Zheng, Y. Fan, Z. L. Wang, and Z. Li, Adv. Mater.**30**(32), 1801895 (2018).
[18]L. Chen, Q. Shi, Y. Sun, T. Nguyen, C. Lee, and S. Soh, Adv. Mater. **30**, 1802405 (2018).
[19]S. Roundy, IEEE Pervasive Comput. **4**(1), 28–36 (2005).
[20]S. Roundy and P. K. Wright, Smart Mater. Struct. **13**(5), 1131–1142 (2004).
[21]Z. Yang, S. Zhou, J. Zu, and D. Inman, Joule, S2542435118301260 (2018).
[22]Z. L. Wang, ACS Nano **7**(11), 9533 (2013).
[23]Z. L. Wang, Nano Energy **54**, 477–483 (2018).
[24]F. U. Khan, J. Renewable Sustainable Energy **8**(4), 044702 (2016).
[25]F. K. Shaikh and S. Zeadally, Renewable Sustainable Energy Rev. **55**, 1041–1054 (2016).
[26]Y. Bai, H. Jantunen, and J. Juuti, Adv. Mater. **30**(34), 1707271 (2018).
[27]E. Arroyo, A. Badel, and F. Formosa, Sens. Actuators, A **183**, 148–156 (2012).
[28]A. R. M. Siddique, S. Mahmud, and B. V. Heyst, Energy Convers. Manage. **106**, 728–747 (2015).
[29]K. Y. Lee, M. K. Gupta, and S. W. Kim, Nano Energy **14**, 139–160 (2015).
[30]H. Li, C. Tian, and Z. D. Deng, Appl. Phys. Rev. **1**(4), 041301 (2014).
[31]A. Toprak and O. Tigli, Appl. Phys. Rev. **1**(3), 031104 (2014).
[32]C. R. Bowen, H. A. Kim, and P. M. Weaver, Energy Environ. Sci. **7**(1), 25–44 (2014).
[33]G. M′boungui, K. Adendorffand, and R. Naidoo, Renewable Sustainable Energy Rev. **49**, 1136–1144 (2015).
[34]S. Saadon and O. Sidek, Energy Convers. Manage. **52**(1), 500–504 (2011).
[35]M. T. Todaro, F. Guido, and V. Mastronardi, Microelectron. Eng. **183–184**, 23–36 (2017).
[36]J. Briscoe and S. Dunn, Nano Energy **14**, 15–29 (2015).
[37]S. H. Lee, K. J. Chang, and G. T. Hwang, Nano Energy **14**, 111–125 (2015).
[38]H. Wu, Y. Huang, and F. Xu, Adv. Mater. **28**(45), 9881–9919 (2016).
[39]A. Erturk and D. J. Inman, *Piezoelectric Energy Harvesting* (John Wiley & Sons, New York, 2011).

[40]T. Rödig, A. Schönecker, and G. Gerlach, J. Am. Ceram. Soc. **93**(4), 901–912 (2010).
[41]S.-H. Baek, M. S. Rzchowski, and V. A. Aksyuk, MRS Bull. **37**(11), 1022–1029 (2012).
[42]X. Chou, J. Zhu, S. Qian, X. Niu, J. Qian, X. Hou, J. Mu, W. Geng, J. Cho, J. He, and C. Xue, Nano Energy **53**, 550–558 (2018).
[43]K. Shibata, R. Wang, T. Tou, and J. Koruza, MRS Bull. **43**(8), 612–616 (2018).
[44]Q. M. Wang, X. H. Du, B. Xu, and L. E. Cross, J. Appl. Phys. **85**(3), 1702–1712 (1999).
[45]B. S. Lee, S. C. Lin, W. J. Wu, X. Y. Wang, P. Z. Chang, and C. K. Lee, J. Micromech. Microeng. **19**(6), 065014 (2009).
[46]S. B. Kim, H. Park, S. H. Kim, H. C. Wikle III, J. H. Park, and D. J. Kim, J. Micorelectromech. Syst. **22**(1), 26–33 (2013).
[47]L. Mateu and F. Moll, J. Intell. Mater. Syst. Struct. **16**(10), 835–845 (2005).
[48]S. Roundy, J. Intell. Mater. Syst. Struct. **16**(16), 809–823 (2005).
[49]J. Baker, S. Roundy, and P. Wright, in Proceeding of the 3rd International Energy Conversion Engineering Conference, San Francisco, California, 15–18 August 2005.
[50]N. Sharpes, A. Abdelkefi, and S. Priya, Energy Harvesting Syst. **1**(3–4), 209–216 (2014).
[51]M. A. Karami and D. J. Inman, J. Intell. Mater. Syst. Struct. **22**(3), 271–282 (2011).
[52]A. M. Karami and D. J. Inman, J. Microelectromech. Syst. **21**(1), 145–160 (2012).
[53]N. Sharpes, A. Abdelkefi, and S. Priya, Appl. Phys. Lett. **107**(9), 093901 (2015).
[54]M. Deterre, E. Lefeuvre, and E. Dufour-Gergam, Smart Mater. Struct. **21**(8), 085004 (2012).
[55]S. Kim, W. W. Clark, and Q. M. Wang, J. Intell. Mater. Syst. Struct. **16**(10), 847–854 (2005).
[56]S. B. Horowitz, M. Sheplak, L. N. Cattafesta, and T. Nishida, J. Micromech. Microeng. **16**(9), S174–S181 (2006).
[57]C. K. Mo, L. J. Radziemski, and W. W. Clark, Smart Mater. Struct. **19**(7), 075010 (2010).
[58]X.-r. Chen, T.-q. Yang, W. Wang, and X. Yao, Ceram. Int. **38**, S271–S274 (2012).
[59]H. Florian, F. Fabien, B. Adrien, C. Jean-Fabien, and L. Mickaël, Sens. Actuators, A **247**, 12–23 (2016).
[60]T. B. Xu, E. J. Siochi, J. H. Kang, L. Zuo, W. Zhou, X. Tang, and X. Jiang, Smart Mater. Struct. **22**(6), 065015 (2013).
[61]H. W. Kim, A. Batra, S. Priya, K. Uchino, D. Markley, R. E. Newnham, and H. F. Hofmann, Jpn. J. Appl. Phys., Part 1 **43**(9A), 6178–6183 (2004).
[62]J. Feenstra, J. Granstrom, and H. Sodano, Mech. Syst. Signal Process. **22**(3), 721–734 (2008).
[63]E. Tufekcioglu and A. Dogan, Sens. Actuators, A **216**, 355–363 (2014).
[64]S. Wen, IEEE Sens. J. **18**(10), 3989–4000 (2018).
[65]L. Wang, S. Chen, W. Zhou, T. B. Xu, and L. Zuo, J. Intell. Mater. Syst. Struct. **28**(9), 1175–1187 (2017).
[66]A. Manbachi and R. Cobbold, Ultrasound **19**(4), 187–196 (2011).
[67]O. E. Mattiat, *Ultrasonic Transducer Materials* (Springer, 1971).
[68]S. R. Anton and H. A. Sodano, Smart Mater. Struct. **16**(3), R1–R21 (2007).
[69]H. Kim, J. Kim, and J. Kim, Int. J. Precis. Eng. Manuf. **12**(6), 1129–1141 (2011).
[70]D. Polsongkram, P. Chamninok, S. Pukird, L. Chow, O. Lupan, G. Chai, H. Khallaf, S. Park, and A. Schulte, Physica B **403**(9), 3713–3717 (2008).
[71]E. Ohshima, H. Ogino, I. Niikura, K. Maeda, M. Sato, M. Ito, and T. Fukuda, J. Cryst. Growth **260**(1), 166–170 (2004).
[72]L. E. Greene, M. Law, J. Goldberger, F. Kim, C. Justin, Y. Zhang, J. Richard, and P. Yang, Angew. Chem., In. Ed. **42**(26), 3031–3014 (2003).
[73]Z. Wang and J. Song, Science **312**(5771), 242–246 (2006).
[74]R. Feng, W. Tang, and Z. Wang, Adv. Mater. **28**(22), 4283 (2016).
[75]G. Zhu, A. Wang, Y. Liu, Y. Zhou, and Z. Wang, Nano Lett. **12**(6), 3086–3090 (2012).
[76]R. Yang, Y. Qin, L. Dai, and Z. Wang, Nat. Nanotechnol. **4**(1), 34–39 (2009).
[77]S. Cha, J. Seo, S. Kim, H. Kim, Y. Park, S. Kim, and J. Kim, Adv. Mater. **22**(42), 4726 (2010).
[78]Y. Qi and M. McAlpine, Energy Environ. Sci. **3**(9), 1275–1285 (2010).
[79]G. Zhu, R. Yang, S. Wang, and Z. Wang, Nano Lett. **10**(8), 3151–3155 (2010).
[80]S. Lee, S. Bae, L. Lin, Y. Yang, C. Park, S. Kim, N. Seung, H. Kim, J. Young, and Z. Wang, Adv. Funct. Mater. **23**(19), 2445–2449 (2013).
[81]Z. Gao, J. Zhou, Y. Gu, P. Fei, Y. Hao, G. Bao, and Z. Wang, J. Appl. Phys. **105**(11), 113707 (2009).
[82]W. Wu, L. Wang, Y. Li, F. Zhang, L. Lin, S. Niu, D. Chenet, X. Zhang, Y. Hao, T. Heinz, J. Hone, and Z. Wang, Nature **514**(7523), 470–474 (2014).
[83]T. Cao, G. Wang, W. Han, H. Ye, C. Zhu, J. Shi, Q. Niu, P. Tan, E. Wang, B. Liu, and J. Feng, Nat. Commun. **3**, 887 (2012).
[84]K. H. Michel and B. Verberck, Phys. Rev. B **80**, 224301 (2009).
[85]J. Lee, Y. Jae, B. Eun, Y. Tae, A. Sang, T. Kim, Y. Liu, K. Sung, J. Chang, H. Yoon, H. Ryu, W. Seung, S. Jong, J. Lee, and S. Kim, Adv. Mater. **29**, 1606667 (2017).
[86]H. Song, I. Karakurt, M. Wei, N. Liu, Y. Chu, J. Zhong, and L. Lin, Nano Energy **49**, 7 (2018).
[87]K. Duerloo, M. Ong, and E. Reed, J. Phys. Chem. Lett. **3**, 2871 (2012).
[88]X. Chen, S. Xu, N. Yao, and Y. Shi, Nano Lett. **10**, 2133 (2010).
[89]G. Hwang, J. Yang, H. Seong, H. Lee, M. Lee, Y. Dae, H. Jae, J. Seung, K. Chang, J. Kim, K. Park, and J. Keon, Adv. Energy Mater. **5**, 1500051 (2015).
[90]L. Bellaiche and D. Vanderbilt, Phys. Rev. Lett. **83**, 1347 (1999).
[91]C. Jeong, S. Cho, J. Han, D. Park, S. Yang, K. Park, J. Ryu, H. Sohn, Y. Chung, and K. Lee, Nano Res. **10**, 437 (2017).
[92]G. Tang, B. Yang, J. Liu, B. Xu, H. Zhu, and C. Yang, Sens. Actuators, A **205**, 150 (2014).
[93]F. Li, D. Lin, Z. Chen, Z. Cheng, J. Wang, C. Li, Z. Xu, Q. Huang, X. Liao, L. Chen, T. Shrout, and S. Zhang, Nat. Mater. **17**, 349 (2018).
[94]G. Hwang, V.Annapureddy, H. Jae, J. Daniel, C. Baek, Y. Dae, H. Dong, H. Jung, K. Chang, K. Park, J. Choi, K. Do, J. Ryu, and J. Keon, Adv. Energy Mater. **6**, 1600237 (2016).
[95]C. Jeong, K. Park, J. Ryu, G. Hwang, and K. Lee, Adv. Funct. Mater. **24**(18), 2620 (2014).
[96]V. Misra, A. Bozkurt, B. Calhoun, T. Jackson, J. S. Jur, J. Lach, B. Lee, J. Muth, Ö. Oralkan, M. Öztürk, S. Trolier-McKinstry, D. Vashaee, D. Wentzloff, and Y. Zhu, Proc. IEEE **103**, 665 (2015).
[97]See https://en.wikipedia.org/wiki/Lead_zirconate_titanate for crystal Atomic model of PZT.
[98]J. Fang, X. Wang, and T. Lin, J. Mater. Chem. **21**, 11088 (2011).
[99]C. Pan, C. Yen, S. Wang, Y. Lai, L. Lin, J. Huang, and S. Kuo, RSC Adv. **5**(103), 85073–85081 (2015).
[100]Z. H. Liu, C. T. Pan, L. W. Lin, J. C. Huang, and Z. Y. Ou, Smart Mater. Struct. **23**(2), 25003–25013 (2014).
[101]G. Zhu, Z. Zeng, L. Zhang, and X. Yan, Comput. Mater. Sci. **44**(2), 224–229 (2008).
[102]C. Chang, V. Tran, J. Wang, Y. Fuh, and L. Lin, Nano Lett. **10**(2), 726 (2010).
[103]L. Persano, C. Dagdeviren, Y. Su, Y. Zhang, S. Girardo, D. Pisignano, Y. Huang, and J. Rogers, Nat. Commun. **4**(3), 1633 (2013).
[104]N. Soin, T. Shah, S. Anand, J. Geng, W. Pornwannachai, P. Mandal, D. Reid, S. Sharma, R. H. Bayramol, and E. Siores, Energy Environ. Sci. **7**(5), 1670–1679 (2014).
[105]A. Savolainen and K. Kirjavainen, J. Macromol. Sci. Chem. **26**(2–3), 583 (1989).
[106]N. Wu, X. Cheng, Q. Zhong, J. Zhong, W. Li, B. Wang, B. Hu, and J. Zhou, Adv. Funct. Mater. **25**(30), 4788–4794 (2015).
[107]Q. Zhong, J. Zhong, X. Cheng, X. Yao, B. Wang, W. Li, N. Wu, K. Liu, B. Hu, and J. Zhou, Adv. Mater. **27**(44), 7130 (2015).
[108]B. Wang, C. Liu, Y. Xiao, J. Zhong, W. Li, Y. Cheng, B. Hu, L. Huang, and J. Zhou, Nano Energy **32**, 42–49 (2017).
[109]X. Zhang, G. M. Sessler, and Y. Wang, J. Appl. Phys. **116**(7), 074109 (2014).
[110]J. J. Wang, C. E. Lu, S. C. Lo, Y. C. Su, and W. Fang, paper presented at the19th International Conference on Solid-State Sensors, Actuators and Microsystems (TRANSDUCERS), Kaohsiung, Taiwan, 18–22 June 2017.
[111]J. Zhong, Q. Zhong, X. Zang, N. Wu, W. Li, Y. Chu, and L. Lin, Nano Energy **37**, 268 (2017).
[112]X. Zhang, P. Pondrom, G. Sessler, and X. Ma, Nano Energy **50**, 52 (2018).
[113]T. Yucel, P. Cebe, and D. Kaplan, Adv. Funct. Mater. **21**, 779 (2011).
[114]M. Otter, J. Shoenung, and W. S. Williams, J. Orthop. Res. **3**, 321–324 (1985).
[115]S. Ghosh and D. Mandal, Appl. Phys. Lett. **109**, 103701 (2016).
[116]B. Lee, J. Zhang, C. Zueger, W. Chung, S. Yoo, E. Wang, J. Meyer, R. Ramesh, and S. Lee, Nat. Nanotechnol. **7**(6), 351–356 (2012).

[117]S. Ghosh and D. Mandal, Nano Energy **28**(8), 356–365 (2016).
[118]K. Park, S. Xu, Y. Liu, G. Hwang, S. Kang, Z. Wang, and K. Lee, Nano Lett. **10**(12), 4939–4943 (2010).
[119]F. Stoppel, C. Schröder, F. Senger, B. Wagner, and W. Benecke, Procedia Eng. **25**(35), 721–724 (2011).
[120]J. Doll, B. Petzold, B. Ninan, R. Mullapudi, and B. Pruitt, J. Micromech. Microeng. **20**(2), 025008 (2010).
[121]D. Vasilescu, R. Cornillon, and G. Mallet, Nature **225**(5233), 635 (1970).
[122]V. V. Lemanov, Ferroelectrics **238**(1), 211–218 (2000).
[123]A. Kholkin, N. Amdursky, I. Bdikin, E. Gazit, and G. Rosenman, ACS Nano **4**(2), 610–614 (2010).
[124]S. Vasilev, P. Zelenovskiy, D. Vasileva, A. Nuraeva, V. Y. Shur, and A. L. Kholkin, J. Phys. Chem. Solids. **93**, 68–72 (2016).
[125]J.-H. Lee, K. Heo, K. Schulz-Schönhagen, J. H. Lee, M. S. Desai, H.-E. Jin, and S.-W. Lee, ACS Nano **12**(8), 8138–8144 (2018).
[126]V. Nguyen, R. Zhu, K. Jenkins, and R. Yang, Nat. Commun. **7**, 13566 (2016).
[127]R. W. Schwartz, T. J. Boyle, S. J. Lockwood, M. B. Sinclair, D. Dimos, and C. D. Buchheit, Integr. Ferroelectr. **7**(1–4), 259–277 (1995).
[128]D. P. Vijay and S. B. Desu, J. Electrochem. Soc. **140**(9), 2640–2645 (1993).
[129]T. Maeder, L. Sagalowicz, and P. Muralt, Jpn. J. Appl. Phys., Part 1 **37**(4A), 2007–2012 (1998).
[130]H. B. Fang, J. Q. Liu, Z. Y. Xu, L. Dong, L. Wang, D. Chen, B. C. Cai, and Y. Liu, Microelectron. J. **37**(11), 1280–1284 (2006).
[131]J. Q. Liu, H. B. Fang, Z. Y. Xu, X. H. Mao, X. C. Shen, D. Chen, H. Liao, and B. C. Cai, Microelectron. J. **39**(5), 802–806 (2008).
[132]D. Shen, J. H. Park, J. Ajitsaria, S. Y. Choe, H. C. Wikle III, and D. J. Kim, J. Micromech. Microeng. **18**(5), 055017 (2008).
[133]D. Shen, J. H. Park, J. H. Noh, S. Y. Choe, S. H. Kim, H. C. Wikle III, and D. J. Kim, Sens. Actuators, A **154**(1), 103–108 (2009).
[134]H. Liu, C. J. Tay, C. Quan, T. Kobayashi, and C. Lee, J. Micorelectromech. Syst. **20**(5), 1131–1142 (2011).
[135]H. Liu, C. Lee, T. Kobayashi, C. J. Tay, and C. Quan, Microsyst. Technol. **18**(4), 497–506 (2012).
[136]L. Deng, Z. Wen, and X. Zhao, J. Microelectromech. Syst. **23**(4), 855–861 (2014).
[137]Y. B. Jeon, R. Sood, J. H. Jeong, and S. G. Kim, Sens. Actuators, A **122**(1), 16–22 (2005).
[138]J. C. Park, J. Y. Park, and Y. P. Lee, J. Microelectromech. Syst. **19**(5), 1215–1222 (2010).
[139]S. B. Kim, J. H. Park, S. H. Kim, H. Ahn, H. C. Wikle, and D. J. Kim, J. Micromech. Microeng. **22**(10), 1922–1931 (2012).
[140]E. K. Reilly and P. K. Wright, J. Micromech. Microeng. **19**, 095014 (2009).
[141]K. Morimoto, I. Kanno, K. Wasa, and H. Kotera, Sens. Actuators, A **163**(1), 428–432 (2010).
[142]D. Isarakorn, D. Briand, P. Janphuang, A. Sambri, S. Gariglio, J. M. Triscone, F. Guy, J. W. Reiner, C. H. Ahn, and N. F. de Rooij, Smart Mater. Struct. **20**(2), 025015 (2011).
[143]T. Harigai, H. Adachi, and E. Fujii, J. Appl. Phys. **107**(9), 096101 (2010).
[144]C. W. Ahn, C. H. Choi, H. Y. Park, S. Nahm, and S. Priya, J. Mater. Sci. **43**, 6784 (2008).
[145]V. M. Le, M. Hara, and H. Kuwano, J. Microelectromech. Syst. **24**(6), 1887–1895 (2015).
[146]S. S. Won, J. Lee, and V. Venugopal, Appl. Phys. Lett. **108**(23), 232908 (2016).
[147]S. Trolier-McKinstry and P. Muralt, J. Electroceram. **12**(1–2), 7–17 (2004).
[148]T.-T. Yen, T. Hirasawa, P. K. Wright, A. P. Pisano, and L. Lin, J. Micromech. Microeng. **21**(8), 085037 (2011).
[149]P. Wang and H. Du, Rev. Sci. Instrum. **86**(7), 075002 (2015).
[150]M. Renaud, K. Karakaya, T. Sterken, P. Fiorini, C. van Hoof, and R. Puers, Sens. Actuators, A **145–146**(1), 380–386 (2008).
[151]B. Yang, H. Liu, J. Liu, and C. Lee, *Micro and Nano Energy Harvesting Technologies* (Artech House, Boston, 2014).
[152]M. Akiyama, K. Nagao, N. Ueno, H. Tateyama, and T. Yamada, Vacuum **74**(3), 699–703 (2004).
[153]J. B. Lee, J. P. Jung, M. H. Lee, and J. S. Park, Thin Solid Films **447**, 610–614 (2004).
[154]A.Toprak and O. Tigli, Sens. Actuators, A **269**, 412–418 (2018).
[155]R. Elfrink, T. M. Kamel, M. Goedbloed, S. Matova, D. Hohlfeld, Y. van Andel, and R. van Schaijk, J. Micromech. Microeng. **19**(9), 094005 (2009).
[156]Z. Wang, R. Elfrink, and M. Rovers, J. Microelectromech. Syst. **23**(3), 539–548 (2014).
[157]Z. Wang, S. Matova, and R. Elfrink, paper presented at the 29th IEEE International Conference on Micro Electro Mechanical Systems, Paris, France, 2012.
[158]R. Andosca, T. G. McDonald, V. Genova, S. Rosenberg, J. Keating, C. Benedixen, and J. Wu, Sens. Actuators, A **178**(5), 76–87 (2012).
[159]S. L. Kok, N. M. White, and N. R. Harris, Meas. Sci. Technol. **20**(12), 124010 (2009).
[160]A. Lei, R. Xu, A. Thyssen, A. C. Stoot, T. L. Christiansen, K. Hansen, R. Lou-Moller, E. V. Thomesen, and K. Birkelund, in *Proceedings of MEMS, Cancun, Mexico*, 23–27 January 2011, pp. 125–128.
[161]R. Xu, A. Lei, and T. L. Christiansen, Sens. Actuators, A **188**(8), 383–388 (2012).
[162]A. Lei, R. Xu, and L. M. Borregaard, J. Microelectromech. Syst. **23**(4), 842–854 (2014).
[163]Y. Liao and H. A. Sodano, Smart Mater. Struct. **17**(17), 065026 (2008).
[164]A. Erturk and D. J. Inman, Smart Mater. Struct. **18**(2), 25009–25018 (2009).
[165]K. Tanaka, T. Konishi, M. Ide, and S. Sugiyama, J. Micromech. Microeng. **16**(4), 815–820 (2006).
[166]E. E. Aktakka, R. L. Peterson, and K. Najafi, paper presented at the Int. Electron Devices Meeting (IEDM), San Francisco, USA, 6–8 December 2010, pp. 31.5.1–31.5.4.
[167]E. E. Aktakka, R. L. Peterson, and K. Najafi, paper presented at Transducer's 2011, Beijing, China, 5–9 June 2011, pp. 1649–1652.
[168]E. E. Aktakka, R. L. Peterson, and K. Najafi, IEEE Trans. Electron Devices **60**(6), 2022–2030 (2013).
[169]X. H. Xu and J. R. Chu, J. Micromech. Microeng. **18**(18), 065001 (2008).
[170]Z. H. Wang, J. M. Miao, and C. W. Tan, Sens. Actuators, A **149**(2), 277–283 (2009).
[171]G. Tang, J. Q. Liu, B. Yang, J. B. Luo, H. S. Liu, Y. G. Li, C. S. Yang, D. N. He, V. D. Dao, K. Tanaka, and S. Sugiyama, J. Micromech. Microeng. **22**(6), 065017 (2012).
[172]P. Janphuang, R. Lockhart, and N. Uffer, Sens. Actuators, A **210**(1), 1–9 (2014).
[173]B. Yang, Y. Zhu, and X. Wang, Sens. Actuators, A **214**(4), 88–94 (2014).
[174]G. Tang, J. Q. Liu, and H. S. Liu, Phys. Status Solidi **208**(12), 2913–2919 (2011).
[175]H. Y. Lin, P. L. Hsu, H. C. Liu, T. Chen, and L. N. Sun, in Proceedings of 13th IEEE International Conference on Nano/Micro Engineered and Molecular Systems (IEEE NEMS 2018), Singapore, 22–26 April 2018.
[176]S. C. Lin and W. J. Wu, Smart Mater. Struct. **22**(4), 045016 (2013).
[177]C. L. Kuo, S. C. Lin, and W. J. Wu, Smart Mater. Struct. **25**(10), 105016 (2016).
[178]G. Tang, B. Yang, H. Cheng, G. Li, J. Liu, X. Chen, and C. Yang, Sci. Rep. **6**(1), 38798 (2016).
[179]Z. Yi, B. Yang, and G. Li, Appl. Phys. Lett. **111**(1), 013902 (2017).
[180]Y. Tian, G. Li, and Z. Yi, J. Phys. Chem. Solids **117**, 21–27 (2018).
[181]D. Wang, G. Yuan, and G. Hao, Nano Energy **43**, 351–358 (2018).
[182]A. I. Kingon and S. Srinivasan, Nat. Mater. **4**, 233–237 (2005).
[183]H. G. Yeo, X. Ma, C. Rahn, and S. Trolier-McKinstry, Adv. Funct. Mater. **26**(32), 5940–5946 (2016).
[184]Q.- L. Zhao, G.-P. He, J.-J. Di, W.-L. Song, Z.-L. Hou, P.-P. Tan, D.-W. Wang, and M.-S. Cao, ACS Appl. Mater. Interfaces **9**(29), 24696–24703 (2017).
[185]C. K. Jeong, K.-I. Park, J. H. Son, G.-T. Hwang, S. H. Lee, D. Y. Park, H. E. Lee, H. K. Lee, M. Byun, and K. J. Lee, Energy Environ. Sci. **7**(12), 4035–4043 (2014).
[186]K. I. Park, J. H. Son, G. T. Hwang, C. K. Jeong, J. Ryu, M. Koo, I. Choi, S. H. Lee, M. Byun, Z. L. Wang, and K. J. Lee, Adv. Mater. **26**(16), 2514–2520 (2014).
[187]J. Kwon, W. Seung, B. K. Sharma, S. W. Kim, and J. H. Ahn, Energy Environ. Sci. **5**(10), 8970–8975 (2012).
[188]Y. Chen, Y. Zhang, L. Zhang, F. Ding, and O. G. Schmidt, Nano Energy **31**, 239–246 (2017).
[189]W. W. Wu, S. Bai, M. M. Yuan, Y. Qin, Z. L. Wang, and T. Jing, ACS Nano. **6**(7), 6231–6235 (2012).
[190]Y. Zhang, M. Y. Xie, J. Roscow, K. Zhou, Y. X. Bao, D. Zhang, and C. R. Bowen, J. Mater. Chem. A **5**(14), 6569–6580 (2017).
[191]W. Jin, Z. Wang, H. Huang, X. K. Hu, Y. H. He, M. Li, L. Y. Li, Y. H. Gao, Y. M. Hu, and H. Gu, RSC Adv. **8**(14), 7422–7427 (2018).

[192]Y. Qi, J. Kim, T. D. Nguyen, B. Lisko, P. K. Purohit, and M. C. McAlpine, Nano Lett. **11**(3), 1331–1336 (2011).
[193]S. Y. Xu, G. Poirier, and N. Yao, Nano Lett. **12**(5), 2238–2242 (2012).
[194]S. Y. Xu, Y. Yeh, G. Poirier, M. C. McAlpine, R. A. Register, and N. Yao, Nano Lett. **13**(6), 2393–2398 (2013).
[195]K. Y. Lee, B. Kumar, J. S. Seo, K. H. Kim, J. I. Sohn, S. N. Cha, D. Choi, Z. L. Wang, and S.-W. Kim, Nano Lett. **12**(4), 1959–1964 (2012).
[196]Z. L. Wang, Adv. Funct. Mater. **18**(22), 3553–3567 (2008).
[197]M. Lee, C. Y. Chen, S. Wang, S. N. Cha, Y. J. Park, J. M. Kim, and Z. L. Wang, Adv. Mater. **24**(13), 1759–1764 (2012).
[198]A. Koka, Z. Zhou, and H. Sodano, Energy Environ. Sci. **7**(1), 288–296 (2014).
[199]J. Chang, M. Dommer, C. Chang, and L. Lin, Nano Energy **1**(3), 356–371 (2012).
[200]T. Ma, M. Guo, M. Zhang, Y. J. Zhang, and X. D. Wang, Nanotechnology **18**(3), 035605 (2007).
[201]S. Xu, C. S. Lao, B. Weintraub, and Z. L. Wang, J. Mater. Res. **23**(8), 2072–2077 (2008).
[202]Y. Qin, R. Yang, and Z. L. Wang, J. Phys. Chem. C. **112**(48), 18734–18736 (2008).
[203]D. Farrar, K. Ren, D. Cheng, S. Kim, W. Moon, W. L. Wilson, J. E. West, and S. M. Yu, Adv. Mater. **23**(34), 3954–3959 (2011).
[204]C. Ribeiro, V. Sencadas, J. L. G. Ribelles, and S. Lanceros-, Mendez, Soft Mater. **8**(3), 274–287 (2010).
[205]A. Gheibi, R. Bagherzadeh, A. A. Merati, and M. Latifi, J. Polym. Res. **21**(11), 571 (2014).
[206]B. S. Lee, B. Park, H. S. Yang, J. W. Han, C. Choong, J. Bae, K. Lee, W. R. Yu, U. Jeong, U. I. Chung, J. J. Park, and O. Kim, ACS Appl. Mater. Interfaces **6**(5), 3520–3527 (2014).
[207]S. Siddiqui, D. I. Kim, E. Roh, L. T. Duy, T. Q. Trung, M. T. Nguyen, and N. E. Lee, Nano Energy **30**, 434–442 (2016).
[208]A. Wang, Z. Liu, M. Hu, C. C. Wang, X. D. Zhang, B. J. Shi, Y. B. Fan, Y. G. Cui, Z. Li, and K. L. Ren, Nano Energy **43**, 63–71 (2018).
[209]K. Maity and D. Mandal, ACS Appl. Mater. Interfaces **10**(21), 18257–18269 (2018).
[210]A. L. Yarin, S. Koombhongse, and D. H. Reneker, J. Appl. Phys. **90**(9), 4836–4846 (2001).
[211]D. H. Renekerand and A. L. Yarin, Polymer **49**(10), 2387–2425 (2008).
[212]D. H. Sun, C. Chang, S. Li, and L. W. Lin, Nano Lett. **6**(4), 839–842 (2006).
[213]C. Chang, K. Limkrailassiri, and L. W. Lin, Appl. Phys. Lett. **93**(12), 123111 (2008).
[214]L. Yu and P. Cebe, Polymer **50**(9), 2133–2141 (2009).
[215]W. Zeng, X. M. Tao, S. Chen, S. M. Shang, H. L. W. Chan, and S. H. Choy, Energy Environ. Sci. **6**(9), 2631–2638 (2013).
[216]Y. Ahn, J. Y. Lim, S. M. Hong, J. Lee, J. Ha, H. J. Choi, and Y. Seo, J. Phys. Chem. C **117**(22), 11791–11799 (2013).
[217]H. B. Kang, J. Chang, K. Koh, L. Lin, and Y. S. Cho, ACS Appl. Mater. Interfaces **6**(13), 10576–10582 (2014).
[218]H. Sodano, D. J. Inman, and G. Park, Shock Vib. Dig. **36**(3), 197–205 (2004).
[219]H. Sodano, D. J. Inman, and G. Park, J. Intell. Mater. Syst. Struct. **16**(1), 67–75 (2005).
[220]L. Tang, Y. Yang, and C. K. Soh, J. Intell. Mater. Syst. Struct. **21**(18), 1867–1897 (2010).
[221]B. P. Mann and N. D. Sims, J. Sound Vib. **319**(1), 515–530 (2009).
[222]B. P. Mann, Appl. Mech. Rev. **66**(4), 045501 (2014).
[223]J. W. Yi, Y. S. Wan, and W. H. Shih, J. Appl. Phys. **91**(3), 1680–1686 (2002).
[224]D. B. Zhu, M. J. Tudor, and S. P. Beeby, Meas. Sci. Technol. **21**(2), 022001 (2009).
[225]M. Ferrari, V. Ferrari, M. Guizzetti, D. Marioli, and A. Taroni, Sens. Actuators, A **142**(1), 329–335 (2008).
[226]S. M. Shahruz, J. Sound Vib. **292**(3), 987–998 (2006).
[227]H. A. Xue, Y. T. Hu, and Q. M. Wang, IEEE Trans. Ultrason., Ferroelectr., Freq. Control **55**(9), 2092–2096 (2008).
[228]X. D. Tang and L. Zuo, J. Sound Vib. **330**(21), 5199–5209 (2011).
[229]X. D. Tang and L. Zuo, Smart Mater. Struct. **21**(7), 075025 (2012).
[230]L. Tang and Y. Yang, J. Intell. Mater. Syst. Struct. **23**(14), 1631–1647 (2012).
[231]H. Xiao, X. Wang, and S. John, Mech. Syst. Signal Process. **58–59**, 355–375 (2015).
[232]H. Y. Wang and L. H. Tang, Mech. Syst. Signal Process. **86**, 29–39 (2017).
[233]B. Yang, J. Q. Liu, G. Tang, J. B. Luo, C. S. Yang, and Y. G. Li, Appl. Phys. Lett. **99**(22), 223505 (2011).
[234]R. J. M. Vullers, R. Elfrink, S. Matova, and Z. Wang, paper presented at PowerMEMS 2012 (2012), pp. 211–214.
[235]J. E. Kim and Y. Y. Kim, AIP Adv. **3**(7), 072103 (2013).
[236]Y. T. Hu and Y. Xu, Appl. Phys. Lett. **104**(5), 53902 (2014).
[237]M. M. R. El-Hebeary, M. H. Arafa, and S. M. Megahed, Sens. Actuators, A **193**, 35–47 (2013).
[238]R. M. Toyabur, M. Salauddin, and J. Y. Park, Ceram. Int. **43**, S675–S681 (2017).
[239]L. J. Gong, Q. S. Pan, W. Li, G. Y. Yan, Y. B. Liu, and Z. H. Feng, Appl. Phys. Lett. **107**(3), 033904 (2015).
[240]R. L. Harne, A. Sun, and K. W. Wang, J. Sound Vib. **363**, 517–531 (2016).
[241]L. G. H. Staaf, A. D. Smith, E. Köhler, P. Lundgren, P. D. Folkow, and P. Enoksson, J. Sound Vib. **420**, 165–173 (2018).
[242]D. F. Berdy, B. Jung, J. F. Rhoads, and D. Peroulis, Sens. Actuators, A **188**, 148–157 (2012).
[243]M. Rezaeisaray, M. E. Gowini, S. Dan, D. Raboud, and W. Moussa, Sens. Actuators, A **228**, 104–111 (2015).
[244]S. Dhote, J. Zu, and Y. Zhu, Appl. Phys. Lett. **106**(16), 163903 (2015).
[245]S. Dhote, Z. Yang, and J. Zu, Mech. Syst. Signal Process. **98**, 268–280 (2018).
[246]Q. B. He and T. Jiang, Appl. Phys. Lett. **110**(21), 213901 (2017).
[247]J. Iannacci, E. Serra, R. D. Criscienzo, G. Sordo, M. Gottardi, A. Borrielli, M. Bonaldi, T. Kuenzig, G. Schrag, G. Pandraud, and P. M. Sarro, Microsyst. Technol. **20**(4–5), 627–640 (2014).
[248]J. Iannacci, G. Sordo, E. Serra, and U. Schmid, Microsyst. Technol. **22**(7), 1865–1881 (2016).
[249]W. J. Su and J. Zu, Appl. Phys. Lett. **103**(20), 203901 (2013).
[250]K. Q. Fan, F. B. Chao, J. G. Zhang, W. D. Wang, and X. H. Che, Energy Convers. Manage. **86**, 561–567 (2014).
[251]H. Wang, F. Hu, K. Wang, and W. Zhao, Appl. Phys. Lett. **110**(16), 163905 (2017).
[252]R. W. Chen, L. Ren, H. K. Xia, X. W. Yuan, and X. J. Liu, Sens. Actuators, A **230**, 1–8 (2015).
[253]C. F. Hung, T. K. Chung, P. C. Yeh, C. C. Chen, C. M. Wang, and S. H. Lin, IEEE Sens. J. **15**(10), 5601–5615 (2015).
[254]J. W. Xu and J. Tang, Appl. Phys. Lett. **107**(21), 213902 (2015).
[255]Q. M. Yu, J. Yang, X. H. Yue, and P. Li, AIP Adv. **5**(4), 047144 (2015).
[256]H. J. Zhang, S. L. Jiang, and X. F. He, Appl. Phys. Lett. **110**(22), 223902 (2017).
[257]A. H. Nayfeh, *Perturbation Methods* (Wiley Interscience, 1973).
[258]A. Triplett and D. D. Quinn, J. Intell. Mater. Syst. Struct. **20**(16), 1959–1967 (2009).
[259]H. Fang and K. W. Wang, J. Sound Vib. **391**, 153–169. (2017).
[260]Z. Yang and J. Zu, IEEE/ASME Trans. Mech. **21**(3), 1787–1791 (2016).
[261]A. M. Wickenheiser and E. Garcia, Smart Mater. Struct. **19**(6), 065020 (2010).
[262]R. Masana and M. F. Daqaq, J. Vib. Acoust. **133**(1), 011007 (2011).
[263]M. Marzencki, M. Defosseux, and S. Basrour, J. Microelectromech. Syst. **18**(6), 1444–1453 (2009).
[264]A. Hajati and S. G. Kim, Appl. Phys. Lett. **99**(8), 083105 (2011).
[265]P. C. Huang, T. H. Tsai, and Y. J. Yang, Microelectron. Eng. **111**, 214–219 (2013).
[266]B. Marinkovic and H. Koser, Appl. Phys. Lett. **94**(10), 103505 (2009).
[267]B. Marinkovic and H. Koser, Smart Mater. Struct. **21**(6), 065006 (2012).
[268]R. Masana and M. F. Daqaq, J. Sound Vib. **330**(24), 6036–6052 (2011).
[269]R. Masana and M. F. Daqaq, J. Sound Vib. **332**(25), 6755–6767 (2013).
[270]L.-C. J. Blystad and E. Halvorsen, Microsyst. Technol. **17**(4), 505–511 (2011).
[271]S. Moss, A. Barry, I. Powlesland, S. Galea, and G. P. Carman, Appl. Phys. Lett. **97**(23), 234101 (2010).
[272]X. Wang, C. Chen, N. Wang, H. San, Y. Yu, E. Halvorsen, and X. Chen, Appl. Energy **190**, 368–375 (2017).
[273]Z. Zeng, B. Ren, Q. Xu, D. Lin, W. Di, H. Luo, and D. Wang, Appl. Phys. Lett. **107**(17), 173502 (2015).
[274]H. Liu, C. Lee, T. Kobayashi, C. J. Tay, and C. Quan, Smart Mater. Struct. **21**(3), 035005 (2012).
[275]S. C. Stanton, C. C. McGehee, and B. P. Mann, Appl. Phys. Lett. **95**(17), 174103 (2009).
[276]G. Sebald, H. Kuwano, D. Guyomar, and B. Ducharne, Smart Mater. Struct. **20**(10), 102001 (2011).
[277]L. H. Tang and Y. W. Yang, Appl. Phys. Lett. **101**(9), 094102 (2012).

[278]K. Q. Fan, Q. X. Tan, Y. W. Zhang, S. H. Liu, M. L. Cai, and Y. M. Zhu, Appl. Phys. Lett. **112**(12), 123901 (2018).
[279]A. Erturk and D. J. Inman, J. Sound Vib. **330**(10), 2339–2353 (2011).
[280]R. L. Harne and K. W. Wang, Smart Mater. Struct. **22**(2), 023001 (2013).
[281]C. McInnes, D. Gorman, and M. Cartmell, J. Sound Vib. **318**(4), 655–662 (2008).
[282]R. Benzi, G. Parisi, A. Sutera, and A. Vulpiani, Tellus **34**(1), 10–16 (1982).
[283]F. Cottone, H. Vocca, and L. Gammaitoni, Phys. Rev. Lett. **102**(8), 080601 (2009).
[284]A. Erturk, J. Hoffmann, and D. J. Inman, Appl. Phys. Lett. **94**(25), 254102 (2009).
[285]R. L. Harne, M. Thota, and K. W. Wang, Appl. Phys. Lett. **102**(5), 053903 (2013).
[286]S. P. Pellegrini, N. Tolou, M. Schenk, and J. L. Herder, J. Intell. Mater. Syst. Struct. **24**(11), 1303–1312 (2013).
[287]S. Zhao and A. Erturk, Appl. Phys. Lett. **102**(10), 103902 (2013).
[288]C. B. Lan, L. Tang, and R. L. Harne, J. Sound Vib. **421**, 61–78 (2018).
[289]S. X. Zhou, J. Y. Cao, A. Erturk, and J. Lin, Appl. Phys. Lett. **102**(17), 173901 (2013).
[290]J. Cao, S. Zhou, D. J. Inman, and Y. Chen, Nonlinear Dyn. **80**(4), 1705–1719 (2015).
[291]S. X. Zhou, J. Y. Cao, D. J. Inman, J. Lin, S. S. Liu, and Z. Z. Wang, Appl. Energy **133**, 33–39 (2014).
[292]J. Cao, S. X. Zhou, W. Wang, and J. Lin, Appl. Phys. Lett. **106**(17), 173903 (2015).
[293]W. Wang, J. Y. Cao, C. R. Bowen, S. X. Zhou, and J. Lin, Energy **118**, 221–230 (2017).
[294]L. Gammaitoni, I. Neri, and H. Vocca, Appl. Phys. Lett. **94**(16), 164102 (2009).
[295]S. C. Stanton, C. C. McGehee, and B. P. Mann, Physica D **239**(10), 640–653 (2010).
[296]S. C. Stanton, B. A. M. Owens, and B. P. Mann, J. Sound Vib. **331**(15), 3617–3627 (2012).
[297]M. Ferrari, V. Ferrari, M. Guizzettia, B. Ando, S. Bagliob, and C. Trigonab, Sens. Actuators, A **162**(2), 425–431 (2010).
[298]M. Ferrari, M. Baù, M. Guizzetti, and V. Ferrari, Sens. Actuators, A **172**(1), 287–292 (2011).
[299]H. Vocca, I. Neri, F. Travasso, and L. Gammaitoni, Appl. Energy **97**, 771–776 (2012).
[300]L. Tang, Y. Yang, and C. K. Soh, J. Intell. Mater. Syst. Struct. **23**(13), 1433–1449 (2012).
[301]B. Ando, S. Baglio, C. Trigona, N. Dumas, L. Latorre, and P. Nouet, J. Micromech. Microeng. **20**(12), 125020 (2010).
[302]W. Yang and S. Towfighian, Mech. Syst. Signal Process. **90**, 317–333 (2017).
[303]Z. Y. Zhou, W. Y. Qin, and P. Zhu, Mech. Syst. Signal Process. **84**, 158–168 (2017).
[304]Z. Y. Zhou, W. Y. Qin, and P. Zhu, Mech. Syst. Signal Process. **110**, 260–272 (2018).
[305]G. W. Kim and J. Kim, Smart Mater. Struct. **22**(1), 014005 (2013).
[306]R. Masana and M. F. Daqaq, J. Appl. Phys. **111**(4), 044501 (2012).
[307]H. Vocca, F. Cottone, I. Neri, and L. Gammaitoni, Eur. Phys. J.: Spec. Top. **222**(7), 1699–1705 (2013).
[308]C. D. Xu, Z. Liang, B. Ren, W. N. Di, H. S. Luo, D. Wang, K. L. Wang, and Z. F. Chen, J. Appl. Phys. **114**(11), 114507 (2013).
[309]B. Ando, S. Baglio, A. R. Bulsara, V. Marletta, V. Ferrari, and M. Ferrari, IEEE Sens. J. **15**(6), 3209–3220 (2015).
[310]Y. Zhu and J. W. Zu, Appl. Phys. Lett. **103**(4), 041905 (2013).
[311]M. I. Friswell, S. F. Ali, O. Bilgen, S. Adhikari, A. W. Lees, and G. Litak, J. Intell. Mater. Syst. Struct. **23**(13), 1505–1521 (2012).
[312]A. F. Arrieta, P. Hagedorn, A. Erturk, and D. J. Inman, Appl. Phys. Lett. **97**(10), 104102 (2010).
[313]D. N. Betts, C. R. Bowen, H. A. Kim, N. Gathercole, C. T. Clarke, and D. J. Inman, Eur. Phys. J.: Spec. Top. **222**(7), 1553–1562 (2013).
[314]L. Van Blarigan, P. Danzl, and J. Moehlis, Appl. Phys. Lett. **100**(25), 253904 (2012).
[315]H. Kulah and K. Najafi, IEEE Sens. J. **8**(3), 261–268 (2008).
[316]M. Umeda, K. Nakamura, and S. Ueha, Jpn. J. Appl. Phys., Part 1 **35**(5B), 3267–3273 (1996).
[317]M. Umeda, K. Nakamura, and S. Ueha, Jpn. J. Appl. Phys., Part 1 **36**(5B), 3146–3151 (1997).
[318]M. Renaud, P. Fiorini, R. van Schaijk, and C. van Hoof, Smart Mater. Struct. **18**(3), 035001 (2009).
[319]X. F. He, K. S. Teh, S. Y. Li, L. X. Dong, and S. L. Jiang, Sens. Actuators, A **259**, 171–179 (2017).
[320]M. A. Halim and J. Y. Park, Microsyst. Technol. **24**(5), 2099–2107 (2018).
[321]L. Gu, Microelectron. J. **42**(2), 277 (2011).
[322]L. Gu and C. Livermore, Smart Mater. Struct. **20**(4), 045004 (2011).
[323]M. A. Halim, S. Khym, and J. Y. Park, J. Appl. Phys. **114**(4), 044902 (2013).
[324]M. A. Halim and J. Y. Park, Sens. Actuators, A **208**(2), 56 (2014).
[325]X. Zhang, S. Gao, D. Li, L. Jin, Q. Wu, and F. Liu, Appl. Phys. Lett. **112**(16), 163902 (2018).
[326]H. Liu, C. Lee, T. Kobayashi, C. J. Tay, and C. Quan, Sens. Actuators, A **186**(4), 242 (2012).
[327]J. Zhang, L. Kong, L. Zhang, F. Li, W. Zhou, S. Ma, and L. Qin, Appl. Sci. **6**(12), 402 (2016).
[328]D. G. Lee, G. P. Carman, D. Murphy, and C. Schulenbury, paper presented at IEEE Transducer 07 (2007).
[329]P. Janphuang, R. A. Lockhart, D. Isarskorn, S. Henein, D. Briand, and N. F. D. Rooij, J. Microelectromech. Syst. **24**(3), 742–754 (2015).
[330]M. Pozzi and M. Zhu, Smart Mater. Struct. **20**(5), 055007 (2011).
[331]M. Pozzi, M. S. H. Aung, M. Zhu, R. K. Jones, and J. Y. Goulermas, Smart Mater. Struct. **21**(7), 075023 (2012).
[332]Y. Kuang and M. Zhu, Sens. Actuators, A **263**, 510–520 (2017).
[333]S. Priya, Appl. Phys. Lett. **87**(18), 184101 (2005).
[334]H. Liu, C. J. Tay, C. Quan, T. Kobayashi, and C. Lee, Microsyst. Technol. **17**(12), 1747–1754 (2011).
[335]S. M. Jung and K. S. Yun, Appl. Phys. Lett. **96**(11), 111906 (2010).
[336]D. Han and K. S. Yun, Microsyst. Technol. **21**(8), 1669–1676 (2015).
[337]B. Ando, S. Baglio, A. R. Bulsara, V. Marletta, and A. Pistorio, IEEE Trans. Instrum. Meas. **66**(5), 1067–1075 (2017).
[338]B. Ando, S. Baglio, V. Marletta, A. Pistorio, and A. R. Bulsara, IEEE Trans. Instrum. Meas. **66**(5), 992–1001 (2017).
[339]T. Galchev, H. Kim, and K. Najafi, J. Microelectromech. Syst. **20**(4), 852–866 (2011).
[340]T. Galchev, E. E. Aktakka, and K. Najafi, J. Microelectromech. Syst. **21**(6), 1311–1320 (2012).
[341]Q. Tang and X. Li, IEEE/ASME Trans. Mech. **20**(1), 115–121 (2015).
[342]T. K. Chung, C. M. Wang, P. C. Yeh, and T. W. Liu, IEEE Sens. J. **14**(9), 3152–3163 (2014).
[343]K. Fan, J. Chang, F. Chao, and W. Pedrycz, Energy Convers. Manage. **96**, 430–439 (2015).
[344]K. Fan, J. Chang, W. Pedrycz, Z, Liu, and Y. Zhu, Appl. Phys. Lett. **106**(22), 223902 (2015).
[345]P. Pillatsch, E. M. Yeatman, and A. S. Holmes, Sens. Actuators, A **206**(3), 178–185 (2014).
[346]P. Pillatsch, E. M. Yeatman, A. S. Holmes, and P. K. Wright, Sens. Actuators, A **244**, 77–85 (2016).
[347]R. Ramezanpour, H. Nahvi, and S. Ziaei-Rad, J. Sound Vib. **370**, 280–305 (2016).
[348]H. Fu and E. M. Yeatman, Energy **125**, 152–161 (2017).
[349]T. Xue and S. Roundy, Sens. Actuators, A **253**, 101–111 (2017).
[350]G. Poulin, E. Sarraute, and F. Costa, Sens. Actuators, A **116**, 461–471 (2004).
[351]T. Wacharasindhu and J. W. Kwon, J. Micromech. Microeng. **18**(10), 104016 (2008).
[352]V. R. Challa, M. G. Prasad, and F. T. Fisher, Smart Mater. Struct. **18**(9), 095029 (2009).
[353]B. Yang, C. Lee, W. Kee, and S. P. Lim, J. Micro/Nanolithogr., MEMS, MOEMS **9**(2), 023002 (2010).
[354]Y. Sang, X. Huang, H. Liu, and P. Jin, IEEE Trans. Magn. **48**(11), 4495–4498 (2012).
[355]M. Wischke, M. Masur, and P. Woias, paper presented at Transducers 2009, Denver, CO, 21–25 June 2009, pp. 521–552.
[356]P. Li, S. Gao, and H. Cai, Microsyst. Technol. **21**(2), 401–414 (2015).
[357]P. Li, S. Gao, and B. Cong, AIP Adv. **8**(3), 035017 (2018).
[358]P. Li, S. Gao, X. Zhou, and H. Liu, Microsyst. Technol. **24**(2), 1017–1024 (2018).
[359]P. Li, S. Gao, X. Zhou, H. Liu, and J. Shi, Microsyst. Technol. **23**(12), 5281–5292 (2017).
[360]H. Lin, P. Hsu, T. Chen, H. Liu, H. Huang, L. Sun, and L. Cui, paper presented at the 16th International Conference on Nanotechnology (IEEE Nano 2016), Sendai, Japan, 22–25 August 2016.
[361]K. Fan, S. Liu, H. Liu, Y. Zhu, W. Wang, and D. Zhang, Appl. Energy **216**, 8–20 (2018).

[362]M. D. Han, X. S. Zhang, W. Liu, X. M. Sun, X. H. Peng, and H. X. Zhang, Sci. China: Technol. Sci. **56**(8), 1835–1841 (2013).
[363]T. Chen, Y. Xia, W. Liu, H. C. Liu, L. N. Sun, and C. Lee, J. Microelectromech. Syst. **25**(5), 845–847 (2016).
[364]X. He, Q. Wen, Y. Sun, and Z. Wen, Nano Energy **40**, 300–307 (2017).
[365]T. Starner, IBM Syst. J. **35**(3–4), 618–629 (1996).
[366]T. Starner and J. Paradiso, *Low Power Electronics Design* (CRC Press, New York, 2004), Chap. 45.
[367]S. Khalifa, G. Lan, M. Hassan, A. Seneviratne, and S. K. Das, IEEE Trans. Mobile Comput. **17**(6), 1353–1368 (2018).
[368]J. L. Gonzalez, A. Rubio, and F. Moll, Int. J. Soc. Mater. Eng. Resour. **10**, 34–40 (2002).
[369]P. Niu, P. Chapman, R. Riemer, and X. Zhang, paper presented at the 35th Annual Power Electronics Specialists Conf. (2004), pp. 2100–2106.
[370]N. S. Shenck and J. A. Paradiso, IEEE Micro **21**(3), 30–42 (2001).
[371]K. Ishida, T. C. Huang, K. Honda, Y. Shinozuka, H. Fuketa, T. Yokota, U. Zschieschang, H. Klauk, G. Tortissier, T. Sekitani, H. Toshiyoshi, M. Takamiya, T. Someya, and T. Sakurai, IEEE J. Solid-State Circuits **48**(1), 255–264 (2013).
[372]J. Zhao and Z. You, Sensors **14**(7), 12497–12510 (2014).
[373]Y. Han, Y. Cao, J. Zhao, Y. Yin, L. Ye, X. Wang, and Z. You, Sensors **16**(9), 1502 (2016).
[374]K. Fan, Z. Liu, H. Liu, L. Wang, Y. Zhu, and B. Yu, Appl. Phys. Lett. **110**(14), 143902 (2017).
[375]W. S. Jung, M. J. Lee, M. G. Kang, H. G. Moon, S. K. Yoon, S. H. Baek, and C. Y. Kang, Nano Energy **13**, 174–181 (2015).
[376]R. Shukla and A. J. Bell, Sens. Actuators, A **222**, 39–47 (2015).
[377]Y. Kuang, T. Ruan, J. C. Zheng, and M. Zhu, Sens. Actuators, A **254**, 69–77 (2017).
[378]I. Izadgoshasb, Y. Y. Lim, N. Lake, L. Tang, R. V. Padilla, and T. Kashiwao, Energy Convers. Manage. **161**, 66–73 (2018).
[379]C. Sun, J. Shi, D. J. Bayerl, and X. Wang, Energy Environ. Sci. **4**(11), 4508–4512 (2011).
[380]H. Xue, Q. Yang, D. Wang, W. Luo, W. Wang, M. Lin, D. Liang, and Q. Luo, Nano Energy **38**, 147–154 (2017).
[381]Q. Zheng, B. Shi, Z. Li, and Z. L. Wang, Adv. Sci. **4**(7), 1700029 (2017).
[382]S. H. Lee, C. K. Jeong, G.-T. Hwang, and K. J. Lee, Nano Energy **14**, 111–125 (2015).
[383]M. Kindermann, B. Schwaab, M. Berg, and G. Frohlig, Pacing Clin. Electrophysiol. **24**(5), 810–815 (2001).
[384]J. C. Deharo and P. Djiane, Ann. Cardiol. Angeiol. **54**(1), 26–31 (2005).
[385]V. R. Vorperian, S. Lawrence, and K. Chlebowski, Pacing Clin. Electrophysiol. **22**(5), 698–705 (1999).
[386]M. A. Wood and K. A. Ellenbogen, Circulation **105**(18), 2136–2138 (2002).
[387]Q. Zheng, B. Shi, F. Fan, X. Wang, L. Yan, W. Yuan, S. Wang, H. Liu, Z. Li, and Z. L. Wang, Adv. Mater. **26**(33), 5851–5856 (2014).
[388]Q. Zheng, H. Zhang, B. Shi, X. Xue, Z. Liu, Y. Jin, Y. Ma, Y. Zou, X. Wang, Z. An, W. Tang, W. Zhang, F. Yang, Y. Liu, X. Lang, Z. Xu, Z. Li, and Z. L. Wang, ACS Nano **10**, 6510 (2016).
[389]Y. Ma, Q. Zheng, Y. Liu, B. Shi, X. Xue, W. Ji, Z. Liu, Y. Jin, Y. Zou, Z. An, W. Zhang, X. Wang, W. Jiang, Z. Xu, Z. L. Wang, Z. Li, and H. Zhang, Nano Lett. **16**(10), 6042 (2016).
[390]Z. Li, G. Zhu, R. Yang, A. C. Wang, and Z. L. Wang, Adv. Mater. **22**(23), 2534–2537 (2010).
[391]X. Cheng, X. Xue, Y. Ma, M. Han, W. Zhang, Z. Xu, H. Zhang, and H. Zhang, Nano Energy. **22**, 453–460 (2016).
[392]Y. Yu, H. Sun, H. Orbay, F. Chen, C. G. England, W. Cai, and X. Wang, Nano Energy **27**, 275–281 (2016).
[393]C. Dagdeviren, Y. Shi, P. Joe, R. Ghaffari, G. Balooch, K. Usgaonkar, O. Gur, P. L. Tran, J. R. Crosby, M. Meyer, Y. Su, R. Chad Webb, A. S. Tedesco, M. J. Slepian, Y. Huang, and J. A. Rogers, Nat. Mater. **14**(7), 728 (2015).
[394]G. T. Hwang, M. Byun, C. K. Jeong, and K. J. Lee, Adv. Healthcare Mater. **4**, 646 (2015).
[395]H. Zhang, X.-S. Zhang, X. Cheng, Y. Liu, M. Han, X. Xue, S. Wang, F. Yang, A. S. Smitha, H. Zhang, and Z. Xu, Nano Energy **12**, 296 (2015).
[396]S. R. Platt, S. Farritor, and H. Haider, IEEE/ASME Trans. Mech. **10**(2), 240–252 (2005).
[397]S. R. Platt, S. Farritor, and H. Haider, IEEE/ASME Trans. Mech. **10**(4), 455–461 (2005).
[398]M. Deterre, E. Lefeuvre, Y. Zhu, M. Woytasik, B. Boutaud, and R. D. Molin, J. Microelectromech. Syst. **23**(3), 651–660 (2014).
[399]G. T. Hwang, Y. Kim, J. H. Lee, S. Oh, C. K. Jeong, D. Y. Park, J. Ryu, H. S. Kwon, S. G. Lee, B. Joung, D. Kim, and K. J. Lee, Energy Environ. Sci. **8**(9), 2677–2684 (2015).
[400]C. Dagdeviren, B. D. Yang, Y. Su, P. L. Tran, P. Joe, E. Anderson, J. Xia, V. Doraiswamy, B. Dehdashti, X. Feng, B. Lu, R. Poston, Z. Khalpey, R. Ghaffari, Y. Huang, M. J. Slepian, and J. A. Rogers, Proc. Natl. Acad. Sci. U. S. A. **111**, 1927 (2014).
[401]D. H. Kim and K. J. Lee, Adv. Funct. Mater. **27**(25), 1700341 (2017).
[402]N. Elvin, A. Elvin, and D. H. Choi, J. Strain Anal. Eng. Des. **38**, 115–124 (2003).
[403]S. W. Arms, C. P. Townsend, D. L. Churchill, J. H. Galbreath, and S. W. Mundell, Proc. SPIE **5763**, 267–275 (2005).
[404]E. E. Aktakka, R. L. Peterson, and K. Najafi, in *Proceeding of the IEEE Conference on Industrial Automation and Control Emerging Technology Applications* (2011), Vol. 6, p. 409.
[405]D. Zhu, S. P. Beeby, M. J. Tudor, and N. R. Harris, Sens. Actuators, A **169**(2), 317–325 (2011).
[406]See https://www.microgensystems.com/ for MicroGen BOLT energy harvesting product.
[407]K. B. Singh, V. Bedekar, S. Taheri, and S. Priya, Mechatronics **22**(7), 970–988 (2012).
[408]Q. C. Tang, X. Y. Xia, and X. X. Li, in *Proceeding of the 25th International Conference on Micro Electro Mechanical Systems* (IEEE MEMS, 2012), pp. 1273–1276.
[409]R. V. Schaijk, R. Elfrink, J. Oudenhoven, V. Pop, Z. Wang, and M. Renaud, Proc. SPIE **8763**, 876305 (2013).
[410]J. Lee and B. Choi, Energy Convers. Manage. **78**, 32–38 (2014).
[411]Y. Zhang, R. Zheng, K. Shimono, T. Kaizka, and K. Nakano, Sensors **16**(10), 1727 (2016).
[412]Y. Zhang, R. Zheng, K. Nakano, and M. P. Cartmell, Appl. Phys. Lett. **112**(14), 143901 (2018).
[413]J. M. McCarthy, S. Watkins, A. Deivasigamani, and S. J. John, J. Sound Vib. **361**(8), 355–377 (2016).
[414]A. Abdelkefi, Int. J. Eng. Sci. **100**, 112–135 (2016).
[415]D. Li, Y. Wu, A. D. Ronch, and J. Xiang, Prog. Aerosp. Sci. **86**, 28–62 (2016).
[416]L. Zhao and Y. Yang, Shock Vib. **2017**, 3585972.
[417]J. Zhang, Z. Fang, C. Shu, J. Zhang, Q. Zhang, and C. Li, Sens. Actuators A: Phys. **262**, 123–129 (2017).
[418]S. M. Frayne, "Generator utilizing fluid-induced oscillations," U.S. patent 20090,309,362 (2009).
[419]W. B. Hobbs and D. L. Hu, J. Fluids Struct. **28**(1), 103–114 (2012).
[420]H. C. Liu, S. Zhang, R. Kathiresan, T. Kobayashi, and C. Lee, Appl. Phys. Lett. **100**(22), 223905 (2012).
[421]H. L. Dai, A. Abdelkefi, Y. Yang, and L. Wang, Appl. Phys. Lett. **108**(5), 053902 (2016).
[422]P. V. Biswas, M. A. Uddin, M. A. Islam, M. A. Sarkar, V. G. Desa, M. H. Khan, and A. M. A. Huq, paper presented at the International Conference On Mechanical Engineering, Dhaka, 2009.
[423]V. K. Wong, J. H. Ho, and A. B. Chai, Energy **124**, 364–371 (2017).
[424]M. Al Ahmad, J. Electron. Mater. **43**(2), 452–458 (2014).
[425]C. H. Wong, Z. Dahari, A. A. Manaf, and M. A. Miskam, J. Electron. Mater. **44**(1), 13–21 (2015).
[426]M. A. Ilyas and J. Swingler, Energy **90**, 796–806 (2015).
[427]Z. Z. Ong, V. K. Wong, and J. H. Ho, Sens. Actuators, A **252**, 154–164 (2016).
[428]N. A. K. Z. Abidin, N. M. Nayan, M. M. Azizan, and A. Ali, Mech. Syst. Signal Process. **101**, 211–218 (2018).
[429]G. Acciari, M. Caruso, R. Miceli, L. Riggi, P. Romano, G. Schettino, and F. Viola, IEEE Trans. Ind. Appl. **54**(1), 458–468 (2018).
[430]A. Delorme, D. Karbowski, R. Vijayagopal, and P. Sharer, *Evaluation of fuel consumption potential of medium and heavy duty vehicles through modeling and simulation*, National Academy of Sciences, Washington, D.C., 2009.
[431]H. Xiong and L. Wang, Appl. Energy **174**, 101–107 (2016).
[432]M. Peigney and D. Siegert, Smart Mater. Struct. **22**(9), 095019 (2013).
[433]M. Wischke, M. Masur, M. Kroner, and P. Woias, Smart Mater. Struct. **20**(8), 085014 (2011).
[434]H. Zhao, J. Ling, and J. Yu, J. Ceram. Soc. Jpn. **120**(1404), 317–323 (2012).
[435]H. J. Xiang, J. J. Wang, Z. F. Shi, and Z. W. Zhang, Smart Mater. Struct. **22**(9), 095024 (2013).
[436]X. Jiang, Y. Li, J. Li, J. Wang, and J. Yao, J. Renewable Sustainable Energy **6**(4), 043110 (2014).

[437]A. Moure, M. A. I. Rodríguez, S. H. Rueda, A. Gonzalo, F. Rubio-Marcos, D. U. Cuadros, A. Pérez-Lepe, and J. F. Fernández, Energy Convers. Manage. **112**, 246–253 (2016).
[438]I. Jung, Y. H. Shin, S. Kim, J. Y. Choi, and C. Y. Kang, Appl. Energy **197**, 222–229 (2017).
[439]Y. H. Shin, I. Jung, M. S. Noh, J. H. Kim, J. Y. Choi, S. Kim, and C. Y, Kang, Appl. Energy **216**, 741–750 (2018).
[440]H. Wang, A. Jasim, and X. Chen, Appl. Energy **212**, 1083–1094 (2018).
[441]G. W. Taylor, J. R. Burns, S. M. Kammann, W. B. Powers, and T. R. Welsh, IEEE J. Oceanic Eng. **26**, 539–547 (2001).
[442]N. Wu, Q. Wang, and X. D. Xie, Appl. Ocean Res. **50**, 110–118 (2015).
[443]N. V. Viet, X. D. Xie, K. M. Liew, N. Banthia, and Q. Wang, Energy **112**, 1219–1226 (2016).
[444]W. S. Hwang, J. H. Ahn, S. Y. Jeong, H. J. Jung, S. K. Hong, J. Y. Choi, J. Y. Cho, J. H. Kim, and T. H. Sung, Sens. Actuators, A **260**, 191–197 (2017).
[445]H. Mutsuda, Y. Tanaka, R. Patel, Y. Doi, Y. Moriyama, and Y. Umino, Appl. Ocean Res. **68**, 182–193 (2017).
[446]X. D. Xie and Q. Wang, Compos. Struct. **178**, 447–454 (2017).